Breast ductal carcinoma *in situ*, MCF10DCIS, and the proprotein convertase PCSK5

A DISSERTATION

Presented to
the faculty of the School of Engineering and Applied Science
in partial fulfillment of the requirements
for the degree of

Doctor of Philosophy

---

by TAYLOR MAROHL

May 2025

DEPARTMENT OF BIOMEDICAL ENGINEERING
UNIVERSITY *of* VIRGINIA

Approval Sheet

This

Dissertation

is submitted in partial fulfillment of the requirements

for the degree of

Doctor of Philosophy

Taylor Marohl, Author

This Dissertation has been read and approved by the examining committee:

Dr. Kevin A. Janes, Dissertation Advisor
Department of Biomedical Engineering

Dr. Kristen M. Naegle, Committee Chair
Department of Biomedical Engineering

Dr. Daniel Gioeli, Committee Member
Department of Microbiology, Immunology, and Cancer Biology

Dr. Mohammad Fallahi-Sichani, Committee Member
Department of Biomedical Engineering

Dr. Marc Hafner, Committee Member
Computational Biology and Translational Oncology, Genentech

Accepted for the School of Engineering and Applied Science:

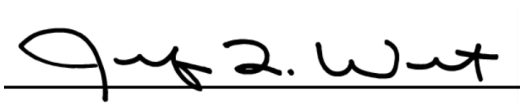

Jennifer L. West, School of Engineering and Applied Science

May 2025

Abstract

Ductal carcinoma *in situ* (DCIS) is a premalignancy characterized by the hyperproliferation of breast ductal cells without invasion into the surrounding tissue. The preeminent model for estrogen receptor-negative DCIS is the MCF10DCIS cell line; MCF10DCIS is a member of the MCF10 series of cell lines, which were serially derived from a single patient sample and represent the progression from normal breast to invasive ductal carcinoma. MCF10 is used for *in vitro*, 3D spheroid, and intraductal xenograft research and underlies impactful studies of DCIS malignancy, metastasis, metabolism, and mechanotransduction. The TGFβ-superfamily ligand GDF11 is important for the maintenance of epithelial properties in MCF10DCIS spheroids and xenografts. GDF11 is synthesized as an inactive protein precursor and is activated by proprotein convertase PCSK5; in triple-negative breast cancer, GDF11 activity is lost due to PCSK5 silencing. The heterozygous PCSK5 mutation M452I arose during derivation of the MCF10 series but is not documented in breast or any other type of cancer.

Through a carefully-designed set of experiments spanning all complexity levels at which MCF10DCIS is used, we show that PCSK5^{M452I} is not hypermorphic but hypomorphic. Using an optimized in-cell GDF11 maturation assay, we found that overexpressed PCSK5^{M452I} had measurable but significantly decreased activity compared to wildtype PCSK5. Co-expression of wildtype PCSK5 and PCSK5^{M452I} yielded an intermediate activity level. In a PCSK5$^{-/-}$ clone of MCF10DCIS reconstituted with different PCSK5 alleles, PCSK5^{M452I} was mildly defective in anterograde transport. However, the multicellular organization of PCSK5^{M452I} addback cells in 3D matrigel cultures was significantly less compact than wildtype and the growth of intraductal MCF10DCIS xenografts was similarly impaired along with the frequency of comedo necrosis and stromal activation. In the same settings, we found that a PCSK5^{T288P} null allele, which had GDF11-processing activity akin to –PCSK5 control, remained in the cis- and particularly the trans-Golgi compartments of the secretory pathway, formed acircular spheroids, and had impaired xenograft growth compared to wildtype PCSK5.

This dissertation reinforces an important role for PCSK5 in the promotion of pro-epithelial phenotype in DCIS. It also reassures the DCIS research community that a PCSK5 mutation unique to MCF10 cell lines is not responsible for the salient characteristics of the MCF10DCIS cell line and xenograft model.

Acknowledgements

I am immensely grateful to so many people for supporting me during graduate school and for making this work possible. First, thank you to my advisor, Kevin Janes, for teaching me to be rigorous in my approach to science, for being incredibly reliable, and for always looking out for my best interests. Lixin, thank you for dedicating so much time and effort to my project; I couldn't have done it without you. Cheryl, thank you for all of the hard work you do to keep the lab running smoothly; everything you do has an immense positive impact on the lab and the research we are able to accomplish. To the Janes Lab grad students and postdocs, thank you for creating and maintaining the best lab culture I could have asked for. Every day of grad school, you provided exactly what I needed to keep going; I am so fortunate to have been able to work and learn and laugh alongside you. You guys made it fun to come to work even when my experiments failed and I had absolutely no clue how my research was going to become a story. Each individual in this lab is an incredible human being, and you all inspire me every day to be a better scientist and person. I am very grateful to have all of you in my life. To Sham, thank you for being my lab role model, for being insanely impressive yet also so down to earth, and for always cheering me on. To Andrew, thank you for being my lab twin and the most wonderful co-senior grad student for so many years; it was an absolute pleasure working and mentoring with you, in addition to all the time we spent together during classes and outside the lab. To Wisam, thank you for listening to pop music with me during early morning dissections, for assisting me with basic (and complex) math, and for always understanding my sarcasm (even when literally no one else got it). To Najwa, thank you for lifting me up out of the dregs of the pandemic by rotating with us; your companionship during that summer meant more to me than you know, and I am so glad I could single-handedly convince you to join the lab because you have continued to lift my spirits day-after-day. To Bishal and Cameron, thank you for bringing postdoc wisdom and a lot of humor to our lab; it has been an honor to watch you develop into passionate and skilled scientists and leaders.

Thank you to my committee members, especially my chair, Kristen Naegle, and Dan Gioeli, for providing outspoken and unyielding support for my professional development and personal wellbeing. Thank you to Marc Hafner, Ciara Metcalfe, and others at Genentech for helping me learn about another type of breast cancer, an entirely new set of bioinformatics skills, and careers in industry; and especially thank you to Marc for your ongoing collaboration and mentorship. Thank you to Dr. Kristen Atkins for your enthusiasm and patience as you dedicated numerous hours to teaching me to understand histology. Thank you to Cameron Wells for providing updated versions of Organoseg and for your crucial help with my analyses. Thank you to Sameer Bajikar for doing so much of the work upon which my project was built and for answering obscure questions about experiments you did numerous years prior. Thank you to the UVA core labs, especially Alex Wendling with the Flow Core, Sheri VanHoose with the Research Histology Core, and Pat Pramoonjago with the BTRF, all of whom were invaluable to my research progress. Thank you especially to my funding sources, including NSF, NIH, and the UVA School of Engineering and Applied Science.

I have been privileged to make many wonderful friends during grad school. Delaney, thank you for being my best friend from start to finish. Everything is more fun when we do it together, and over the past 7 years I feel like we've faced just about everything. I look forward to many more years of friendship ahead. Thank you to my covid bubble, Thaddeus, Keric, Anna, and Matt, for puzzles and roommate dinners and kitchen climbing and keeping each other sane. Thank you to Gabe, Dawson, Michael, Yoni, Keric, and others for backpacking, hiking, skiing, climbing, and other outdoor adventures.

Thank you to Delaney and Justin for being wonderful housemates. Thank you to everyone who has helped make Friendsgiving a special tradition over the years.

To my mom and dad, thank you for being so supportive of me, my entire life. Thank you for coming to visit me in Charlottesville, for exploring hikes and breweries, and for getting to know my friends. Thank you for encouraging me to work hard and do my best, and thank you for always believing in me. I love you both. To my dad in particular, losing you was the hardest part of grad school. I wish more than anything that you were still here with us. You were always my #1 fan, and I know just how proud you would be to see me graduate. I miss you so much and will always, always love you.

To Thaddeus, thank you for being goofy, loving, and excited to try so many new experiences with me - like forging, pottery, and adopting a dog despite being a cat person. Thank you for traveling with me, going on hikes, and enjoying the farmer's market and Mariebette with me on Saturday mornings. Thank you especially for ceaselessly supporting me no matter what life throws at us. You are a fantastic partner. I love you.

Finally, thank you to Bruno for providing me with a limitless tap of serotonin. Only people who have experienced firsthand the deep bond between humans and dogs know how special it is to share a relationship with a creature who speaks only through actions. Importantly, he has no clue and does not care one bit about my role as a grad student. He highlights the simple pleasures in life: going for a walk, basking in the sunshine, learning new tricks, and being present with those you love.

Table of Contents

List of Figures

List of Tables

Acronyms/Abbreviations Used

Genes/Proteins

ACTH = adrenocorticotropic hormone

ACVR = activin receptor

ALK = activin receptor-like kinase (type I receptors)

cAMP = cyclic adenosine monophosphate

EGFR = epidermal growth factor receptor

ER = estrogen receptor

FGF = fibroblast growth factor

GDF11 = growth differentiation factor 11 (also: BMP11)

HER2 = human epidermal growth factor receptor 2 (also: ERBB2)

HSPG = heparan sulfate proteoglycans

MAPK = mitogen activated protein kinase

MMP = matrix metalloproteinase

PC = proprotein convertase

PCSK5 = proprotein convertase subtilisin/kexin type 5, A form (also: PC5A)

PCSK5b = proprotein convertase subtilisin/kexin type 5, B form (also: PC5B)

PDGF = platelet-derived growth factor

PR = progesterone receptor

TGFβ = transforming growth factor beta

TIMP = tissue inhibitor of metalloproteinases

Other

CRD = Cys-rich domain

DCIS = ductal carcinoma in situ

ECM = extracellular matrix

ER = endoplasmic reticulum

HTAN = Human Tumor Atlas Network

IDC = invasive ductal carcinoma

IHC = immunohistochemistry

KO = knock-out

MCF10DCIS = MCF10DCIS.COM cell line

PDX = patient-derived xenografts

TCGA = The Cancer Genome Atlas

TGN = trans-Golgi network

VAF = variant allele plot

Chapter 1: Introduction

1.1 Ductal Carcinoma in Situ (DCIS)

The human breast consists of glandular, adipose, and fibrous connective tissue (Cooper, 1840; Hassiotou & Geddes, 2013). Within the glandular tissue is a network of ducts that connect a number of breast lobes to the nipple (**Figure 1.01, left**). Each lobe is comprised of smaller units called lobules, which are responsible for producing milk during lactation. The duct wall contains an inner layer of epithelial cells, which are cuboidal and interface with the ductal lumen (**Figure 1.01, left**). Surrounding the luminal epithelial cells is a layer of myoepithelial cells that have contractile properties and interface with the stroma, which supports the ducts and lobes. These structures play critical roles in normal breast function following pregnancy but are also subject to disease.

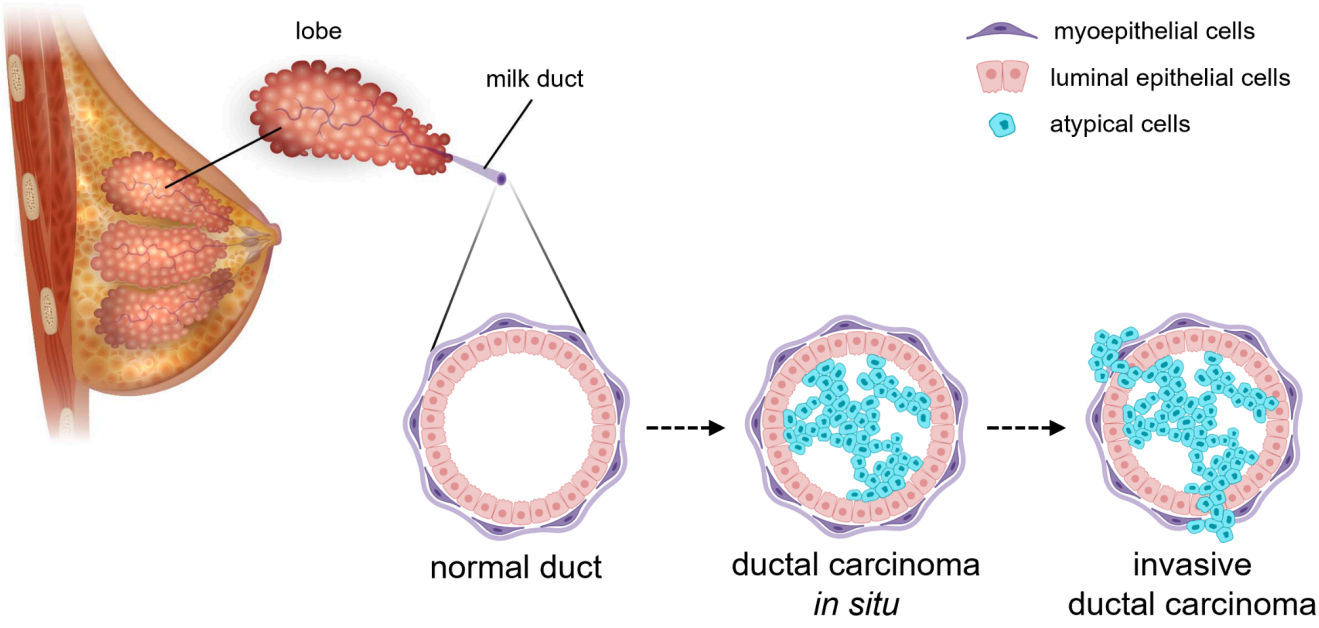

Figure 1.01. Normal breast anatomy, ductal carcinoma *in situ*, and invasive ductal carcinoma. **Left**, Normal breast consisting of multiple lobes, each of which contain round, hollow milk ducts. **Right**, Ductal cross-sections showing proliferation of atypical cells as in ductal carcinoma *in situ* and invasion into the surrounding tissue as in invasive ductal carcinoma. *Adapted with permission from Rocky Mountain Cancer Centers. Produced in part using Biorender.*

Ductal carcinoma *in situ* (DCIS) is a premalignant condition characterized by proliferation of ductal epithelial cells into the ductal lumen; importantly, myoepithelial cells and an intact basement membrane confine the DCIS cells to the intraductal space (**Figure 1.01, right**). Invasive ductal carcinoma (IDC), the most common type of breast cancer, occurs when tumor cells break through the duct wall, invading into the surrounding breast tissue and metastasizing to other sites of the body (**Figure 1.01, right**). DCIS is a non-obligate precursor of IDC (Wellings & Jensen, 1973), with

approximately 20-50% of untreated DCIS cases later progressing to IDC (Betsill et al., 1978; Collins et al., 2005; Erbas et al., 2006; Page et al., 1982, 1995; Sanders et al., 2005). Despite its recognition going back decades, we still have a limited understanding of the mechanisms governing DCIS and lack a reliable way to predict which cases of DCIS will progress to IDC and which will not (Brock et al., 2019; Puleo & Polyak, 2021; Schwartz et al., 2000).

1.1.1 DCIS Biology

While all DCIS is confined to the breast duct, much diversity exists. DCIS cells produce multiple architectural patterns as they proliferate. These patterns include cribriform, where cells polarize around punched-out spaces; solid, where cells proliferate as monomorphic sheets that fill the lumen; papillary, where epithelial proliferation covers fibrovascular cores; micropapillary, where tufts of cells project into the lumen and form narrow slits that lack a fibrovascular core; and comedo necrosis, where necrotic cells and cell material form a core at the center of the duct (Bellamy et al., 1993; Sanati, 2019). It is common for a single lesion to exhibit multiple growth patterns (Scripcaru & Zardawi, 2012). While the prognostic utility of DCIS architecture is limited, the patterns are useful for the histological recognition of DCIS (Bellamy et al., 1993; Sanati, 2019).

DCIS lesions are categorized by their histological markers. Like IDC, DCIS can be positive or negative for estrogen receptor (ER) and progesterone receptor (PR) expression, and HER2 amplification can be present or absent. A set of RNA expression-based, or “molecular”, subtypes was first defined for IDC (Perou et al., 2000; Sorlie et al., 2001) and later extended to DCIS (Bryan et al., 2006; Clark et al., 2011; Doebar et al., 2016; Livasy et al., 2007; Tamimi et al., 2008; Yu et al., 2011). The luminal A subtype is characterized by high estrogen signaling, high RB1 expression, and low proliferation, while the luminal B subtype has less estrogen signaling than luminal A, some cyclin D1 amplification, and high proliferation. The HER2-amplified subtype is characterized by ERBB2 gene amplification, high protein expression and phosphorylation of HER2 and EGFR, high proliferation, high prevalence of TP53 mutations, and high genomic instability. Finally, the basal-like subtype is mostly triple-negative (ER-/PR-/HER2-), has high expression of CDKN2A and DNA repair proteins, high proliferation, very prevalent TP53 mutations, rare PIK3CA mutations, and high genomic instability (Brenton et al., 2005; Koboldt et al., 2012; Perou et al., 2000; Sorlie et al., 2001). These subtypes are generally identified by the histological markers ER, HER2, EGFR, and cytokeratin 5/6+ (**Table 1.01**) (Abd El-Rehim et al., 2004; Brenton et al., 2005; Cheang et al., 2008; Nielsen, 2004; Nielsen & Perou, 2015). While the same subtypes are identified in both DCIS and IDC, the prevalence of each differs; luminal A and basal-like subtypes are more common in IDC, while luminal B and HER2 are more common in DCIS (**Table 1.01**) (Livasy et al., 2007; Tamimi et al., 2008).

Table 1.01. Prevalence of molecular subtypes among DCIS and IDC cases. (Clark et al., 2011; Livasy et al., 2007; Tamimi et al., 2008)

Molecular Subtype	Histological Signature	Prevalence in DCIS	Prevalence in IDC
Luminal A	ER+ and/or PR+, HER2-	~57-63%	~73%
Luminal B	ER+ and/or PR+, HER2+	~9-13%	~5%
HER2	ER-, PR-, HER2+	~14-22%	~6%
Basal-like	ER-, PR-, HER2-, EGFR+ and/or CK5/6+	~8-11%	~11%

More recently, the subtypes for DCIS have been redefined by the Human Tumor Atlas Network (HTAN) analysis of the Translational Breast Cancer Research Consortium (TBCRC) and Resource of Archival Breast Tissue (RAHBT) cohorts (Strand et al., 2022). An 812-gene differential expression signature was established that predicts subsequent invasive ipsilateral breast events in both cohorts. The signature was not prognostic for invasive breast carcinoma cases in The Cancer Genome Atlas (TCGA), in support of prior work highlighting the distinctions in biological patterns between DCIS and invasive breast carcinoma. The signature was enriched for genes involved with proliferation, immune response, and metabolism. Unsupervised clustering of RNAseq data from both cohorts yielded three distinct clusters: ER_{low}, quiescent, and ER_{high}. The ER_{low} cluster was associated with higher HER2 and lower ER expression and enrichment of progression-associated MYC, mTOR signaling, and cell cycle pathways; the ER_{high} cluster was associated with higher ER expression, depletion of UV response down and enrichment of oxidative phosphorylation pathways, and increased myoepithelial E-cadherin abundance; and the quiescent cluster was associated with higher ER expression, lack of enrichment for recurrence-associated pathways, and depletion of Ki67 and GLUT1.

1.1.2 Laboratory Models of DCIS

Progression from the normal breast to DCIS to IDC is a highly complex process that occurs through myriad paths (Lopez-Garcia et al., 2010). To study the characteristics of DCIS and the principles governing its development and its progression to IDC requires perturbation and analysis of the relevant biology in the laboratory. DCIS laboratory models have been extensively reviewed (Behbod et al., 2018; Brock et al., 2019; Hutten & Jonkers, 2023; van Amerongen et al., 2023; J. Wang et al., 2024). Generally, DCIS models facilitate assessment at four different complexity scales, each with benefits and limitations: 2D cell culture in a dish, 3D spheroid culture with extracellular matrix substrate, xenograft of cell lines or patient-derived cells in immune-deficient mice, and genetically-engineered mouse models. Cell lines (Barnabas & Cohen, 2013; Lee et al., 2012; Miller et al., 2000; Rizki et al., 2008; Samson et al., 2021; Yong et al., 2014) are easily manipulable by genetic engineering and *in vitro*

perturbation with drugs or environmental modifications and allow straightforward read-out at DNA, RNA, protein, and phenotypic levels, but carry obvious limitations involved with their far-from-physiological growth environment. Cell culture in 3D involves the study of cells in a microenvironment, allowing manipulation of specific environmental variables with a higher-level phenotypic read-out (Jedeszko et al., 2009; Pereira et al., 2020). Original xenograft models involve the implantation of cell lines or patient-derived samples into the flank, tail vein, or mammary fat pad of mice (Eck et al., 2009; Miller et al., 2000; Rizki et al., 2008), while the more modern mouse-intraductal (MIND) model involves the direct injection of cells into the mouse mammary duct (Behbod et al., 2009; Hong et al., 2022; Hutten et al., 2023; Kittrell et al., 2016; Valdez et al., 2011). These strategies convey a physiological environment, particularly the ductal environment of the MIND model, but require the use of immune-deficient mice. Finally, genetically engineered mouse models (GEMMs) are the most physiologically-relevant and the optimal system for studying immune-tumor interactions, but are complex to produce, expensive to maintain, and do not allow the study of human-derived cells (Green et al., 2000; Pfefferle et al., 2013). Arguably the most useful models are those that span multiple complexity scales, thereby leveraging the benefits of each.

1.1.2.1 MCF10 Series

MCF10DCIS.com is one of the most widely used cell line and xenograft models of DCIS. It belongs to a family of cell lines, MCF10, that were all derived from a single patient and span across the phases of breast ductal carcinogenesis. The derivation of MCF10DCIS.com was complex and warrants attention as it provides context that is important for understanding the model's characteristics and utility.

The MCF10 cell line was established from mammary tissue collected during a mastectomy on a 36-year old premenopausal woman (**Figure 1.02, blue box**) (Soule et al., 1990). The histology revealed a diagnosis of extensive fibrocystic disease; the woman had no other disease and no family history of breast cancer. The primary cells were cultured for 6 days in DMEM/F-12 medium followed by 10 days in low-calcium medium (0.06 mM Ca^{2+}) before being transferred into low-calcium serum-free medium, where they were maintained until day 677 of *in vitro* culture. These cells grew very slowly and were mortal (designated MCF10M), as evidenced by their undergoing senescence when cultured in DMEM/F-12 containing normal levels of calcium (1.05 mM Ca^{2+}), and grew as a combination of adhered and free-floating cells. All passages were performed by transferring the subset of cells that were free-floating to a new vessel. MCF10M cells were switched to serum-containing medium with low calcium (0.04 mM Ca^{2+}) at day 677 (Soule et al., 1990). At day 754, free-floating cells from several passages were combined to initiate passage 8. Between then and passage 12 at 840 days, the cells underwent spontaneous immortalization; when cultured in DMEM/F-12 with normal calcium levels, they no longer senesced. The cultures of this immortalized cell line (designated MCF10F) continued to produce floating cells.

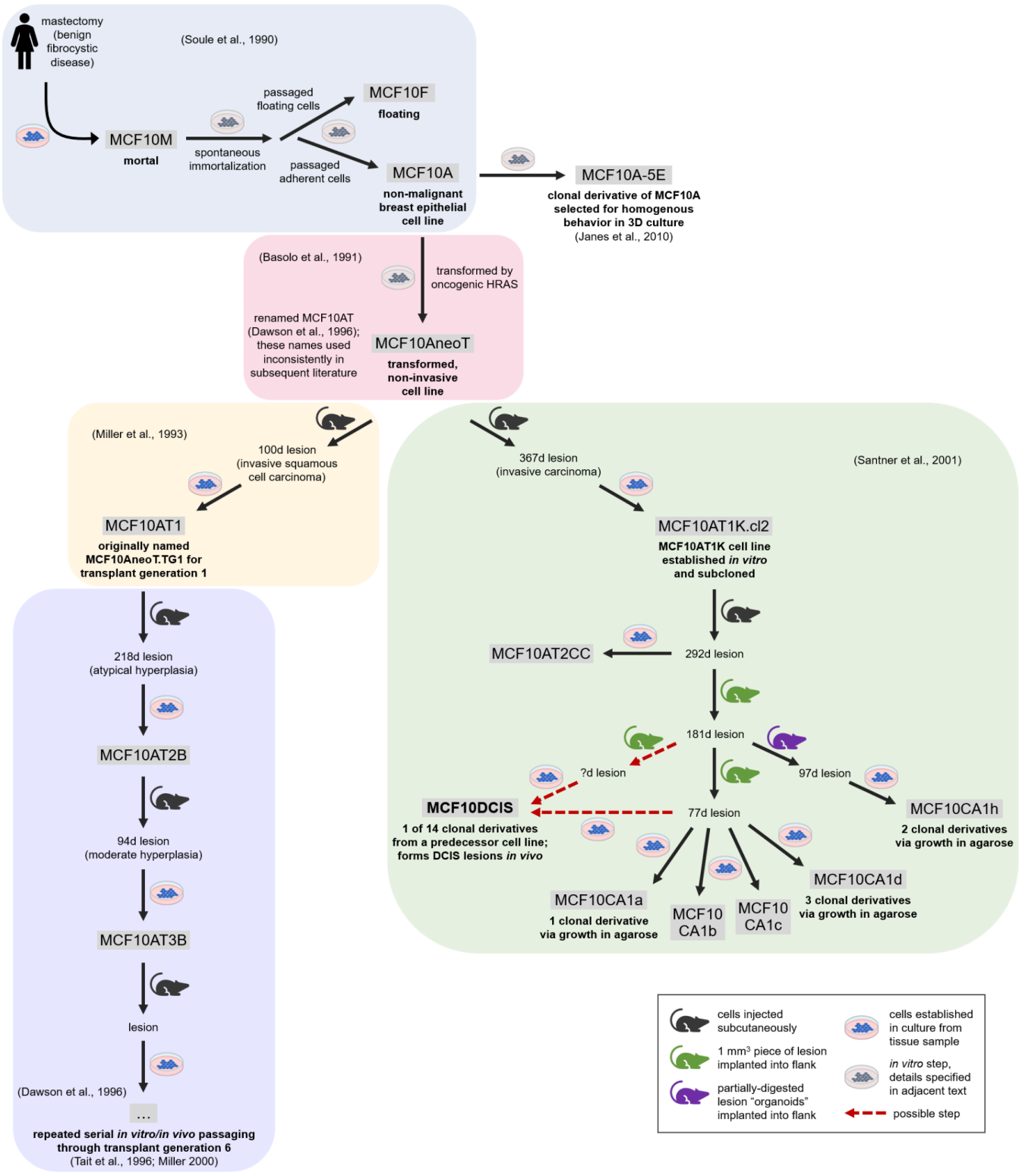

Figure 1.02. Derivation of MCF10 cell lines.

Blue box, Initial establishment of MCF10M from mastectomy sample and subsequent derivation of MCF10F and MCF10A (Soule et al., 1990). **Red box**, Transformation of MCF10A by oncogenic HRAS to produce MCF10AneoT/MCF10AT (Basolo et al., 1991). **Yellow box**, Xenograft of MCF10AneoT *in vivo* and establishment of MCF10AT1 from a resulting lesion (Miller et al., 1993). **Purple box**, Cyclical xenograft and establishment of cell lines *in vitro* from resulting lesions (Dawson et al., 1996; Miller, 2000; L. Tait et al.,

1996). **Green box**, Serial passage of MCF10AneoT-derivative lesions *in vivo* to derive MCF10DCIS and MCF10CA cell lines (Miller, 2000; Miller et al., 2000; Santner et al., 2001). Red dashed arrows indicate possible routes by which MCF10DCIS was derived. *Produced in part using Biorender.*

At day 849 of culture, a subline was established by transferring free-floating cells into DMEM/F-12 medium (**Figure 1.02, blue box**). This subline was subsequently passaged via collection of adhered cells using trypsin and EDTA, and was adherent (designated MCF10A) (Soule et al., 1990). Confluent regions of MCF10A grow as domes and floating cells represent less than 5% of the total population. MCF10A cells at and above passage 50 (after 3+ years of *in vitro* culture) failed to grow at an appreciable rate unless growth factors and hormones (cortisol, EGF, insulin, cholera toxin) were included in the medium along with horse serum. Both MCF10A and MCF10F exhibit characteristics of breast epithelial cells, specifically luminal ductal cells, and not of myoepithelial cells (L. Tait et al., 1990).

With the goal of developing a model of proliferative human breast disease, MCF10A cells at passage 98 were transformed *in vitro* with human $HRAS^{G12V}$ (T24-mutated c-Ha-*ras* oncogene) (**Figure 1.02, red box**) (Basolo et al., 1991). The transfected cells formed approximately 30 colonies, which were pooled to yield the MCF10AneoT (also called MCF10AT) cell line. Compared to MCF10A, MCF10AneoT cells were more cuboidal in shape, larger, and generally less uniform in their nuclear and cytoplasmic appearance (Russo et al., 1991). The MCF10AneoT cells lost their requirement for hormones and EGF in culture media; exhibited loss of contact-inhibition, anchorage-independent growth, increased motility, and invasion through matrigel; and were tumorigenic when injected in to the mouse mammary fat pad (Basolo et al., 1991). MCF10AneoT cells thus represent an *in vitro*-derived derivative of MCF10A that underwent transformation by transfection of mutant HRAS.

To establish an animal model, MCF10A or MCF10AneoT cells were xenografted by subcutaneous injection into the dorsal flank of male nude/beige mice (**Figure 1.02, yellow box**) (Miller et al., 1993). MCF10A cells formed small palpable nodules *in vivo* that regressed and disappeared after 3-4 weeks. While nodules arising from MCF10A were transient, nodules that arose from xenograft of MCF10AneoT cells persisted for at least one year, with many representing benign ductal aggregates or atypical hyperplastic lesions and a few progressing to carcinomas. A tumor that arose in an MCF10AneoT xenograft and was harvested at 100 days was an invasive squamous cell carcinoma; cells from this tumor were established in tissue culture to form the cell line MCF10AneoT.TG1 (transplant generation 1; this cell line was later designated MCF10AT1 (Dawson et al., 1996)), which itself was xenografted into another round of mice (Miller et al., 1993). MCF10AneoT.TG1 xenografts formed lesions that resembled histologic features of human breast atypical hyperplasia after 23 weeks, and lesions resembling carcinoma in situ after 31 and 39 weeks; ducts surrounded by epithelial

proliferation as well as cribriform and papillary growth patterns were prominent (**Figure 1.02, purple box**).

The cycle of (1) xenograft a cell line in mice, (2) harvest a lesion and subject it to enzymatic dissociation, (3) establish cells from the lesion in culture, was repeated numerous times starting from MCF10AT1 (MCF10AneoT.TG1) cells to produce at least 6 transplant generations of lesions and cell lines, which were denoted MCF10AT2, MCF10AT3, etc. (**Figure 1.02, purple box**) (Dawson et al., 1996; Miller, 2000; L. Tait et al., 1996). The mice used for these xenograft experiments were from several cohorts: male nude/beige, male nude, female nude/beige, and female nude; the authors reported that results were similar across mouse sex and strains (Dawson et al., 1996). Inocula consistently began by forming simple ducts, some of which remained as simple ducts for two years, while others progressed asynchronously over time through stages of breast proliferative disease (Iravani et al., 1998; Miller, 2000; L. Tait et al., 1996). Resulting lesions represented a wide range of morphologies, including mild hyperplasia with only one or two layers of epithelial cells lining a small duct, ducts containing cystic spaces surrounded by several layers of epithelial cells, cribriform spaces surrounded by monotonic cells, ducts near-completely filled with enlarged but uniform cells, carcinoma filling large ductal spaces or infiltrating among smaller glands, and glands of various sizes filled with mucin-secretion (Dawson et al., 1996). Progression of lesions to moderate or atypical hyperplasia was sporadic but was significantly more common in later transplant generations compared to earlier transplant generations. However, the number of lesions that progressed to invasive carcinoma remained unchanged from MCF10neoT (Dawson et al., 1996; Miller, 2000).

The MCF10AT system is notable in its ability to repeatedly produce simple ducts and premalignant lesions that progress over a range of timescales to hyperplasia, carcinoma *in situ*, and invasive carcinoma. While abundantly useful for the study of premalignancy and progression, this feature made it difficult to establish derivative lines that were promptly and reliably tumorigenic (H Heppner et al., 2000). This was finally achieved by serially passaging pieces of MCF10AT lesions directly into another mouse, skipping the establishment of a cell line *in vitro* (**Figure 1.02, green box**) (H Heppner et al., 2000; Santner et al., 2001; Strickland et al., 2000). Starting with xenografts of MCF10AneoT, a 367-day invasive carcinoma lesion was dissociated and established *in vitro* as MCF10AT1K; this cell line was subsequently subcloned to produce the line MCF10AT1K.cl2, which was xenografted to produce a second transplant generation (Santner et al., 2001). A 292-day lesion was harvested and a small tissue sample was directly passaged into another mouse, from which a 181-day lesion was harvested. This time, two different methods were used to initiate subsequent xenografts: (1) a small tissue sample was directly implanted into another mouse as before, or (2) the tissue was partially digested first by overnight incubation with collagenase, and the resulting “organoids” were implanted into another mouse. A 77-day lesion was harvested from the mouse receiving the small

tissue sample (method 1) and dissociated into small partly-digested tumor pieces, which were established in culture as MCF10CA1a, MCF10CA1b, MCF10CA1c, and MCF10CA1d. Separately, a 97-day lesion was harvested from the mouse receiving the “organoids” (method 2) and dissociated into partly-digested pieces, which was established in culture as MCF10CA1h. The resulting MCF10CA1 lines produce rapidly-growing invasive carcinomas upon injection, some of which are metastatic (Santner et al., 2001; Strickland et al., 2000).

In addition to the MCF10CA lines, MCF10neoT derivatives yielded a clonal cell line called MCF10DCIS.com (hereafter referred to as MCF10DCIS) (**Figure 1.02, green box**) (Miller et al., 2000). While it is unclear exactly where MCF10DCIS falls in the MCF10AT family tree (**Figure 1.02, green box, red dashed arrows**), it seems most likely that belongs to the branch derived from MCF10AT1K.cl2, in which derivatives were passaged *in vivo* without intermediate reestablishment of cell lines *in vitro* (Santner et al., 2001). The publication introducing MCF10DCIS describes it as being “cloned from a cell culture initiated from a xenograft lesion obtained after two successive trocar passages of a lesion formed by premalignant MCF10AT cells” (Miller et al., 2000). A review published the same year describes the tumorigenic MCF10CA1 variants and continues: “One tumorigenic variant produced very heterogeneous tumors including areas of DCIS as well as invasive cancer. One of 14 clones derived from that variant produces comedo DCIS. Unlike the MCF10AT xenografts, this variant, MCF10DCIS.com, has a high proliferative rate and produces large tumors within a few weeks. Early passage cells produce nearly pure comedo DCIS. Invasive cancers develop within the MCF10DCIS.com xenografts but all lesions so far examined retain a DCIS component” (Miller, 2000). Despite a lack of clarity regarding its exact origin, the establishment of the MCF10DCIS model was an important milestone in DCIS research.

Injection of MCF10DCIS into immunocompromised mice leads to consistent formation of lesions resembling comedo DCIS (Miller, 2000; Miller et al., 2000; Puleo & Polyak, 2021). The cells first form a tightly-packed network of ducts, followed by proliferation within those ducts and central necrosis, which is often infiltrated with neutrophils (Miller et al., 2000). The epithelial cells have large nuclei and a foamy cytoplasm, and mitosis is common. The lesions are surrounded by a distinct layer of myoepithelial cells and an intact basement membrane. MCF10DCIS cells also exhibit properties in cell culture that distinguish them from their immortalized but untransformed progenitor, MCF10A. In 2D culture, MCF10A cells grow as clusters, taking on a cobblestone morphology at confluence that is characteristic of epithelial cells grown on plastic (Debnath et al., 2003), while MCF10DCIS cells do not exhibit an epithelial organization, instead displaying a spindle-shaped morphology characteristic of fibroblasts and mesenchymal-like cells (Q. Li & Mattingly, 2008). MCF10A cells are incapable of anchorage-independent growth, while MCF10DCIS is capable (Samson et al., 2021; Soule et al., 1990). When cultured in the presence of reconstituted basement membrane, MCF10 series cells form

into three-dimensional growth-arrested spheroid structures reminiscent of breast acini (Debnath et al., 2003). MCF10A cells grown in 3D (**Figure 1.03, top**) divide and self-organize into a spherical layer of polarized, growth-arrested epithelial cells that surround a hollow lumen, where the basal surface contacts the surrounding extracellular matrix (ECM) and the luminal surface faces the lumen (Debnath et al., 2003; McKeen Polizzotti et al., 2012). When visualized by immunofluorescence, integrin-α6 clearly outlines the basal surface and integrin-α3 is localized along the lateral cell membranes. By contrast, MCF10DCIS cells (**Figure 1.03, bottom**) form structures that lack the regular organization that characterizes MCF10A spheroids. Integrin-α6 and -α3 are localized much more sporadically around the spheroid and tend to colocalize in dense accumulations. Thus, at multiple levels of complexity, MCF10DCIS cells exhibit DCIS-like behavior.

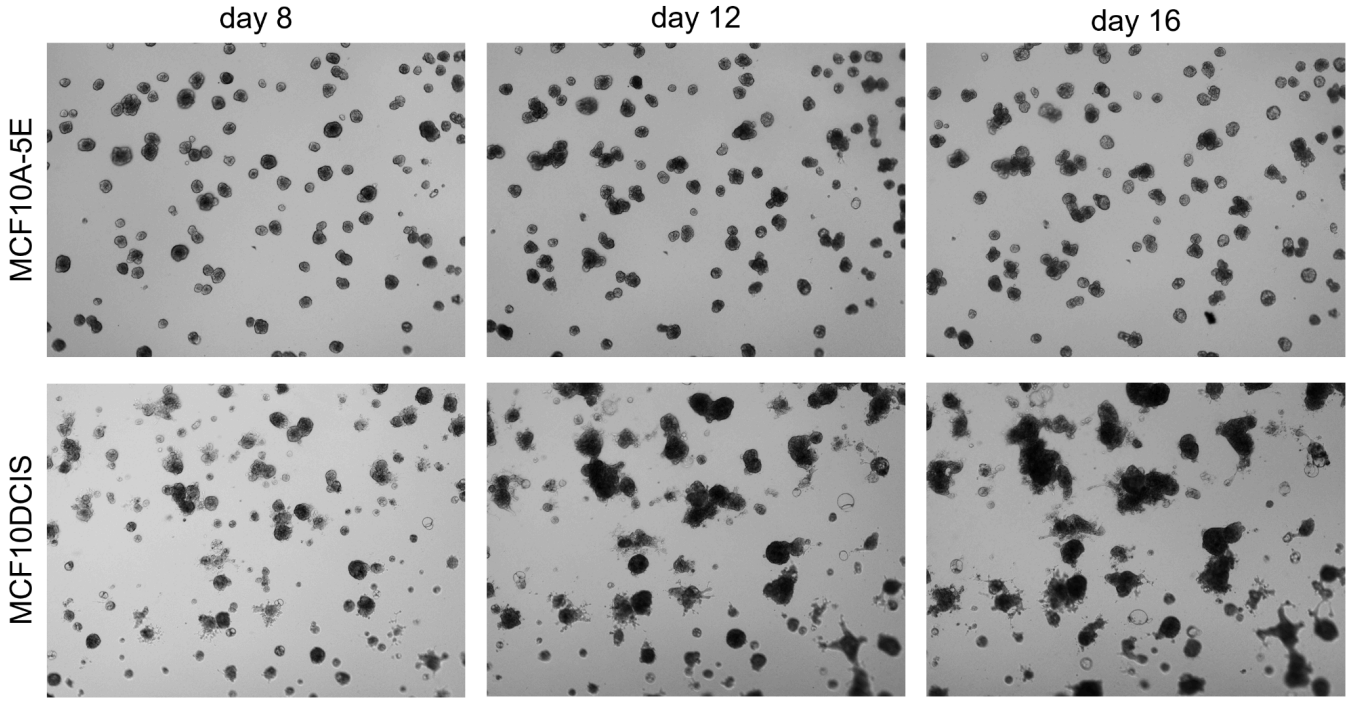

Figure 1.03. MCF10A-5E and MCF10DCIS spheroids.

MCF10A-5E (**top**) and MCF10DCIS (**bottom**) cells grown in 3D culture in the presence of Matrigel, imaged at days 8, 12, and 16 after seeding.

Nine years after the initial publication of the MCF10DCIS line, a new method for xenograft was put forward. Instead of injecting cells subcutaneously into the flanks or in the mammary fat pad of immunodeficient mice, human breast cancer cell lines were injected intraductally through the nipple (Behbod et al., 2009). Suspensions of MCF10DCIS and SUM225, a HER2-overexpressing DCIS cell line, were the first to be tested, and they established DCIS-like lesions inside the mouse ducts. The preexisting ductal system of the mouse confines the injected cells to an environment that is more relevant than the flank or fat pad and thus provides an excellent system for studying DCIS from its early

establishment in the duct to its eventual invasion into the periductal basement membrane (Behbod et al., 2009, 2018; Hong et al., 2022; Hutten & Jonkers, 2023; Kittrell et al., 2016; Russell et al., 2015).

MCF10DCIS.com cells underlay impactful studies of malignancy (Hu et al., 2008; Russell et al., 2015), metastasis (W. Zhou et al., 2014), metabolism (Kalaany & Sabatini, 2009; Possemato et al., 2011), and mechanotransduction (Wei et al., 2015). For example, in the early 2000s it was suspected that myoepithelial cells played an important role in breast tumor progression, but the prior lack of experimental models of DCIS had precluded direct evaluation of this hypothesis (Polyak & Hu, 2005). Once MCF10DCIS became an established model, it was found that subcutaneously-inoculated xenografts contained both epithelial (cytokeratin-positive) and myoepithelial (SMA-positive) cells of human origin, while myofibroblast (SMA-positive) cells in the surrounding stroma were of mouse origin; the normal human myoepithelial cells gradually decreased in abundance over time, coinciding with the progression of DCIS lesions to invasive tumors (Hu et al., 2008). A later study using the intraductal MCF10DCIS model supported these results, finding that intraductally-established DCIS lesions use the endogenous mouse myoepithelial layer rather than generating their own of human origin, and that the mouse myoepithelial cells progressively lose their myoepithelial differentiation markers (α-SMA, calponin, p63) leading up to invasion of the DCIS (Russell et al., 2015). Both of these studies provided important *in vivo* results that support the notion that disruptions to the ductal myoepithelium may contribute to the transition from *in situ* to invasive disease (Hu et al., 2008; Russell et al., 2015).

The MCF10 series has been categorized most closely with the “basal-like” subgroup of human breast cancers, based on the MCF10A parental line clustering most closely with the “basal B” subtype by expression profiling and its lack of functional estrogen or progesterone receptors, as well as the lack of HER2 locus amplification in MCF10A or its derivatives (Kadota et al., 2010; Kao et al., 2009; Neve et al., 2006; Shekhar et al., 1998; Sorlie et al., 2001). MCF10DCIS was independently identified as basal subtype by flow cytometry, which found the cell line to have high expression of the basal markers CD44 and CD49f and low expression of the luminal markers CD24 and MUC-1 (Behbod et al., 2009). Further, immunofluorescence of intraductal xenografts found MCF10DCIS lesions to be positive for cytokeratins 5 and 8 and negative for cytokeratin 19 and estrogen receptor. Therefore, MCF10DCIS is used as one of the few cell culture and xenograft models of basal-like or hormone receptor-negative DCIS.

As the field continues to employ the MCF10DCIS cell line and xenograft model to inform our understanding of DCIS, it remains important to reassess the relevance of the model itself. The improvement of sequencing technologies, for example, has led to better characterization of the genetic and transcriptional landscapes of the MCF10 series as well as clinical specimens. A 2016 study completed whole genome, exome, and RNA sequencing of MCF10-series cell lines with the goal of identifying potential driver genetic alterations of breast cancer progression (Maguire et al., 2016). Their analysis revealed four predicted driver mutations that arose during model series generation between

MCF10A cells and MCF10DCIS cells: $HRAS^{G12V}$ (engineered), $EPHA7^{A713S}$, $MAP3K12^{A662D}$, and $PCSK5^{M452I}$. The PCSK5 mutation is present at variant allele frequency (VAF) below 50% in all derivative lines except for MCF10DCIS, in which the VAF is 50%. The increased VAF of $PCSK5^{M452I}$ specifically in MCF10DCIS cells could indicate that it confers some advantage in the DCIS-like state, which is a delicate balance between mesenchymal- and epithelial-promoting forces. Indeed, the selective pressures at play in the MCF10 series are multifaceted; the cells underwent transduction with mutant HRAS and numerous alternating rounds of establishment as *in vitro* cell lines and *in vivo* xenograft, some of which involved outgrowth from a single clone (Basolo et al., 1991; Dawson et al., 1996; Miller et al., 1993, 2000; Soule et al., 1990). Finally, MCF10DCIS cells underwent selection by the researchers for their formation of DCIS-like lesions *in vivo*. All of these environments select for different cellular adaptation mechanisms. In later sections of this dissertation, I will discuss PCSK5 in detail; its known functions suggest that it could be highly relevant to the biology of DCIS, and so an unusual mutation in a DCIS cell line warrants investigation.

1.1.2.2. Modern alternatives to MCF10DCIS.COM

In 2009, Behbod, *et al.* published the first report of the intraductal injection of human breast cancer cells in immunodeficient mice (Behbod et al., 2009). They implanted suspensions of MCF10DCIS or SUM225 (ER-, PR-, HER2-overexpressing DCIS) cell lines via the nipple and saw DCIS-like lesions weeks later inside the mouse ducts. Importantly, they also injected primary human DCIS cells from a lesion that was finely chopped with a razor blade and enzymatically digested overnight, resulting in HER2-overexpressing DCIS growth (Behbod et al., 2009; Kittrell et al., 2016). They went on to establish DCIS xenografts from eight patient biopsy samples and found that at least some recapitulated the ER and HER2 staining positivity seen in the patient biopsy (Valdez et al., 2011).

In 2016, an international consortium of researchers reported on the collective development of 537 breast cancer patient-derived xenograft (PDX) lines, 56% of which were from patients with triple-negative breast cancer, 35% from patients with ER+ breast cancer, and 8% from HER2+ breast cancer (Dobrolecki et al., 2016). These stably transplantable xenografts, generally defined as PDXs that can undergo at least 3 serial passages in mice, were a great improvement over xenografts of established breast cancer cell lines because only a small subset of cell lines grow as xenografts and an even smaller subset form metastases, which is essential for many breast cancer-focused studies. However, the take rates for breast cancer PDXs were much higher than for lower grade tumors, DCIS, and normal breast epithelium, so the explosion of PDX use for breast cancer was not yet attainable for DCIS; this emphasized the importance of the MCF10DCIS and SUM225 models (Behbod et al., 2018; Dobrolecki et al., 2016).

In 2023, the Jonkers group published a landmark study of 130 patient-derived DCIS samples that were xenografted by intraductal injection and grown in immunodeficient *NOD-scid;Il2rg^{null}* (NSG)

mice for one year before excision and analysis by whole-mount 3D imaging, immunohistochemistry, genomics, and transcriptomics for comparison with each primary lesion (Hutten et al., 2023). Surgically-removed patient DCIS tissue was enzymatically digested overnight before intraductal injection and mice were supplemented with with estradiol (E2) for an overall take rate of 88% (Hutten et al., 2023). The PDX lesions had high concordance with the original patient samples in terms of histological expression (ER, PR, HER2, and Ki67), genomics, copy number alteration, and transcriptomic-based hallmark gene set signatures and PAM50 gene expression. Just over one-third of samples were successfully re-transplanted to a second-generation PDX and a small number of those were also successfully re-transplanted again; growth patterns, molecular subtype, and invasive potential were consistent across transplantations. The group established a collection of 19 models, including 2 luminal A, 4 luminal B, 2 ER+/HER2+, and 11 ER-/HER2+ models, that are banked and able to be shared for future research.

The advantages of PDX models are numerous. They allow expansive profiling opportunities over short- and long-term studies and are highly conducive to pre-clinical treatment evaluation (Dobrolecki et al., 2016; Hutten et al., 2023; Hutten & Jonkers, 2023). Compared to cell lines that have been passaged in labs for decades and exposed to clonal selection and loss of heterogeneity, PDXs are much more closely related to their source tumors and have shown to be highly faithful to the molecular and phenotypic characteristics of the original sample. However, for basal-like DCIS in particular, PDX models have thus far fallen short. Of the nine patient DCIS samples from which cells were xenografted in the original intraductal injection studies, none were triple-negative (Behbod et al., 2009; Valdez et al., 2011), and although the Jonkins effort included 8 basal-like patient samples, none of these PDX models were able to be re-transplanted and so they are not distributable for further study (Hutten et al., 2023). From my own lab's experience collecting patient samples from our surgical oncology collaborators, we know that the University of Virginia Comprehensive Cancer Center operates on fewer than four patients per year who have ER-negative DCIS. The rarity with which hormone-negative DCIS presents in the clinic plainly illustrates the unsustainability of a PDX-centric approach to studying basal-like DCIS and underscores the importance of the MCF10DCIS cell line model.

1.2 GDF11 Signaling in Development and Disease

The transforming growth factor-beta (TGFβ) family is well-known for its myriad involvement in development, normal physiological function, and disease. Growth differentiation factor 11 (GDF11; also known as bone morphogenic protein 11, BMP11) is a secreted TGFβ-family ligand that binds a variety of TGFβ receptors to stimulate SMAD transcription factor activity. GDF11 was discovered because of its high homology with GDF8/myostatin, which is a regulator of skeletal muscle growth during development

(McPherron et al., 1997). Indeed, GDF11 also plays an important role in skeletal development (Gamer et al., 1999; McPherron et al., 1999; Nakashima et al., 1999). GDF11 is also implicated in disease, including multiple types of cancer (Simoni-Nieves et al., 2019).

1.2.1 GDF11 is Essential for Development

The earliest studies of GDF11 established its importance in skeletal development (Gamer et al., 1999; McPherron et al., 1999; Nakashima et al., 1999). During mouse embryogenesis, Gdf11 expression appears around days 8-9 post-coitus first in the primitive streak and then in the embryonic tail bud, both of which serve as early sources of mesodermal cells. Over the next few days of embryogenesis, Gdf11 expression extends to the limb bud and the developing nervous system and spinal cord (Gamer et al., 1999; Nakashima et al., 1999). $Gdf11^{-/-}$ mice exhibit shortened or absent tails and die within 24 hours after birth (McPherron et al., 1999). The mutant animals have skeletal abnormalities indicating that the typical posterior skeletal patterning was replaced with anterior-like patterning; this occurred in both the thoracic and cervical vertebral regions. Almost all $Gdf11^{-/-}$ mice also have kidney defects, which begin to appear around day 11 when the ureteric bud fails to form; by day 12, the normal kidney precursor tissues have failed to develop (Esquela & Lee, 2003). Heterozygous $Gdf11^{+/-}$ mice exhibit similar abnormalities as those seen in $Gdf11^{-/-}$ mice, but to a less severe degree, suggesting a dose-dependent effect of Gdf11 action during development (McPherron et al., 1999).

Complex regulation of developmental processes is achieved by GDF11 signaling with an ensemble of binding partners and effectors. GDF11 binds directly to activin type II receptors (Acvr2 or Acvr2b) before it is able to bind type I receptors (Andersson et al., 2006; Oh et al., 2002). The GDF11-Acvr2b complex is able to interact with type I receptors ALK4, ALK5, and ALK7, but the strongest signal is achieved upon binding to ALK4 or ALK5. During mouse development, GDF11 signals through Acvr2b, or to a lesser degree Acvr2, and ALK5 to promote Smad2- and Smad3-mediated transcription of Hox genes. Hox gene expression along the anterior-posterior axis of the embryo is determined by the combination of opposing gradients of retinoic acid, highest at the anterior end, and GDF11 and fibroblast growth factor (FGF), highest at the posterior end (Andersson et al., 2006; Deschamps & van Nes, 2005; Dubrulle & Pourquié, 2004). In particular, GDF11-Acvr2b-ALK5 signaling is required for Hoxc10 expression in mouse embryos at day 9, governing the anterior-posterior patterning associated with GDF11 function during embryogenesis (Andersson et al., 2006; Oh et al., 2002). The kidney development effects of GDF11 are carried out by Gdf11 signaling upstream of glial cell line-derived neurotrophic factor (Gdnf), which signals through c-Ret and Gfrα1 to direct the outgrowth of the ureteric bud in the first stage of kidney development (Esquela & Lee, 2003). GDF11 has also been shown to signal non-canonically through MAPK to activate p38, AKT, and JNK

(Z. Wang et al., 2018). Thus, GDF11 interacts with numerous other proteins to exact precise control over important developmental processes.

GDF11, like other TGFβ-family members, is synthesized as a proprotein and requires cleavage of its pro-domain to become active. Many secreted proproteins that require pro-domain cleavage at basic sites are substrates of a protease family called the proprotein convertases (PCs) (Cui et al., 2001). GDF11 is activated near-exclusively by the PC family member PCSK5; PACE4 can process proGDF11 *in vitro* but much less efficiently than PCSK5, and furin and PC7 do not process proGDF11 at all (Essalmani et al., 2008). The specificity for proGDF11 cleavage by PCSK5 is due to an Asn at the first residue after the cleavage site, as substitution of this amino acid for Asp permitted cleavage by PCSK5, PACE4, furin, and PC7, with PCSK5 remaining the most efficient. In the mouse embryo at days 9-10, Pcsk5 and Gdf11 mRNA expression overlaps in the tail bud and the developing nervous system and brain, although Pcsk5 expression is also detected elsewhere in the embryo. Conditional KO of Pcsk5 in the mouse epiblast results in phenotypes that closely resemble $Gdf11^{-/-}$ developmental defects, including lack of tail, altered anteroposterior patterning, and kidney agenesis. Pcsk5 conditional KO mice have some additional abnormalities as well, consistent with the broader expression of Pcsk5 than Gdf11 in the embryo, suggesting the importance of PCSK5 in development is not exclusively enacted via GDF11.

1.2.2 The Complex Role of GDF11 in Cancer

GDF11 is widely expressed in normal tissues and its expression remains widespread in cancer (Hoadley et al., 2018; Lonsdale et al., 2013). In some settings, GDF11 has been shown to play a tumor suppressor-like role (Bajikar et al., 2017; Gerardo-Ramírez et al., 2019), while in others it is associated with metastasis and poorer outcomes (Qin et al., 2017; Yokoe et al., 2007). This contradiction may be due in part to the role of TGFBR3, a co-receptor that mediates GDF11 binding to its type II and type I receptors; my colleague and friend Wisam Fares is extending a model of GDF11 receptor binding to include the co-receptor, which may aid in our understanding of the complex effects of GDF11 in cancer (personal communication; manuscript in preparation).

1.3 Proprotein Convertase PCSK5

1.3.1 The Proprotein Convertase (PC) Family

Since the early 1900s, there had been hypotheses that hormones might be stored in a “prohormone” state, analogous to zymogen enzymes, but it wasn’t until 1967 that the first prohormone was actually discovered: proinsulin (Chrétien & Li, 1967; Seidah & Chrétien, 1992; Steiner, 2011; Steiner et al., 1967). Proinsulin inspired a body of work focused on the processing of precursor proteins in the secretory pathway (Lazure et al., 1983; Steiner, 2011). In particular, identification of the yeast

enzyme Kex2 as a calcium-dependent serine protease opened the doors for the discovery of the human proprotein convertase family (Fuller et al., 1989b; Seidah & Chrétien, 1992). It had been shown that Kex2 could cleave mammalian precursor proteins and so the amino acid sequence of the Kex2 active site was subjected to computer alignment with a database of mammalian protein sequences (Fuller et al., 1989a; Seidah & Chrétien, 1992). This led to the identification of the human gene Furin, the first member of the human proprotein convertase family. Two additional members, PC1 and PC2, were identified shortly thereafter (Seidah et al., 1990, 1991; Smeekens & Steiner, 1990). In all, nine proprotein convertase family members were identified (Seidah, 2011; Seidah et al., 2008, 2013; Seidah & Chrétien, 1999; Seidah & Prat, 2012).

The proprotein convertase (PC) genes were eventually renamed with the PCSK nomenclature, standing for proprotein convertase subtilisin/kexin. Herein I refer to the proprotein convertases collectively as PCs and individually by their PCSK or traditional nomenclature (**Table 1.02**). The PCs have been reviewed extensively and their properties are summarized in **Table 1.02** (Seidah, 2011; Seidah et al., 2008, 2013; Seidah & Chrétien, 1999; Seidah & Prat, 2012). The PCs are calcium-dependent serine proteases; they belong, along with yeast kexin, to the eukaryotic branch of the subtilase family (Seidah & Prat, 2012). The subtilases are serine proteases that are more closely related to bacterial subtilisin, whereas the alternative serine protease family is related to (chymo)trypsin (Siezen & Leunissen, 1997). PCs themselves are produced as precursors and undergo autocatalytic cleavage to their mature forms. PC cleavage regulates the activity of important substrates including hormones, growth factors, receptors, adhesion molecules, and proteins belonging to viruses and bacteria. Due to high homology (50-75%) within their catalytic domains, the PCs have quite a bit of overlap in the substrates they are able to cleave. It has been common to evaluate substrate cleavage in test tube assays with recombinant PCs and candidate substrates. However, while test tube cleavage assays are useful for testing whether a specific PC is capable of processing a specific substrate, the biological relevance of the results is difficult to ascertain. Substrate redundancy can be an evolutionary advantage in terms of back-ups for important processes, but in many cases the PC-substrate specificity is determined by tissue and cell-type expression patterns, subcellular localization, and other factors such as interacting proteins or the microenvironment (J. W. M. Creemers & Khatib, 2008).

Table 1.02. Summary of proprotein convertase family member properties. (Seidah et al., 2013; Seidah & Prat, 2012)

PCSK Nomenclature	Traditional and (Archival) Nomenclature	Tissue Expression	Subcellular Localization	Cleavage Sites	Major Substrates
PCSK1	PC1 (PC1/3, PC3)	endocrine cells, neuronal cells	regulated secretory pathway granules	single or paired basic residues	hormones, neuropeptides
PCSK2	PC2	endocrine cells, neuronal cells	regulated secretory pathway granules	single or paired basic residues	hormones, neuropeptides
PCSK3	Furin, PACE (PC1)	ubiquitous	constitutive secretory pathway	single or paired basic residues	growth factors, receptors, adhesion molecules, metalloproteinases, viral glycoproteins
PCSK4	PC4	testicular germ cells; placenta, ovary	unknown	single or paired basic residues	IGF2, PACAP
PCSK5	PC5/6 (PC5, PC6)	widespread	constitutive secretory pathway	single or paired basic residues	growth factors, receptors, adhesion molecules
PCSK6	PACE4	widespread	constitutive secretory pathway	single or paired basic residues	growth factors, metalloproteinases, viral glycoproteins
PCSK7	PC7 (PC8)	ubiquitous	constitutive secretory pathway	single or paired basic residues	receptors
PCSK8	SKI-1, S1P	ubiquitous	Golgi	non-basic residues	transcription factors, viral glycoproteins
PCSK9	NARC-1	liver, intestine, kidney	secreted; trafficking to lysosomes	only autocatalytic	autocatalytic; acts as binding protein to LDL receptors

1.3.2 PCSK5 Gene and Expression

The proprotein convertase PCSK5 was first identified in 1993 in mouse and rat (Lusson et al., 1993; Nakagawa, Murakami, et al., 1993) and the human gene was mapped to chromosome 9q21 in 1996 (van de Loo et al., 1996). The PCSK5 gene codes for two isoforms produced by alternative splicing: a shorter, soluble PCSK5a form and a longer, membrane-bound PCSK5b form (De Bie et al., 1996; Nakagawa, Murakami, et al., 1993). The majority of this thesis is focused on PCSK5a, referred to simply as PCSK5. When the long form is discussed, it is specified as PCSK5b.

PCSK5 is widely expressed, with PCSK5b being the predominant form in the kidney and digestive tract and PCSK5a predominating in all other tissues (Essalmani et al., 2006). PCSK5

expression is especially high in the adrenal glands. It is expressed in the ovaries and uterus, particularly during embryonic implantation into the uterine epithelium, as well as in the embryo during embryonic development (Essalmani et al., 2006; Heng, Hannan, et al., 2011; Nie et al., 2003, 2005; Rancourt & Rancourt, 1997; Wong et al., 2002).

Several stimuli have been shown to promote PCSK5 expression, including adrenocorticotropic hormone (ACTH) or cAMP in the adrenocortical cell line Y1 (Lusson et al., 1993; Mayer et al., 2008); progesterone and cAMP in human endometrial stromal cells (Heng et al., 2010; Okada et al., 2005); pregnant mare serum gonadotropin along with chorionic gonadotropin in rat ovaries, and pregnant mare serum gonadotropin along with luteinizing hormone or forskolin in rat preovulatory follicles (Bae et al., 2008); activin A in mouse ovarian secondary follicles (Antenos et al., 2011); and platelet-derived growth factor (PDGF)-B or 10% fetal calf serum in rat vascular smooth muscle cells (Stawowy et al., 2002). Nevertheless, a mechanistic understanding of PCSK5 regulation is elusive. One challenge in studying PCSK5 regulation is that in numerous cell lines and tissues, PCSK5 expression is easily detected at the mRNA level but is too low at the protein level to reliably detect with available antibodies (De Bie et al., 1996; Mayer et al., 2008; Szumska et al., 2008). As a result, many studies of PCSK5 use overexpression constructs, negating the potential for conclusions related to regulation of gene expression.

1.3.3 PCSK5 Protein: Post-Translational Regulation, Trafficking, and Function

There are several distinct domains within the PCSK5 protein (**Figure 1.04**): the pre-domain or signal peptide; pro-domain or propeptide, catalytic or peptidase domain, P or Homo B domain, RGD or cell-binding domain, and C-terminal Cys-rich domain (CRD) (Nakagawa, Hosaka, et al., 1993). Each domain contributes to the production, secretion, and/or function of PCSK5.

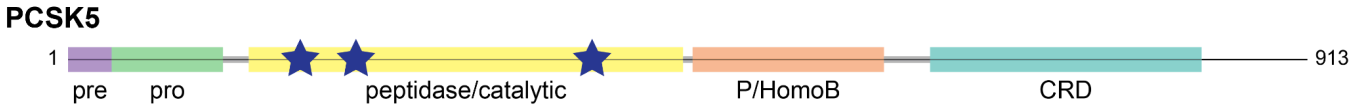

Figure 1.04. PCSK5a protein domains.
Protein domains of PCSK5a, which is 913 amino acids in length, including the pre-domain, pro-domain, peptidase domain containing three sites of the catalytic triad (blue stars), P domain, and Cys-rich domain (CRD). *Uniprot*.

The C-terminus differentiates PCSK5 from the PCSK5b isoform and governs intracellular sorting; the shorter PCSK5a is sorted to dense core granules for secretion via the regulated pathway, while the extended C-terminus of PCSK5b renders it membrane-bound and sorted to the constitutive pathway (De Bie et al., 1996; Nakagawa, Murakami, et al., 1993). Both the constitutive and regulated secretory pathways begin with protein synthesis in the rough ER and transfer to the Golgi apparatus for

processing and packaging into secretory vesicles (Kelly, 1985; Palade, 1975). In the constitutive pathway, vesicles leaving the Golgi reach the cell surface within minutes and immediately fuse with the plasma membrane to release their protein contents without the requirement of any external stimulus (Kelly, 1985). Alteration of protein secretion is achieved by changing the rate of protein synthesis. Conversely, proteins secreted via the regulated pathway are condensed into secretory vesicles that have a half-life of days and therefore accumulate in the cytoplasm. Vesicles fuse to the membrane for exocytosis only upon the signal of calcium or another cytoplasmic secondary messenger, releasing large amounts of protein at once. By immunofluorescence (**Figure 1.05**), PCSK5 is localized weakly to the perinuclear ER and strongly to the perinuclear Golgi, the cytoplasm, and the tips of cellular projections (De Bie et al., 1996). The staining in the cytoplasm and cell periphery is punctate, representing secretory granules (De Bie et al., 1996; Matsuuchi et al., 1988). PCSK5a is distinct from PCSK5b in its path down the secretory pathway and thus its subcellular localization.

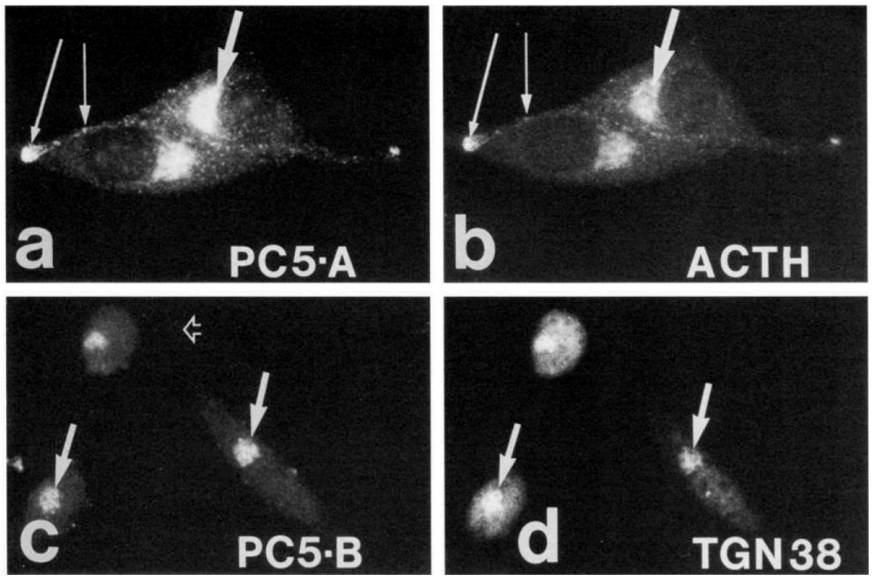

Figure 1.05. PCSK5 intracellular localization by immunofluorescence. [Figure 10 from (De Bie et al., 1996)]

A-B, PCSK5a colocalization with ACTH, a marker of secretory granules and the Golgi. **C-D**, PCSK5b colocalization with TGN38, a marker of the trans-Golgi network. *Used with permission from Rockefeller University Press (license ID 1601667-1, April 21, 2025).*

There are a number of processing and regulatory steps that occur along the secretory pathway. Many proteases are synthesized as pre-pro-proteins that require multiple cleavage steps and environmental changes to become active (Anderson et al., 2002; Baker et al., 1993). First, the signal peptide or “pre-domain” targets the nascent protein to the ER and is removed shortly after translation begins (Baker et al., 1993; Lazure et al., 1983; Steiner et al., 1980). Next, the pro-domain acts as an intramolecular chaperone to mediate folding of the protease domain and is cleaved autocatalytically in the ER (Anderson et al., 1997, 2002; Baker et al., 1993; J. W. M. Creemers et al., 1995; De Bie et al.,

1996; Nour et al., 2003). The autocatalytic cleavage of furin is *intra*molecular, meaning pro-furin catalyzes the removal of its own pro-domain, rather than *inter*molecular, which would require a mature furin to remove the pro-domain of a pro-furin (Leduc et al., 1992). This was demonstrated by expressing human furin with a mutation of the active site aspartate, which yielded only pro-furin; further, simultaneous expression of active furin could not mature the mutant pro-furin. Without studies testing the same question in PCSK5, we presume that it is the same as furin in this regard. The pro-domain is cleaved when the full protein is only partially folded and binds non-covalently but strongly to the protease active site, serving as a steric inhibitor while also mediating conformational changes necessary to achieve the proper folding (Anderson et al., 1999, 2002; Eder et al., 1993a, 1993b; Nour et al., 2003; Shinde et al., 1999). If the pro-domain is missing, the protease folds into a kinetically stable but inactive “molten globule”-like intermediate and remains in the ER; proper folding and trafficking can be achieved by addition of the propeptide in *trans* (Anderson et al., 2002; Baker et al., 1992; J. W. M. Creemers et al., 1995; De Bie et al., 1996; Eder et al., 1993b; Strausberg et al., 1993). The protease and its cleaved but still-bound pro-domain traffic to the early- and mid-Golgi; in some cases, this can occur even if the cleavage step did not happen (e.g. due to mutated active site), as long as the pro-domain is present (Anderson et al., 2002; Nour et al., 2003). Further transport to the TGN, however, only occurs if the initial cleavage took place and the pro-domain remains associated with the protease. A secondary autocatalytic cleavage step at a second pro-domain cleavage site, referred to as “internal” in contrast to the primary cleavage site at the C-terminal end of the pro-domain, is required for dissociation of the propeptide and disinhibition of the protease (Anderson et al., 1997, 2002; Nour et al., 2003). For furin, the acidic environment of the TGN permits this secondary cleavage (Anderson et al., 1997, 2002; Nour et al., 2003); however, some, if not all, of the secondary cleavage, and thus activation, of PCSK5 occurs on the cell surface, as PCSK5 and its pro-domain are both detected in this location (Mayer et al., 2008).

The C-terminal CRD is essential for cell surface localization of PCSK5 (Nour et al., 2005). The PCSK5 CRD binds to the C-terminal domain of tissue inhibitor of metalloproteinases (TIMP)-2 and the complex is bound to the cell surface by heparan sulfate proteoglycans (HSPGs); accordingly, cell-surface tethering of the PCSK5-TIMP-2 complex is displaced upon culture with exogenous heparin which competes for the HSPG binding site. HSPGs involved with anchoring PCSK5 to the cell surface include CD44, syndecan-2, and syndecan-4 (Mayer et al., 2008) and, in addition to TIMP-2, PCSK5 binds TIMPs-1, -3, and -4 (Nour et al., 2005). PCSK5 activation is then stimulated by incubation with adrenocorticotropic hormone (ACTH) or cAMP, either of which reduce PCSK5 pro-domain cell surface localization by more than 60% and increase the activity of PCSK5 released into the media (Mayer et al., 2008). The cell-surface anchoring may serve numerous purposes, including adding a degree of specificity to PCSK5 activity by restricting the spatial distribution in which it is active and acts upon

substrates (Seidah et al., 2008; Turnbull et al., 2001). Given the role of HSPGs in facilitating molecular interactions at the plasma membrane, it is possible that HSPG binding causes a conformational change in PCSK5 that favors the secondary cleavage (Hayashida et al., 2022; Mayer et al., 2008). HSPG binding also sequesters protein ligands at the cell surface and in the ECM, many of which may be PCSK5 substrates, thus facilitating more efficient PCSK5 activity (Hayashida et al., 2022; Mayer et al., 2008; Seidah et al., 2008; Turnbull et al., 2001). PCSK5 cleaves a number of substrates at the cell surface, including proteoglycan-bound endothelial lipase and lipoprotein lipase (Jin et al., 2003, 2005; Mayer et al., 2008; Nour et al., 2005), metalloproteinase ADAMTS-4 (Mayer et al., 2008; Tortorella et al., 2005), and TGFβ-family ligand Lefty (Mayer et al., 2008; M. Tang, Mikhailik, et al., 2005; M. Tang, Taylor, et al., 2005). Furthermore, a secreted 65 kD form of PCSK5 is thought to be cleaved by an MMP late in the secretory pathway, likely at the cell surface (De Bie et al., 1996; Nour et al., 2005). The C-terminal truncation of mature PCSK5 occurs at residue Tyr619 (of mouse PC5A) and is not achieved autocatalytically (Nour et al., 2005). At this point, the purpose of the 65 kD form of PCSK5 and the details of its regulation are unknown.

Within the peptidase domain, subtilisin-like serine proteases share a conserved Asp/His/Ser triad (**Figure 1.04, blue stars**) (De Bie et al., 1996). The P domain, located a short distance downstream of the peptidase domain, is required for PC activity (J. W. Creemers et al., 1993; Gluschankof & Fuller, 1994; A. Zhou et al., 1998). Protein truncation prior to the end of the P domain blocks pro-domain removal and traps PCs in the ER (Gluschankof & Fuller, 1994; A. Zhou et al., 1998). The P domain interacts with the peptidase domain through hydrophobic interactions and contributes to the folding and stability of the PCs (Ueda et al., 2003). Swapping the P domains of various PCs leads to alterations in calcium and pH dependence, suggesting that some of the PC member-specific properties might arise from this domain (A. Zhou et al., 1998). PCSK5 also contains an Arg-Gly-Asp (RGD) sequence within the P domain, which is characteristic of extracellular matrix proteins and is involved in cell adhesion (Nakagawa, Hosaka, et al., 1993). PCSK5 can be further modified post-translationally by glycosylation, which occurs in the Golgi (Kelly, 1985; Palade, 1975). A study of bovine furin with mutations at the three potential sites of N-glycosylation found that glycosylation was not essential for autocatalytic processing of pro-furin or substrate processing (J. W. M. Creemers et al., 1995). Mutagenesis of the four potential N-glycosylation sites of the mouse PC5A CRD found no effect on PCSK5 secretion or surface binding to TIMP-2 (Nour et al., 2005).

Chapter 2: PCSK5^{M452I} is a recessive hypomorph exclusive to MCF10DCIS.com cells[#^]

Taylor Marohl[1], Kristen A. Atkins[2], Lixin Wang[1]*, Kevin A. Janes[1,3]*

[1]Department of Biomedical Engineering, University of Virginia, Charlottesville, VA 22908

[2]Department of Pathology, University of Virginia, Charlottesville, VA 22908

[3]Department of Biochemistry & Molecular Genetics, University of Virginia, Charlottesville, VA 22908

*Co-corresponding authors

Lead contact: Kevin A. Janes (kjanes@virginia.edu)

[#]This work has been preprinted and is available online at: https://www.biorxiv.org/content/10.1101/2025.03.03.641323v1.

[^]At the time of publication of this dissertation, the manuscript comprising Chapter 2 is in revision for resubmission to *Molecular Cancer Research.*

2.1 ABSTRACT

The most widely used cell line for studying ductal carcinoma in situ (DCIS) premalignancy is the transformed breast epithelial cell line, MCF10DCIS.com. During its original clonal isolation and selection, MCF10DCIS.com acquired a heterozygous M452I mutation in the proprotein convertase PCSK5, which has never been reported in any human cancer. The mutation is noteworthy because PCSK5 matures GDF11, a TGFβ-superfamily ligand that suppresses progression of triple-negative breast cancer. We asked here whether PCSK5^{M452I} and its activity toward GDF11 might contribute to the unique properties of MCF10DCIS.com. Using an optimized in-cell GDF11 maturation assay, we found that overexpressed PCSK5^{M452I} was measurably active but at a fraction of the wildtype enzyme. In a *PCSK5*$^{-/-}$ clone of MCF10DCIS.com reconstituted with different PCSK5 alleles, PCSK5^{M452I} was mildly defective in anterograde transport. However, the multicellular organization of PCSK5^{M452I} addback cells in 3D matrigel cultures was significantly less compact than wildtype and indistinguishable from a PCSK5^{T288P} null allele. Growth of intraductal MCF10DCIS.com xenografts was similarly impaired along with the frequency of comedo necrosis and stromal activation. In no setting did PCSK5^{M452I} exhibit gain-of-function activity, leading us to conclude that it is hypomorphic and thus compensated by the remaining wildtype allele in MCF10DCIS.com.

Implications: This work reassures that an exotic PCSK5 mutation is not responsible for the salient characteristics of the MCF10DCIS.com cell line.

2.2 INTRODUCTION

Ductal carcinoma *in situ* (DCIS) is a prevalent yet enigmatic premalignancy of the breast with a ~30% chance of progressing to invasive cancer (Stuart et al., 2015). DCIS latency is thought to be long and variable in women, and its molecular subtypes differ from those of breast carcinoma (Koboldt et al., 2012; Strand et al., 2022). The biology of DCIS is notoriously difficult to access experimentally. There are long-standing genetically-engineered mouse models of breast cancer that have well defined DCIS intermediates. However, they are driven by viral transgenes [polyomavirus middle T antigen (Lin et al., 2003), SV40 large T antigen (Green et al., 2000)] and progress rapidly without the indolence characteristic of human DCIS (Hutten & Jonkers, 2023). This prompted early efforts to derive human cell lines that capture facets of DCIS *in vitro* and *in vivo*.

Nearly 25 years ago, Miller *et al*. described MCF10DCIS.com as a derivative of MCF10A cells (Soule et al., 1990) that was transformed with oncogenic $HRAS^{G12V}$ (Miller et al., 1993), subcloned, and propagated subcutaneously in nude mice (Miller et al., 2000). MCF10DCIS.com is singular among HER2-negative cell lines in initiating durable xenografts with comedo necrosis that are histologically DCIS-like (Hu et al., 2008). It is a pillar of the MCF10 series of cell lines (Puleo & Polyak, 2021) and has served as a reference for DCIS research decades before the exciting recent advances with intraductal xenotransplantation of patient-derived samples (Hutten et al., 2023). MCF10DCIS.com cells underlay impactful studies of malignancy (Hu et al., 2008), metastasis (W. Zhou et al., 2014), metabolism (Kalaany & Sabatini, 2009; Possemato et al., 2011), and mechanotransduction (Wei et al., 2015). The line remains useful for spanning complexity scales—MCF10DCIS.com expands readily in 2D tissue culture and 3D matrigel culture, as well as in the subcutaneous tissue, mammary duct, and mammary fat pad of immunocompromised mice (Behbod et al., 2009; Fattet et al., 2020; Frittoli et al., 2023; Pereira et al., 2020; Peuhu et al., 2022). Although there are valid concerns about the initiating oncogene (Wagner, 2022), MCF10DCIS.com cells are generally viewed as a best-available proxy for human hormone receptor-negative DCIS.

MCF10DCIS.com cells harbor ectopic $HRAS^{G12V}$ (Miller et al., 1993), an acquired $PIK3CA^{H1047R}$ driver mutation (Kalaany & Sabatini, 2009), as well as additional somatic changes of unknown significance (Maguire et al., 2016). Among the most unusual is a M452I point substitution in the proprotein convertase, PCSK5 (Seidah & Prat, 2012). Mutant *PCSK5* is detectable in transformed MCF10 predecessors and increases to 50% allele frequency in MCF10DCIS.com before receding in MCF10 invasive carcinoma lines; no other mutation exhibits this pattern (Maguire et al., 2016). The most-recognized convertase substrate for PCSK5 is GDF11 (Essalmani et al., 2008; McPherron et al., 1999), a secreted TGFβ superfamily ligand that modulates cancer progression (Simoni-Nieves et al., 2019). In breast cancer, we previously showed that GDF11 promotes epithelial organization, restrains invasion, and loses activity when its inactive precursor is not matured due to PCSK5 silencing or

mutation (Bajikar et al., 2017). Multiple breast cancer-derived PCSK5 mutants were validated as loss-of-function in our earlier study. However, M452I is not documented in breast cancer nor in any cancer to date (Tate et al., 2019), and a loss-of-function allele would be counterintuitive given the anti-invasive characteristics of MCF10DCIS.com. More plausible was that PCSK5^{M452I} conferred a non-canonical gain-of-function phenotype and matured endogenous proGDF11 more efficiently than wildtype, as recently demonstrated for a V474I polymorphism in a related proprotein convertase (Mei et al., 2025). If true, it would provide a satisfying explanation for the select characteristics of MCF10DCIS.com and call into question prior conclusions that might have stemmed from a one-off mutation never before documented in human disease.

Here, we performed a detailed investigation of the PCSK5^{M452I} mutant derived from MCF10DCIS.com. Using an orthogonal mammalian-expression system, we designed a proGDF11 convertase assay, which suggested that PCSK5^{M452I} was detectably less active than wildtype PCSK5, with additive effects when the two were coexpressed. MCF10DCIS.com-specific properties were examined by knocking out PCSK5 and inducibly reconstituting with PCSK5, PCSK5^{M452I}, or a known loss-of-function allele [PCSK5^{T288P} (Bajikar et al., 2017)]. In these cells, we quantified subcellular protein localization in 2D monolayers, multicellular organization in 3D cultures, and *in vivo* histopathology of intraductal inocula. The PCSK5^{T288P} addback cells verified PCSK5 loss-of-function and phenocopied prior results involving GDF11 knockdown (Bajikar et al., 2017), but in no context was there a hypermorphic or neomorphic difference between wildtype PCSK5 and PCSK5^{M452I} addback. Our reassuring conclusion is that PCSK5^{M452I} is a hypomorphic allele, which is heterozygous recessive and thus unlikely to drive phenotypes in MCF10DCIS.com.

2.3 RESULTS

2.3.1 The PCSK5^{M542I} allele expressed by MCF10DCIS.com is plausibly altered in function

In the first report of PCSK5^{M452I} (Maguire et al., 2016), computational algorithms disagreed on the predicted severity of an M452I substitution in PCSK5. We revisited these inferences with newer methods (J. Cheng et al., 2023; Liu et al., 2020; Rogers et al., 2021; Steinhaus et al., 2021; H. Tang & Thomas, 2016) and evaluated PCSK5^{M452I} relative to two missense single-nucleotide polymorphisms (SNPs) in the short form of PCSK5—rs138257548 (encoding R486H) and rs145509473 (encoding A565T)—along with a somatic T288P mutation verified as inactive (Bajikar et al., 2017). Whereas PCSK5 SNPs were generally predicted to be neutral or minimally damaging, PCSK5^{M452I} was predicted to be damaging as frequently as PCSK5^{T288P} (**Figure 2.01 A**), warranting further study of PCSK5^{M452I} in MCF10DCIS.com.

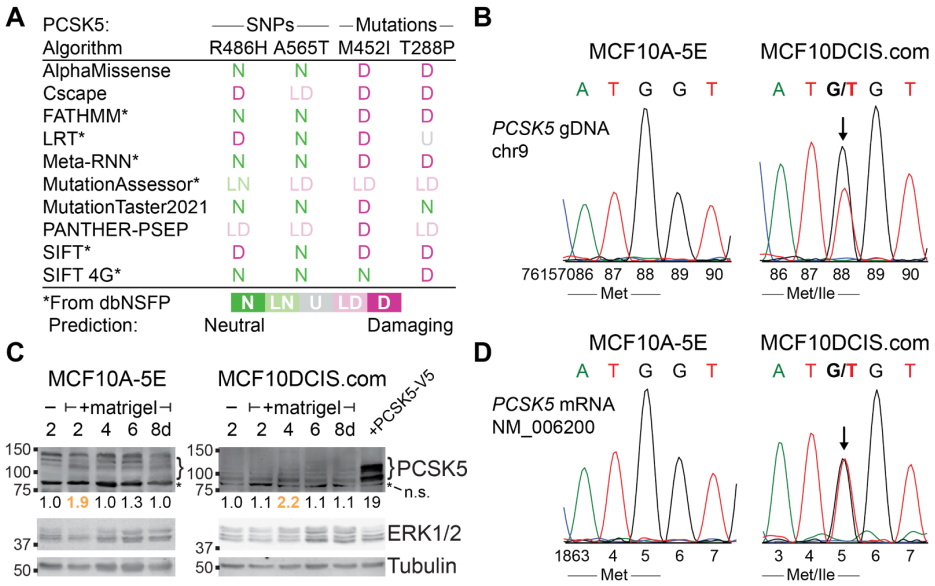

Figure 2.01. MCF10DCIS.com cells express a mutated allele of PCSK5 that is predicted to be damaging.

A, Computational predictions for the PCSK5^{M452I} mutation of MCF10DCIS.com alongside two single-nucleotide polymorphisms (SNPs; R486H and A565T) and a somatic mutation (T288P) confirmed experimentally to be inactive (Bajikar et al., 2017). Outputs for each algorithm were grouped as Neutral (N), Likely Neutral (LN), Unknown (U), Likely Damaging (LD), or Damaging (D) as described in **Table 2.01**. **B,** Confirmation of the M452I mutation in genomic DNA (gDNA) from MCF10DCIS.com cells. **C,** Endogenous PCSK5 is induced when MCF10-series cells are cultured with 2% matrigel for 2–4 days. Cell extracts were immunoblotted for PCSK5 with ERK1/2 and tubulin used as loading controls. Extract from MDA-MB-231 cells overexpressing pro and mature V5-tagged PCSK5 (+PCSK5-V5) was used as a positive control. Asterisk marks a nonspecific band for the PCSK5 antibody. Image gamma = 2 for the PCSK5 immunoblots. **D,** The PCSK5^{M452I} allele is expressed in MCF10DCIS.com cells cultured with 2% matrigel. For (**B**) and (**D**), MCF10A-5E cells (Janes et al., 2010) provide a wildtype reference.

We first confirmed the chr9:67157088G>T substitution in *PCSK5* at roughly 50% allele frequency (Maguire et al., 2016) in genomic DNA prepared from MCF10DCIS.com, using the 5E clone (Janes et al., 2010) of MCF10A cells as a wildtype reference (**Figure 2.01 B**). To ensure both transcripts were equally abundant in MCF10DCIS.com, we required a context in which endogenous PCSK5 was reliably detected. However, *PCSK5* transcripts are very low in breast carcinomas and standard breast cancer cell lines (Bajikar et al., 2017), and commercial reagents for detecting PCSK5 protein were insensitive or nonspecific. We thus raised a new polyclonal antibody against residues 604–619, affinity purified the antisera, and optimized immunoblotting conditions to achieve fmol sensitivity against ectopic PCSK5 (**Figure 2.02**). Using the purified antibody, we discovered that PCSK5 is transiently induced when MCF10-series cells are cultured with 2% matrigel for multiple days (**Figure 2.01 C**). Total RNA extracted from matrigel-treated cells confirmed that both the wildtype and M452I transcripts were present in MCF10DCIS.com (**Figure 2.01 D**). These results supported that PCSK5^{M452I} protein was expressed when MCF10DCIS.com cells were exposed to certain microenvironments.

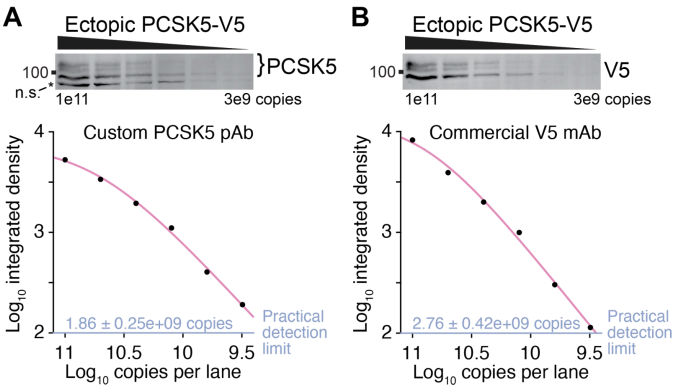

Figure 2.02. Affinity-purified PCSK5 antibody sensitivity and dynamic range.

A and **B,** Extract from MDA-MB-231 cells ectopically expressing V5-tagged PCSK5 was calibrated with recombinant V5-containing Multitag protein (Lopacinski et al., 2021), serially diluted, and immunoblotted for (**A**) PCSK5 and (**B**) V5 as described in the Materials and Methods. Asterisk marks a nonspecific band for the PCSK5 antibody. Bands were quantified by densitometry and fit to a three-parameter logistic equation with regression uncertainties estimated by asymptotic error analysis. Absolute copy-number sensitivities were set to a nominal integrated band intensity of 100 (blue).

2.3.2 An ectopic proGDF11 convertase assay suggests that PCSK5^{M452I} is enzymatically deficient

PCSK5 is the major convertase of proGDF11 (Essalmani et al., 2008; McPherron et al., 1999). To quantify the activity of different PCSK5 alleles *in cellulo*, we developed a high-throughput GDF11 secretion assay by ectopically coexpressing PCSK5 and GDF11 in 293T cells and quantifying GDF11 release with a commercial ELISA. Endogenous GDF11 was barely detectable in conditioned medium from control lipofections and was generally low when GDF11 was overexpressed on its own (**Figure**

2.03 A, Lanes 1–5), confirming that endogenous convertase activity is modest in these cells (Ge et al., 2005). Cotransfection with PCSK5 hyperbolically increased the measured GDF11 ELISA signal, and we optimized wildtype PCSK5 gene dosage to provide dynamic range for increased activity as well as decreased activity (**Figure 2.04 A**). In principle, the capture and detection antibodies of the ELISA might recognize unprocessed proGDF11 in the medium, which would obscure GDF11 maturation by conflating it with proGDF11 release. Using conditioned medium from optimized lipofections, we immunoprecipitated GDF11 by its epitope tag and immunoblotted to separate the pro and mature proteoforms by molecular weight. Consistent with the ELISA results, we observed much less mature GDF11 from cells that were not cotransfected with PCSK5 (**Figure 2.04 B**). Across a range of conditions, the ELISA readout correlated with mature GDF11 abundance and anticorrelated with proGDF11 released into the medium (**Figure 2.04 C and D**). These results indicated that the ELISA is specific for mature GDF11; thus, the secretion assay largely measures proGDF11 conversion by the PCSK5 that is cotransfected.

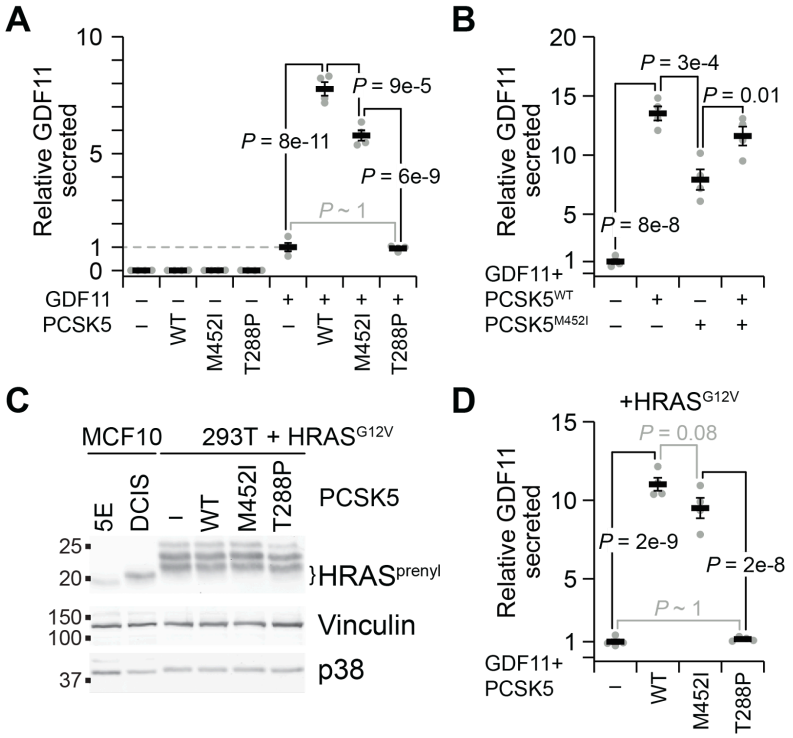

Figure 2.03. 293T cells co-expressing PCSK5^{M452I} secrete mature ectopic GDF11 with intermediate efficiency.

A, Catalytically active PCSK5 promotes ectopic GDF11 secretion. Cells were lipofected with 3 ng of the indicated PCSK5 allele (or EGFP overexpression control) plus 100 ng of GDF11, and conditioned medium was collected after 24 hours to measure GDF11 release by ELISA. PCSK5^{T288P} was included as a catalytically dead control (Bajikar et al., 2017). **B,** GDF11 release by PCSK5^{M452I} plus wildtype PCSK5 (PCSK5^{WT}) is additive. Cells were treated as in (**A**) and compared with 1.5 ng PCSK5^{WT} plus 1.5 ng PCSK5^{M452I}. **C,** Cotransfection with oncogenic HRAS^{G12V} approximates the level of prenylated HRAS (HRAS^{prenyl}) in MCF10DCIS.com. 293T cells were lipofected with 2 ng of HRAS^{G12V} and 3 ng of the indicated PCSK5 allele (or EGFP overexpression control) and immunoblotted for HRAS with vinculin and p38 used as

loading controls. MCF10A-5E cells are a negative control for HRAS overexpression. **D,** $HRAS^{G12V}$ cotransfection does not alter the relative GDF11 secretion efficiencies of wildtype PCSK5, $PCSK5^{M452I}$, and $PCSK5^{T288P}$. Cells were treated as in (**C**) and measured for GDF11 release by ELISA. For (**A**), (**B**), and (**D**), GDF11 ELISA results are normalized to the GDF11-only condition [gray dashed in (**A**)] and shown as the mean ± SEM of *N* = 4 biological replicates. Differences among +GDF11 groups were analyzed by multiway ANOVA with PCSK5 genotype as a fixed effect. Significant factors were followed up pairwise by Tukey-Kramer post hoc analysis.

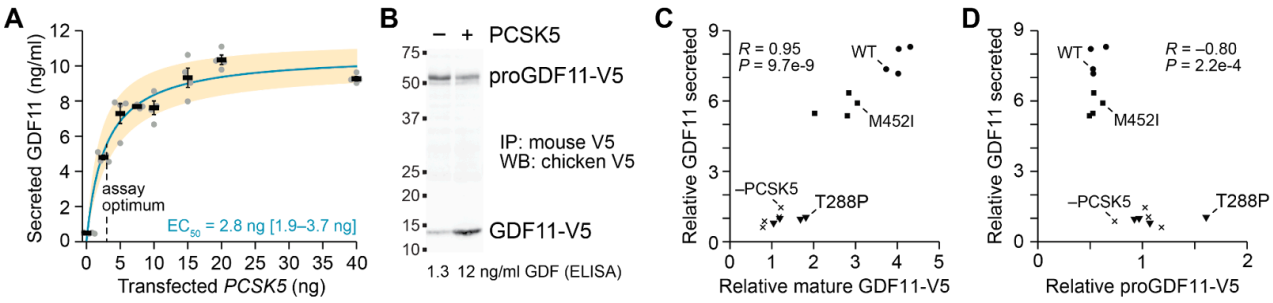

Figure 2.04. Optimization and validation of a proGDF11 convertase assay.

A, 293T cells were lipofected with 100 ng of pLX302 GDF11-V5 plasmid plus the indicated mass of pLX304 PCSK5-V5 plasmid in a 24-well plate, and conditioned medium was analyzed for GDF11 release by ELISA. Data are shown as the mean ± SEM of *N* = 4 biological replicates that were fit to a hyperbolic relationship by nonlinear least squares. The half-maximal PCSK5 mass (EC_{50}) is shown with 95% confidence interval in brackets, and the dashed line indicates the amount used in the optimized assay. **B,** Conditioned medium from optimized lipofections was collected, immunoprecipitated (IP) with mouse anti-V5, and immunoblotted (WB) with chicken anti-V5 to resolve pro and mature forms of GDF11. ELISA results for these samples are reported underneath the immunoblot. **C** and **D,** Correlation between secreted GDF11 measured by ELISA and (**C**) mature GDF11-V5 or (**D**) proGDF11-V5 measured by immunoblotting. ELISA and immunoblots were normalized to the control lipofections lacking PCSK5 (–PCSK5). Data are from *N* = 4 independent experiments for each PCSK5 genotype and the –PCSK5 control. The Pearson correlation (*R*) was tested for nonzero significance after the Fisher *Z* transformation.

We applied the assay to assess enzymatic function of the different PCSK5 alleles. Whereas $PCSK5^{T288P}$ showed no convertase activity, as expected (Bajikar et al., 2017), we found that $PCSK5^{M452I}$ activity was consistently detectable but lower than wildtype PCSK5 (**Figure 2.03 A**, Lanes 5–8). Recognizing that the MCF10DCIS.com genotype is $PCSK5^{M452I/+}$, we mixed equal proportions of wildtype and M452I alleles in the cotransfection and repeated the assay. The resulting GDF11 conversion was an average of the two alleles (**Figure 2.03 B**), suggesting additivity in a heterozygous context. We also considered the possibility that a $PCSK5^{M452I}$-specific effect might depend on the inciting $HRAS^{G12V}$ oncogene of MCF10DCIS.com (Miller et al., 1993). When $HRAS^{G12V}$ was added to the 293T cotransfection and calibrated to the abundance of active prenylated HRAS (Odeniyide et al., 2022) in MCF10DCIS.com, there was no qualitative change in the measured activity of $PCSK5^{M452I}$ relative to wildtype PCSK5 or $PCSK5^{T288P}$ (**Figure 2.03 C** and **D**). Contrary to our original hypothesis, the isolated enzymology of $PCSK5^{M452I}$ suggested that it was not hypermorphic but hypomorphic.

2.3.3 Unmixing PCSK5 alleles in MCF10DCIS.com

The proGDF11 convertase assay estimated enzymatic activity for a transfected PCSK5 allele but did not capture the cellular context of MCF10DCIS.com. We expected that the heterozygous *PCSK5*$^{M452I/+}$ genotype of MCF10DCIS.com cells would blur any role for the M452I mutation specifically (**Figure 2.01 B** and **2.03 B**). A fear of disrupting individual alleles was that heterozygous PCSK5 knockouts would be confounded by clone-to-clone variation given the stem-progenitor characteristics of MCF10DCIS.com (Hu et al., 2008) and the known impact of GDF11 on stem-cell dynamics (Lander et al., 2009). We thus adopted a knockout–addback approach that sought to minimize adaptations caused by loss of autocrine PCSK5–GDF11 signaling (**Figure 2.05 A**). Cells were transduced with lentivirus encoding a destabilization domain-Cas9 (DD-Cas9) fusion (Senturk et al., 2017) and an sgRNA targeting just upstream of the PCSK5 catalytic triad (**Figure 2.05 B**). MCF10DCIS.com transductants were treated with Shield-1 to stabilize DD-Cas9 (Banaszynski et al., 2006) plus 2% matrigel to give Cas9 access to the PCSK5 locus (Horlbeck et al., 2016) for twelve days (**Figure 2.05 A**). Cells were clonally sorted for Venus co-expression, expanded in low-dose GDF11 to maintain basal signaling during colony recovery, and screened for knockout by sequencing. We moved forward with a *PCSK5*$^{-/-}$ clone with morphology and growth characteristics similar to MCF10DCIS.com in 2D culture but with distinct indels yielding premature stop codons for each allele (**Figure 2.05 B**). This clone was then transduced at limiting multiplicity of infection with a doxycycline-regulated, sgRNA-resistant, and V5-tagged PCSK5 allele (short proteoform; C-terminal tag) and polyclonally selected (**Figure 2.05 A**). We quantified induction with a V5-containing recombinant standard (Lopacinski et al., 2021) and detected ~150,000 copies of each PCSK5 allele after 24 hours of doxycycline (**Figure 2.05 C**). These stable, inducible, and pure PCSK5 alleles provided a basis for all subsequent experiments involving MCF10DCIS.com.

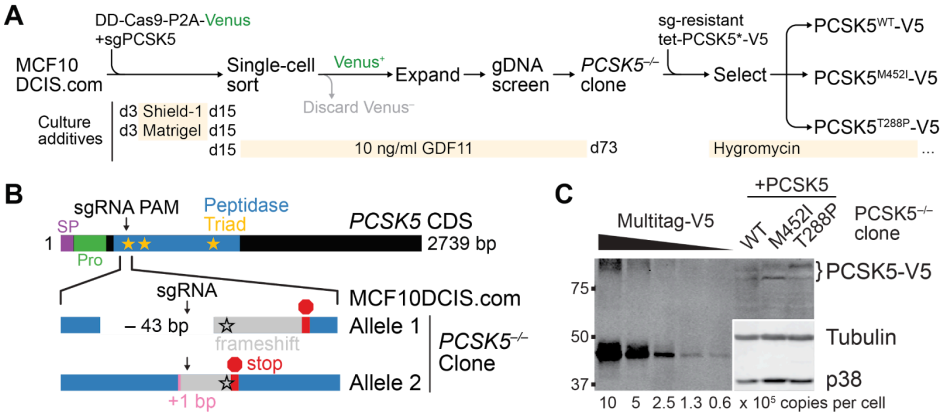

Figure 2.05. Inducible reconstitution of PCSK5 alleles in PCSK5$^{-/-}$ MCF10DCIS.com cells.

A, Approach to MCF10DCIS.com engineering. Cells were transduced with a destabilizing domain (DD)-containing Cas9-P2A-Venus (Senturk et al., 2017) and a single-guide RNA targeting Exon 4 of PCSK5 (sgPCSK5). Transduced cells were treated with 200 nM Shield-1 (Senturk et al., 2017) to stabilize

Cas9-P2A-Venus and 2% matrigel to promote PCSK5 expression (**Figure 2.01 C**) before sorting single Venus-positive cells into 10 ng/ml GDF11 (to aid recovery upon PCSK5 loss) and screening genomic DNA (gDNA) of expanded clones for knockout. One confirmed $PCSK5^{-/-}$ clone was then transduced with sgPCSK5-resistant, tetracycline (tet)-regulated, V5-tagged alleles of PCSK5 and selected polyclonally for hygromycin resistance. **B,** Sequence-confirmed knockout alleles of MCF10DCIS.com clone 3D8. The PCSK5 coding sequence (CDS) is shown with annotations for the signal peptide (SP, purple), proprotein sequence (Pro, green), and peptidase domain (blue) including its catalytic triad (yellow stars). The protospacer adjacent motif (PAM) of sgPCSK5 is just upstream of the first triad amino acid, and deletions (white, Allele 1) or insertions (pink, Allele 2) induce frameshift mutations (gray) removing the first amino acid in the catalytic triad (black outlined stars) and producing premature stop codons (red). **C,** Quantification of reconstituted PCSK5 alleles by calibrating against recombinant V5-containing Multitag protein at the indicated copies per cell (Lopacinski et al., 2021; L. Wang et al., 2023). Cells were treated with 1 µg/ml doxycycline for 24 hours, and total protein from counted cells was immunoblotted for V5 with tubulin and p38 used as loading controls for cells. Copy number estimates are: $PCSK5^{WT}$, 136,000 ± 11,000 copies per cell; $PCSK5^{M452I}$, 164,000 ± 6,000 copies per cell; $PCSK5^{T288P}$, 176,000 ± 15,000 copies per cell (*N* = 4 independent samples).

2.3.4 Localization of PCSK5 alleles along the distal secretory pathway coincides with auto-maturation

The short proteoform of PCSK5 traffics through the ER and Golgi to secretory vesicles (De Bie et al., 1996; Seidah & Prat, 2012), and the M452I mutation could affect steady-state localization to these organelles. We leveraged the higher specificity of the V5 antibody (**Figure 2.01 C**, **2.02**, and **2.05 C**) to co-localize reconstituted PCSK5 alleles with markers of the ER [PDI (Freedman, 1984)], cis Golgi [GM130 (Nakamura et al., 1995)], and trans Golgi [TGN38 (Girotti & Banting, 1996)]. Using diffraction-limited and adaptively deconvolved image stacks collected by laser-scanning confocal microscopy, we calculated the extent of pixel overlap relative to the overall V5 immunoreactivity per cell. Co-localization with the ER was indistinguishable among PCSK5 alleles (**Figure 2.06 A** and **B**), but we noted differences in Golgi localization that coincided with whole-cell convertase activity measured earlier (**Figure 2.03 A**). Compared to wildtype, the inactive T288P mutation accumulated detectably in the cis Golgi and dramatically in the trans Golgi (**Figure 2.06 C–F**). The hypomorphic M452I mutation, by contrast, was localized similarly to wildtype in the cis Golgi and at an intermediate level between wildtype in T288P in the trans Golgi. These differences were consistent with the extent of proPCSK5 auto-maturation observed by mobility shift in these cells (**Figure 2.07**), which occurs after anterograde traffic from the trans Golgi (Mayer et al., 2008). Some V5 was aberrantly immunolocalized to the nucleus, likely from protein that had escaped co-translational import to the ER lumen and undergone nuclear import based on multiple weak localization sequences in the PCSK5 primary structure (**Figure 2.08 A**). However, the mean nuclear V5 staining was unchanged among PCSK5 alleles (**Figure 2.08 B**), arguing that M452I is hypomorphic predominantly by inhibiting autoconversion and thus traffic beyond the trans-Golgi network (Constam, 2014).

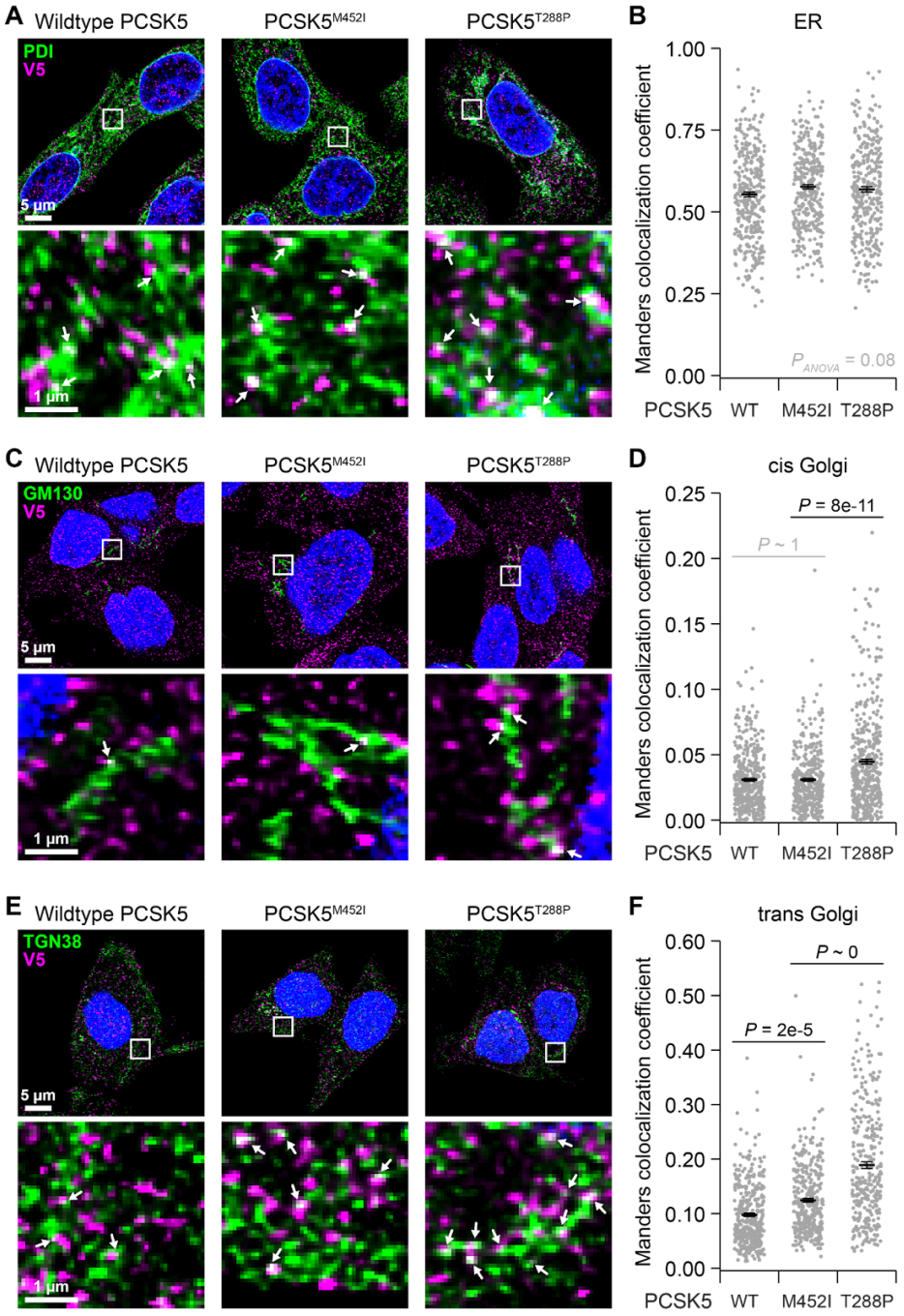

Figure 2.06. Impaired anterograde transport of catalytically deficient PCSK5 alleles in PCSK5$^{-/-}$ MCF10DCIS.com cells.

A, Immuno-colocalization of V5 epitope tag (magenta) with the endoplasmic reticulum (ER) marker PDI (green) for the indicated PCSK5 addback allele. **B**, Whole-cell V5–PDI colocalization quantified by Manders colocalization coefficient as a fraction of total per-cell V5 immunoreactivity in *N* = 348 (wildtype PCSK5), 322 (PCSK5^{M452I}), and 324 (PCSK5^{T288P}) cells. **C**, Immuno-colocalization of V5 epitope tag (magenta) with the cis Golgi marker GM130 (green) for the indicated PCSK5 addback allele. **D**, Whole-cell V5–GM130 colocalization quantified by Manders colocalization coefficient as a fraction of total per-cell V5 immunoreactivity in *N* = 398 (wildtype PCSK5), 373 (PCSK5^{M452I}), and 431 (PCSK5^{T288P}) cells. **E**, Immuno-colocalization of V5 epitope tag (magenta) with the trans Golgi marker TGN38 (green) for the indicated PCSK5 addback allele. **F,** Whole-cell V5–TGN38 colocalization quantified by Manders

colocalization coefficient as a fraction of total per-cell V5 immunoreactivity in *N* = 361 (wildtype PCSK5), 358 (PCSK5^{M452I}), and 324 (PCSK5^{T288P}) cells. For (**A**), (**C**), and (**E**), cells were immunostained for the indicated targets along with tubulin for cell segmentation, counterstained with DAPI (blue), and imaged on a laser-scanning confocal microscope followed by adaptive image deconvolution. Scale bars are 5 μm (upper) and 1 μm (lower). For (**B**), (**D**), and (**F**), arcsine-transformed coefficients were analyzed by multiway ANOVA with PCSK5 genotype as a fixed effect. Significant factors were followed up pairwise by Tukey-Kramer post hoc analysis.

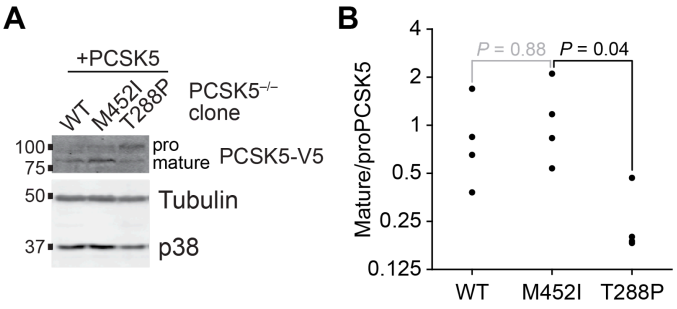

Figure 2.07. Defective maturation of PCSK5^{T288P}, but not PCSK5^{M452I}, in reconstituted PCSK5$^{-/-}$ MCF10DCIS.com cells.

A, Altered relative abundance of pro and mature forms of different PCSK5 alleles. Cells were treated with 1 μg/ml doxycycline for 24 hours, and total protein from counted cells was immunoblotted for V5 with tubulin and p38 used as loading controls. **B,** Densitometry of mature/proPCSK5 for *N* = 4 biological replicates from each genotype. Ratios were analyzed by Kruskal-Wallis test, and significant differences by genotype were followed up by Tukey-Kramer post hoc analysis.

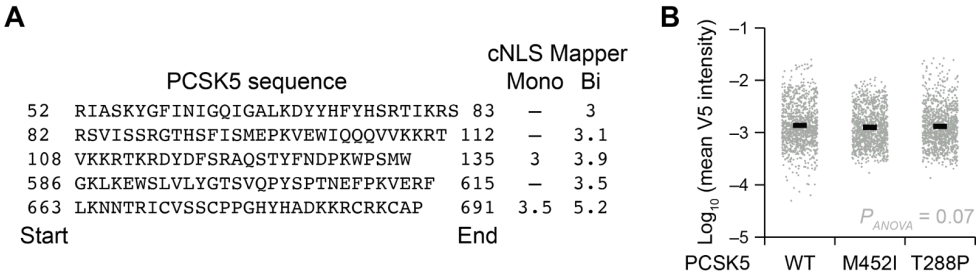

Figure 2.08. Weak nuclear localization signals and observed nuclear localization of PCSK5.

A, PCSK5 sequences predicted by cNLS Mapper (Kosugi et al., 2009) to be mono- or bi-partite nuclear localization sequences (NLS). Scores of 3–5 predict localization to both the nucleus and the cytoplasm. **B,** Mean nuclear V5 signal intensity in *N* = 1107 (wildtype PCSK5), 1053 (PCSK5^{M452I}), and 1079 (PCSK5^{T288P}) cells. Log-transformed mean intensities were analyzed by multiway ANOVA with PCSK5 genotype as a fixed effect.

2.3.5 PCSK5 deficiency perturbs 3D organization of MCF10DCIS.com spheroids

MCF10-series lines exhibit more phenotypes when overlay cultured with matrigel in 3D (Debnath et al., 2002; Muthuswamy et al., 2001; L. Wang et al., 2023). In MCF10DCIS.com cells, for example, acute knockdown of GDF11 has no discernible effect in 2D culture, but the same perturbation causes 3D spheroids to rupture (Bajikar et al., 2017). This result together with the induction of PCSK5

in matrigel (**Figure 2.01 C**) motivated us to characterize the different PCSK5 addback derivatives of MCF10DCIS.com in 3D.

We digitally segmented (Borten et al., 2018) hundreds of organoids at multiple time points but did not see gross changes in 3D growth (Przanowska et al., 2024) among the PCSK5 alleles (**Figure 2.09 A**). However, when comparing parental MCF10DCIS.com cells to the originating *PCSK5*$^{-/-}$ clone (**Figure 2.05 A**), there was a notable change in 3D morphology that was quantifiable as spheroid circularity (**Figure 2.09 B** and **C**). We revisited the three PCSK5 addback lines in 3D and added a high-dose recombinant GDF11 condition to the T288P allele as a positive control for the maximum circularization possible through PCSK5–GDF11 signaling (Bajikar et al., 2017). PCSK5^{T288P} cultures were the least spherical, consistent with the null activity of this allele (**Figure 2.03 A**), and the dramatic increase in circularity with high-dose GDF11 confirmed that they remain responsive to mature ligand (**Figure 2.09 D** and **E**). Wildtype PCSK5 addback cultures were significantly more circular than PCSK5^{T288P} but did not reach the PCSK5^{T288P} + GDF11 condition, reflecting the MCF10DCIS.com response to endogenous, sub-saturating levels of mature GDF11. Despite earlier biochemical and subcellular evidence of intermediate activity (**Figure 2.03 A**, **2.06 E** and **F**), we found that circularity of the PCSK5^{M452I} line was not distinguishably different from the null PCSK5^{T288P} allele (**Figure 2.09 D** and **E**; see Discussion). At the 3D endpoint, we assessed CDH1, TP63, and VIM as markers of epithelial, myoepithelial, and mesenchymal differentiation and did not observe bulk differences among lines without high-dose GDF11 (**Figure 2.09 F** and **G**). We attribute the induction of VIM in GDF11-stimulated PCSK5^{T288P} cultures to the synergy recognized between TGFβ-superfamily ligands and oncogenic HRAS (Janda et al., 2002; Oft et al., 1996). Overall, the multicellular phenotype of PCSK5^{M452I}-reconstituted MCF10DCIS.com provides further support that PCSK5^{M452I} is a hypomorph.

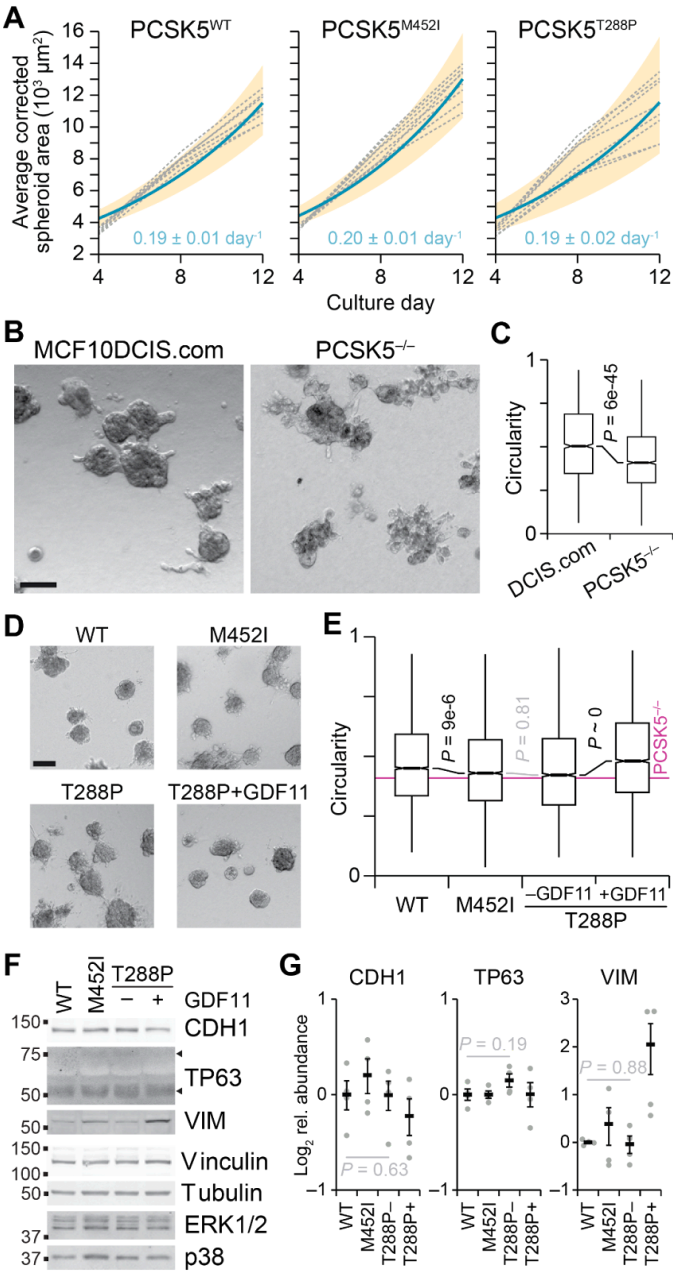

Figure 2.09. PCSK5 activity promotes rounded multi-cell organization in 3D matrigel cultures of MCF10DCIS.com.

A, Spheroid growth rates for the indicated PCSK5 addback lines estimated by nonlinear least-squares regression of cross-sectional area (Przanowska et al., 2024) at 4, 8, and 12 days from N = 8 biological replicates (gray dashed). **B** and **C,** Reduced multi-cell circularity of MCF10DCIS.com upon loss of PCSK5. For (**B**), the scale bar is 100 µm. For (**C**), circularities were calculated from N = 1819 (DCIS.com) and 2028 (PCSK5$^{-/-}$) segmented spheroids collected from 4 biological replicates at 16 days. Arcsine-transformed circularities were analyzed by two-sample homoscedastic t test. **D** and **E,** Multi-cell circularity of PCSK5$^{-/-}$ cells is restored by wildtype PCSK5 or addition of recombinant GDF11, but not PCSK5^{M452I} or PCSK5^{T288P}. For (**D**), the scale bar is 100 µm. For (**E**), circularities were calculated from N = 5503 (wildtype PCSK5), 5016 (PCSK5^{M452I}), 3495 (PCSK5^{T288P}), and 3815 (PCSK5^{T288P}+GDF11) segmented spheroids collected from 8 biological replicates at 8 days, and arcsine-transformed circularities were analyzed by multiway ANOVA with PCSK5 genotype as a fixed effect. Significant factors were followed up pairwise by Tukey-Kramer post

hoc analysis. **F** and **G,** PCSK5 alleles do not alter the differentiation phenotypes of MCF10DCIS.com cells in 3D matrigel culture. Cultures in (**A**) plus PCSK5^{T288P}+GDF11 cultures were lysed and immunoblotted for CDH1, TP63, and VIM with vinculin, tubulin, ERK1/2, and p38 used as loading controls. For (**G**), data from *N* = 4 biological replicates were normalized to the mean of wildtype PCSK5 cultures, and the three unstimulated genotypes were Box-Cox-transformed and compared by multiway ANOVA with PCSK5 genotype as a fixed effect.

2.3.6 Wildtype PCSK5 promotes the in vivo phenotypes of MCF10DCIS.com

MCF10DCIS.com owes its name to the DCIS-like lesions with comedo necrosis formed upon injection in the mammary fat pad (Miller et al., 2000). To investigate a possible role for PCSK5 in this histopathology, we used intraductal injection (Behbod et al., 2009) to inoculate SCID-beige animals with different PCSK5 addback lines of MCF10DCIS.com. Cells were labeled with luciferase to estimate the surviving inoculum at 2, 7, and 14 days, which together served as an internal reference for outgrowth over the subsequent six weeks after PCSK5 expression was induced with doxycycline at Day 7 (Bajikar et al., 2017). We found that wildtype PCSK5 inductions yielded significantly more bioluminescence than PCSK5^{M452I} and PCSK5^{T288P}, which were comparable to one another throughout (**Figure 2.10 A**). Endpoint bioluminescence correlated with estimated tumor volumes upon excision (**Figure 2.10 B**), verifying that the longitudinal images had captured intraductal growth. Notably, from Day 21 onward, the exponential rate of bioluminescence increase was similar for all genotypes (**Figure 2.10 A**). Wildtype PCSK5 was distinctive in its growth from Day 14–21, when MCF10DCIS.com xenografts start organizing as DCIS lesions (L. R. Tait et al., 2007) and PCSK5 is presumably increasing from doxycycline induction. The results suggested a transient role for wildtype PCSK5 activity—and, by extension, MCF10DCIS.com-derived GDF11—in intraductal recovery as xenografts, for which PCSK5^{M452I} cannot compensate.

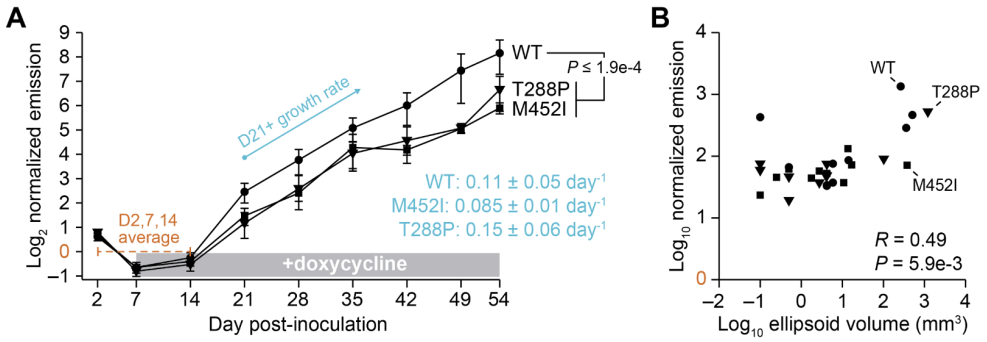

Figure 2.10. Longitudinal tumor bioluminescence and correlation with estimated tumor volume.

A, Peak emission was normalized to the Day 2–14 (D2,7,14) average per gland (brown), and data are reported as the mean ± SEM from *N* = 10 glands per genotype. Doxycycline was added on Day 7. Bioluminescence was compared from Day 21 onward (D21+) by multiway ANOVA with PCSK5 genotype and time point as fixed effects. Significant differences by genotype were followed up by Tukey-Kramer post hoc analysis. Additionally, the D21+ growth rate (blue) was estimated by nonlinear least squares and is shown as the mean ± SEM of the per-day growth rate estimate. **B,** Correlation between peak emission

[normalized as in (**A**)] and estimated tumor volume at the study endpoint (Day 54). The Pearson correlation (*R*) was tested for nonzero significance after the Fisher *Z* transformation.

At the endpoint, glands were harvested and carefully assessed by hematoxylin–eosin staining for the per-lesion frequency of various histological phenotypes. We observed no difference in the prevalence of ducts with (micro)papillary, solid, or cribriform growth patterns among PCSK5 alleles, and there was no discernible effect on the frequency of luminal gaps or secretions (**Figure 2.11**). Interestingly, we identified two differences that distinguished wildtype PCSK5 or PCSK5^{M452I} from the other alleles. First, comedo necrosis at different length scales was most frequent in glands inoculated with cells harboring wildtype PCSK5 (**Figure 2.12 A** and **B**). These results are consistent with recent work implicating GDF11 in cell death mediated by hypoxia (Kraler et al., 2023). Second, there were distinctions in the stroma that evolved inside and around MCF10DCIS.com lesions (L. R. Tait et al., 2007). Instances of stromal proliferation in and around the lesions were most frequent with wildtype PCSK5 and least frequent with PCSK5^{M452I} (**Figure 2.12 C** and **D**). Breast premalignancies with desmoplastic stroma have better clinical outcomes (Strand et al., 2022), suggesting a role for the stromal response in enforcing the DCIS state. Taken together, these *in vivo* data indicate that PCSK5 activity drives both the *in situ* and comedo phenotypes of MCF10DCIS.com; PCSK5^{M452I} is phenotypically at least as weak as the PCSK5^{T288P} null allele and thus should be impenetrant as a *PCSK5*$^{M452I/+}$ heterozygote.

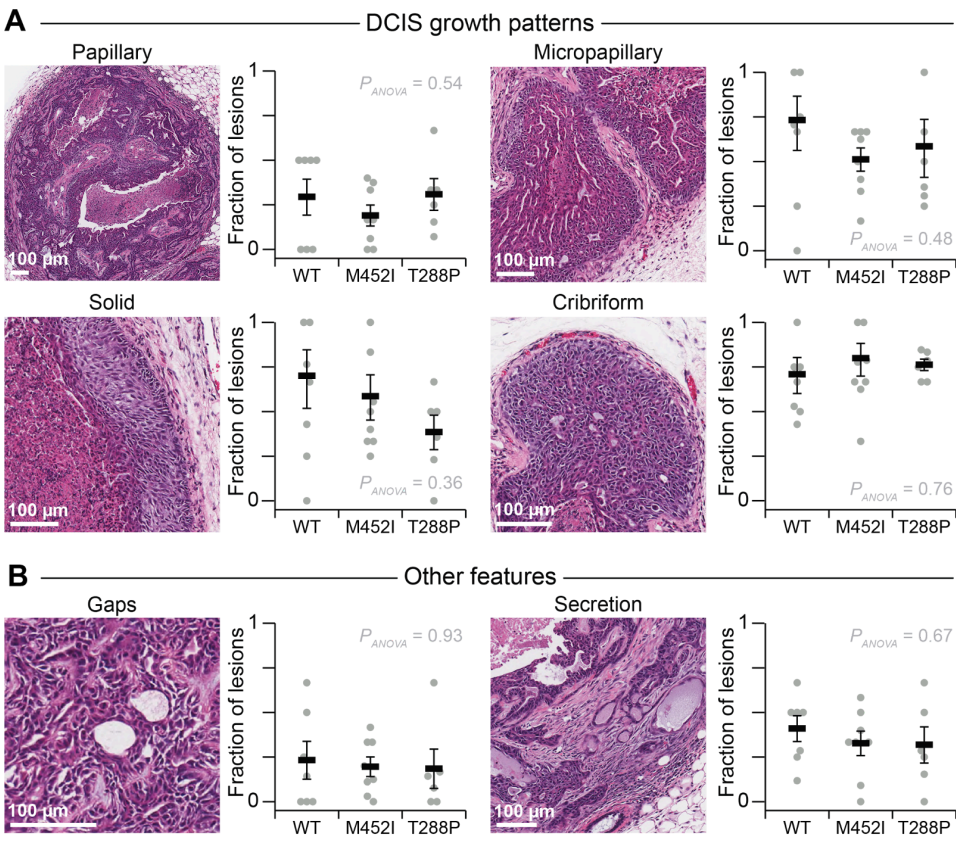

Figure 2.11. Other MCF10DCIS.com histologic phenotypes not detectably altered by PCSK5 activity.

A, Papillary (upper left), micropapillary (upper right), solid (lower left), and cribriform (lower right) DCIS growth patterns quantified by lesion prevalence for each genotype. **B,** Gaps (left) and secretions (right) quantified by lesion prevalence for each genotype. For (**A**) and (**B**), hematoxylin–eosin images of wildtype PCSK5 lesions are shown in the left subpanels at 54 days post-injection. The scale bar is 100 µm. In the right subpanels, prevalence among lesions from N = 6–8 animals per PCSK5 genotype was analyzed by multiway ANOVA with PCSK5 genotype as a fixed effect after arcsine transformation of percentages.

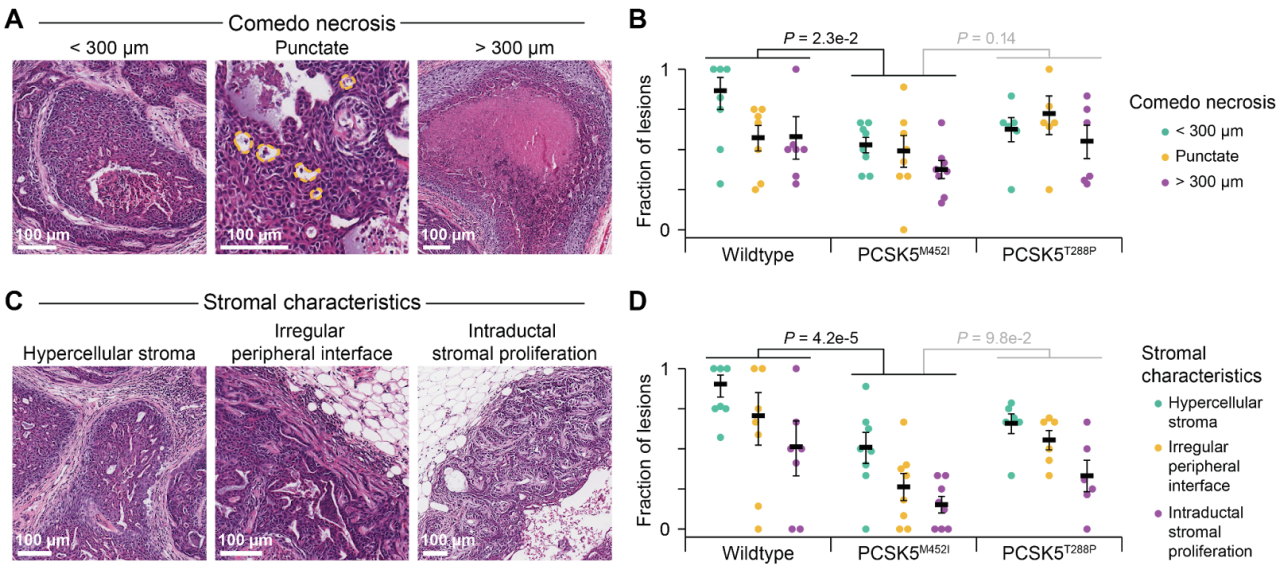

Figure 2.12. PCSK5 activity promotes comedo and stromal phenotypes in MCF10DCIS.com intraductal xenografts.

A, Representative hematoxylin–eosin images of wildtype PCSK5 lesions exhibiting small (less than 300 µm; left), punctate (yellow; middle), or large (greater than 300 µm; right) comedo necrosis at 54 days post-injection. **B,** Prevalence of comedo necrosis phenotypes among lesions from *N* = 6–8 animals per PCSK5 genotype. **C,** Representative hematoxylin–eosin images of wildtype PCSK5 lesions exhibiting hypercellular stroma (left), irregularity at the peripheral DCIS-stromal interface (middle), or intraductal stromal proliferation (right) at 54 days post-injection. **D,** Prevalence of stromal phenotypes among lesions from *N* = 6–8 animals per PCSK5 genotype. For (**A**) and (**C**), the scale bar is 100 µm. For (**B**) and (**D**), arcsine-transformed fractions were analyzed by multiway ANOVA with PCSK5 genotype and sub-phenotype as fixed effects. Significant differences by genotype were followed up by Tukey-Kramer post hoc analysis.

2.4 DISCUSSION

This study carefully examines an exclusive PCSK5^{M452I} somatic mutation found in the widely used cell line, MCF10DCIS.com (Maguire et al., 2016; Miller et al., 2000; Puleo & Polyak, 2021). By comparing to wildtype PCSK5 and catalytically null PCSK5^{T288P} throughout, we exclude PCSK5^{M452I} as a hypermorph and provide strong evidence that it is enzymatically deficient. This deficiency is first reflected as incomplete processing of the inactive zymogen, which retains proPCSK5^{M452I} in the trans Golgi and impedes its anterograde transport to secretory vesicles and the cell surface. Consequently, proGDF11 is unable to mature and accumulates intracellularly (Bajikar et al., 2017). Although PCSK5^{M452I} will process GDF11 when both are overexpressed, our results with endogenous GDF11 and minimally reconstituted PCSK5 indicate that PCSK5 activity is rate limiting in MCF10DCIS.com. Observing such PCSK5-dependent phenotypes may require 3D and *in vivo* microenvironments, which trap autocrine factors like GDF11 locally and evolve with time.

Using a new high-sensitivity PCSK5 antibody, we found that endogenous PCSK5 was induced in MCF10-series cells by long-term exposure to matrigel, a form of reconstituted basement membrane. Although the mechanism of induction is unclear, *PCSK5* transcripts are known to increase in breast epithelia upon overexpression of TP53 (Perez et al., 2007) or knockdown of the BRCA1-interacting protein, BRIP1 (Daino et al., 2013). In 3D matrigel cultures, TP53 is stabilized sporadically by environmental stresses (Pereira et al., 2020), suggesting a similar route may induce *PCSK5* here. Without matrigel, we were repeatedly unable to knock out PCSK5 in MCF10DCIS.com cells, illustrating the importance of basement membrane for opening the genomic locus. Similar pathways may be active during the early intraductal growth of MCF10DCIS.com *in vivo*, and random monoallelic expression of *PCSK5* (Deng et al., 2014) might generate mixtures of cells very similar to the addback lines developed here.

The PCSK5-dependent stromal response in xenografts suggests that mature GDF11 from MCF10DCIS.com cells reaches murine fibroblasts. GDF11 induces fibrosis in multiple tissue contexts [reviewed in (Frohlich & Vinciguerra, 2020)], and SMAD2 phosphorylation is observed at the tumor-stroma interface in MCF10DCIS.com xenografts (L. R. Tait et al., 2007). Although this signaling was originally attributed to TGFβ, GDF11 also triggers phosphorylation of SMAD2 (Bajikar et al., 2017), and their combined action may be important for addressing the stromal compartment in a way that TGFβ alone cannot (Antebi et al., 2017; Su et al., 2022).

Our results give reassurance to hundreds of MCF10DCIS.com-themed studies over the past two-and-a-half decades (Puleo & Polyak, 2021). Although PCSK5^{M452I} is an outlier mutation, it appears to do little more than dilute somewhat the cellular convertase available for proGDF11. PCSK5 cleaves additional substrates shared by other convertases but is unique in its activity toward proGDF11

(Essalmani et al., 2008; Seidah & Prat, 2012). Growth of intraductal MCF10DCIS.com xenografts is not affected when GDF11 itself is inducibly knocked down after 14 days (Bajikar et al., 2017), implying that a mature GDF11 niche is established very early and dispensable thereafter. Complete loss-of-function mutations documented in breast cancer, such as PCSK5^{T288P}, may actually impede breast tumorigenesis if they were to occur during premalignancy.

2.5 MATERIALS AND METHODS

2.5.1 Cell lines

MCF10DCIS.com cells were obtained directly from the Karmanos Cancer Institute through a Material Transfer Agreement, and cell identity was confirmed by STR profiling. MCF10DCIS.com cells were maintained in DMEM/F-12 medium (Gibco, 11320) plus 5% horse serum (Gibco, 16050) and 3D cultured in MCF10A assay medium (Debnath et al., 2003). MCF10A-5E cells were isolated and maintained as previously described (Janes et al., 2010). HEK 293T/17 cells (ATCC, CRL-11268) were cultured in DMEM (Gibco, 11965) plus 10% fetal bovine serum (HyClone, SH303396.03). All base media were supplemented with 1% penicillin–streptomycin (Gibco, 15140), and all cell lines were cultured at 37°C.

2.5.2 Plasmids

GDF11 secretion assay—pLX302 GDF11-V5 puro (Addgene, 83097), pLX304 (wildtype) PCSK5-V5 blast (Addgene, 83100), and pLX304 PCSK5 (T288P)-V5 blast (Addgene, 83101) were described previously (Bajikar et al., 2017). pDONR223 PCSK5 (M452I) (Addgene, 232445) was prepared by QuikChange II XL site-directed mutagenesis (Agilent, 200521) of pDONR223 (wildtype) PCSK5 from the human ORFeome v5.1 and recombined into pLX304 (Addgene, 25890) with LR clonase II (Invitrogen, 11791020) to yield pLX304 PCSK5 (M452I)-V5 blast (Addgene, 232446). pcDNA3 was used as a carrier plasmid for lipofections, and pLX302 EGFP-V5 puro (Addgene, 141348) or pLX304 EGFP-V5 blast (Addgene, 232447) was used when diluting GDF11 or PCSK5 plasmid dosage and for negative controls. pcDNA3.1 HRAS (G12V) was kindly provided by David Kashatus.

Knockout and addback of PCSK5 alleles—For PCSK5 knockout, an sgRNA sequence (sg09, CTACACGGGAAAGAACATTG) was cloned into EDCPV (Addgene, 90085) by conventional restriction digest, oligo annealing, and ligation to yield EDCPV PCSK5_sg09 (Addgene, 232455). For PCSK5 addback, an inducible donor plasmid for PCSK5 was first constructed by PCR cloning of wildtype PCSK5 with a C-terminal V5 epitope tag into the SpeI–MfeI sites of pEN_TTmiRc2 (Addgene, 25752)

to yield pEN_TT PCSK5-V5 (Addgene, 232448). Next, an sgRNA-resistant (sgRR) allele of PCSK5 was prepared by introducing 3 silent mutations into pEN_TT PCSK5-V5 by QuikChange II XL site-directed mutagenesis (Agilent, 200521) to yield pEN_TT PCSK5(sgRR)-V5 (Addgene, 232449). The sgRR plasmid was further mutagenized to yield pEN_TT PCSK5(sgRR,M452I)-V5 (Addgene, 232450) and pEN_TT PCSK5(sgRR,T288P)-V5 (Addgene, 232451). Last, the three sgRR donor plasmids were recombined into pSLIK hygro (Addgene, 25737) with LR clonase II (Invitrogen, 11791020) to yield pSLIK PCSK5(sgRR)-V5 hygro (Addgene, 232452), pSLIK PCSK5(sgRR,M452I)-V5 hygro (Addgene, 232453), and pSLIK PCSK5(sgRR,T288P)-V5 hygro (Addgene, 232454).

Bioluminescence imaging—We removed the V5 epitope tag of pLenti PGK Blast V5-LUC (w528-1) (Addgene, 19166) by BamHI digestion and self-ligation to yield pLenti PGK Blast LUC (w528-1) (Addgene, deposition pending).

2.5.3 Computational assessment of PCSK5 mutations

Computational predictions for the mutations R486H (rs138257548, chr9:76159009G>A), A565T (rs145509473, chr9:76169777G>A), M452I (chr9:76157088G>T), and T288P (COSV65097476, chr9:76071866A>C) were made in November 2024 with PCSK5A (transcript ID NM_006200.6/ENST00000376752.9, protein ID NP_006191.2/ENSP00000365943.4). For AlphaMissense (J. Cheng et al., 2023; Tordai et al., 2024), PCSK5A was not available, and so PCSK5B (transcript ID ENST00000545128.5) was used instead. Predictions using AlphaMissense (J. Cheng et al., 2023; Tordai et al., 2024), Cscape (Rogers et al., 2017), MutationTaster2021 (Steinhaus et al., 2021), and PANTHER-PSEP (H. Tang & Thomas, 2016) were taken directly from the corresponding website with no change in default parameters. Predictions using FATHMM v2.3 (Shihab et al., 2013), LRT (Chun & Fay, 2009), Meta-RNN (C. Li et al., 2022), MutationAssessor r3 (RRID: SCR_024502), SIFT (Sim et al., 2012), and SIFT 4G 2.4 (Vaser et al., 2016) were aggregated by dbNSFP v4.7 (Liu et al., 2020). Predictions from computational tools were categorized as neutral (N), likely neutral (LN), unknown (U), likely damaging (LD), or damaging (D) as described in **Table 2.01**.

Table 2.01. Categorical grouping of PCSK5 mutation predictions.

	Neutral (N)	Likely Neutral (LN)	Unknown (U)	Likely Damaging (LD)	Damaging (D)
AlphaMissense	Likely benign				Likely pathogenic
CScape				Low-confidence oncogenic	High-confidence oncogenic
FATHMM	Tolerated				Damaging
LRT	Neutral		Unreported		Deleterious
Meta-RNN	Tolerated				Damaging
MutationAssessor		Functional—medium		Non-functional—low	
MutationTaster2021	Benign				Deleterious
PANTHER-PSEP				Possibly damaging	Probably damaging
SIFT	Tolerated				Damaging
SIFT 4G	Tolerated				Damaging

2.5.4 PCSK5 genotyping

Genomic DNA was isolated from standard cultures of MCF10DCIS.com and MCF10A-5E cells with the DNeasy Blood & Tissue Kit (Qiagen, 69504). The *PCSK5* locus was PCR amplified and sequenced with the following primers: GTGGGGCCCTGGAGAAAAA (forward), AAGAGCCCAGGGGTAAGCAT (reverse), ATCCCATAGGGTGGTGTCTG (sequencing). Total RNA was isolated from MCF10DCIS.com cells with the RNeasy Mini Kit (Qiagen, 74134) after culturing cells for 6 days in assay medium (Debnath et al., 2003) plus 2% growth factor-reduced matrigel (Corning, 356253) and 5 ng/ml EGF (Peprotech, AF-100-15). Total RNA was similarly isolated from MCF10A-5E cells cultured in growth medium. 250 ng RNA was reverse transcribed with oligo$(dT)_{24}$ and Superscript III (Invitrogen, 18080085), and the transcribed *PCSK5* locus was PCR amplified and sequenced with the following primers: CCCTGCCAGTCTGACATGAA (forward), TTTGTCGGTCTGTGCTCTCC (reverse), GTACCTGGAAGAGTGTTCATCC (sequencing).

2.5.5 PCSK5 antibody

The custom PCSK5 antibody was raised in rabbit to target the peptide sequence Ac-SPTNEFPKVERFRYSRC-amide (PCSK5-A amino acids 604–619) and affinity purified to a stock concentration of 1.82 mg/ml (Covance).

2.5.6 Quantitative immunoblotting

Cells were lysed in RIPA buffer supplemented with proteinase inhibitor cocktail, except for whole-cell PCSK5-V5 quantification, where cells were trypsinized, counted, and lysed in Laemmli sample buffer. Quantitative immunoblotting was performed as described (Janes, 2015) with primary antibodies recognizing the following targets: CDH1 (BD Biosciences, 610182; 1:1000 dilution), ERK1/2 (EMD Millipore, ABS44; 1:2000 dilution), HRAS (Santa Cruz, sc-520; 1:1000 dilution), p38 (Santa Cruz,

sc-535; 1:5000 dilution), PCSK5 (Covance, custom; 1:1000 dilution), TP63 (Biocare, 163A;, 1:500 dilution), tubulin (chicken polyclonal—Abcam, ab89984; 1:20,000 dilution or rabbit polyclonal—Cell Signaling, 2148; 1:2000 dilution), V5 (mouse monoclonal—Invitrogen, 46-0705; 1:5000 dilution or chicken polyclonal—Bethyl Laboratories, A190-118A; 1:5000 dilution), VIM (Abcam, ab16700; 1:300 dilution), and vinculin (Millipore, 05-386; 1:10,000 dilution). Primary antibodies were probed with IRDye 680RD- or 800CW-conjugated secondary antibodies (LI-COR; 1:20,000 dilution) and visualized on a LI-COR Odyssey infrared imaging system. For endogenous PCSK5 detection, a tertiary detection scheme was used involving unconjugated AffiniPure goat anti-rabbit IgG (Jackson ImmunoResearch,111-005-144; 1:1000 dilution) followed by IRDye 800CW-conjugated donkey anti-goat IgG (LI-COR, 926-32214; 1:20,000 dilution). For whole-cell PCSK5-V5 quantification, calibration was performed with serial dilutions of V5-containing recombinant Multitag protein (GenScript, M0101).

2.5.7 ProGDF11 convertase assay

HEK 293T/17 cells (ATCC, CRL-11268) were seeded in 24-well plates at a density of 100,000 cells per cm^2 one day before lipofection with Lipofectamine 3000 (Invitrogen, L3000015) and 500 total ng of pLX304 PCSK5-V5 blast (0–40 ng, with 3 ng optimal), pLX302 GDF11-V5 puro (100 ng), and pcDNA3 carrier plasmid (400–360 ng). Existing medium was removed before gentle addition of lipocomplexes in 100 µl DMEM (Gibco, 11965) combined with 250 µl growth medium per well. Edge wells were left unplated and filled with PBS to minimize evaporation effects of lipofected cells. After 24 hours, conditioned medium was collected, and the concentration of secreted GDF11 was quantified with a GDF11 ELISA (R&D Systems, DY1958). If needed, samples were pre-diluted in Reagent Diluent (R&D Systems, DY008B) to remain within the standard range of the assay (31–2000 pg/mL). The calibration curve was modeled by four parameter logistic regression and used to calculate concentration of mature GDF11 in unknown samples. When PCSK5 or GDF11 were reduced or omitted as controls, the corresponding EGFP plasmid was substituted. For $HRAS^{G12V}$ experiments, cells were co-transfected with a PCSK5 allele, GDF11, and 2 ng pcDNA3 $HRAS^{G12V}$. All secreted GDF11 concentrations were normalized to the GDF11/EGFP control condition from the same experiment.

2.5.8 Immunoprecipitation

GDF11-V5 was immunoprecipitated from 250 µl conditioned medium of transfected HEK 293T/17 cells with 1 µg mouse anti-V5 (Invitrogen, 46-0705) overnight at 4ºC followed by 10 µl Protein A/G Plus Ultralink Resin beads (Thermo Fisher, 53135) for one hour at 4ºC, followed by two washes with ice-cold

PBS. Beads were boiled in 2x Laemmli sample buffer and immunoblotted with chicken anti-V5 (Bethyl Laboratories, A190-118A; 1:5000 dilution).

2.5.9 Lentiviral transduction and cell selection

MCF10DCIS.com cells were seeded in 6-well plates at a density of 50,000 cells per well one day before three serial daily transductions with 500 µl of EDCPV PCSK5_sg09 lentivirus freshly prepared by calcium phosphate transfection of HEK 293T/17 cells (ATCC, CRL-11268) (L. Wang et al., 2011). Transductants were treated with 200 nM Shield-1 (AOBIOUS, AOB1848) in MCF10A assay medium supplemented with 5 ng/ml EGF (Peprotech, AF-100-15) and 2% growth factor-reduced matrigel (Corning, 356253) (Debnath et al., 2003) for 12 days. Venus-expressing cells were clonally sorted into 96-well plates with a Sony MA900 Cell Sorter (Sony MA900) at the University of Virginia Flow Cytometry Core and supplemented with 10 ng/ml recombinant GDF11 (Peprotech, 120-11) during clonal expansion. Genomic DNA was harvested from clones with the PureLink Genomic DNA Mini Kit (Thermo Fisher, K182001) and the PCSK5-sg09 target site was PCR-amplified (Millipore Sigma, 11732650001) with primers CAGCATGCTCTTCTTCTTTCAG (forward) and GAGTGTATGCTGTGGTTAGAAGGTC (reverse). Amplicons were cloned into TOPO plasmids (Invitrogen, 450030) and Sanger sequenced to verify successful PCSK5 knockout. GDF11 supplementation was removed after knockout verification to facilitate the subsequent lentiviral transduction. MCF10DCIS.com PCSK5$^{-/-}$ cells were transduced with 100 µl of pSLIK PCSK5(sgRR)-V5 hygro, pSLIK PCSK5(sgRR,M452I)-V5 hygro, or pSLIK PCSK5(sgRR,T288P)-V5 hygro lentivirus prepared by calcium phosphate transfection of HEK 293T/17 cells and stored at –80ºC (L. Wang et al., 2011). Transductants were selected with 100 µg/ml hygromycin (Sigma, H0654) until control plates had cleared.

2.5.10 Immunofluorescence

PCSK5 addback cells were seeded on coverslips in 6-well plates (275,000 cells per well) in MCF10DCIS.com growth medium supplemented with 100 µg/ml hygromycin (Sigma, H0654) and 1 µg/ml doxycycline. After approximately 24 hours, cells were fixed in ice-cold methanol for 5 minutes at –20ºC, and then immunofluorescence was performed as previously described (L. Wang et al., 2011) for the following targets: PDI (Thermo Fisher, MA3-019, 1:200 dilution), GM130 (BD Biosciences, 610823; 1:750 dilution), TGN38 (Thermo Fisher, MA3-063; 1:200 dilution), V5 (Bethyl, A190-118A; 1:1000 dilution), and α/□-Tubulin (Cell Signaling Technology, 2148; 1:100 dilution). Primary antibodies were visualized with Alexa Fluor 488-conjugated goat anti-mouse (Invitrogen, A11029; 1:200 dilution), Alexa Fluor 555-conjugated goat anti-chicken (Invitrogen, A21437; 1:200 dilution), and Alexa Fluor

647-conjugated goat anti-rabbit (Invitrogen, A21245; 1:200 dilution). After counterstaining with DAPI, coverslips were incubated with 10 mM $CuSO_4$ in 50 mM NH4Ac (pH 5.0) for 10 minutes at room temperature (Schnell et al., 1999) and then washed once with PBS before mounting. Mounted coverslips were imaged as 5–13 optical sections on a Leica STELLARIS 5 LIAchroic confocal laser-scanning microscope with a 63x 1.4 NA plan apochromat oil-immersion objective and the following acquisition parameters: 70.7 nm pixel size at 1.28x optical zoom; 2048 x 2048 $pixels^2$ field of view; 167 ns pixel dwell time; 500 nm z step size; 1 Airy Unit pinhole for a 520 nm emission; line accuracy = 2; 405 nm laser power = 2%; 488 nm laser power = 0.2% (PDI), 0.5% (GM130), or 2% (GM130, TGN38); 561 nm laser power = 2%; 638 nm laser power = 5%; and all detectors in photon-counting mode. Image stacks were deconvolved with Leica LIGHTNING deconvolution software using default parameters and an immersion medium of 90% glycerol + 10% water.

2.5.11 Fluorescence segmentation and image analysis

We used CellProfiler (Stirling et al., 2021) version 4.2.6 to analyze the optical section in each image stack that best captured secretory pathway staining for most cells. Each multicolor image was first thresholded above a photon count of 10 (V5, PDI, GM130, and TGN38) or 5 (DAPI). The DAPI signal was converted to a nuclear mask by a series of morphological operations (fill, diagonal, bridge, majority) to fill holes. The nuclear mask was globally thresholded with a diameter range of 80–350 pixels and then shrunk by 4 pixels. The tubulin signal was smoothed and combined with the nuclear mask to create a cell mask that was subsequently expanded by 10 pixels to ensure complete capture of the cell periphery. Colocalization of V5 with PDI, GM130, and TGN38 in the whole-cell mask of each cell was quantified by the Manders colocalization coefficient relative to total V5 immunoreactivity after excluding pixels with photon counts below the specified threshold for each marker. Colocalization coefficients were arcsine-transformed and batch corrected by study to account for variability in the extent of PCSK5 induction between days. The batch correction was hierarchically defined as the global mean of the arcsine-transformed means of each V5-organelle stain for that day. Mean V5 intensity in the nuclear mask of each cell was log-transformed and batch corrected by study. Cells with no above-threshold organelle staining in the optical section (0.03% of all cells segmented) were excluded from the analysis.

2.5.12 3D matrigel culture

Eight-well chamber slides (Fisher, 354108) were coated with 40 µl growth factor-reduced matrigel (Corning, 356253) and centrifuged at 4°C for 10 minutes at 1824 rcf. MCF10DCIS.com cells were seeded at 5000 cells per well in 400 µl MCF10A assay medium supplemented with 5 ng/ml EGF and

2% matrigel as described (Debnath et al., 2003). Where indicated, assay medium was supplemented with 250 ng/ml recombinant mature GDF11 protein (Peprotech, 120-11) throughout the experiment, or supplemented with 1 µg/ml doxycycline from Day 4 onward. Medium was replaced every 4 days, and cultures were imaged as 3x3 fields with a 4x apochromat air objective on an EVOS M7000 (Thermo Fisher, AMF7000) using DiamondScope software (version 2.0.2094.0).

2.5.13 Brightfield segmentation and image analysis

Spheroids were segmented with an updated OrganoSeg (Borten et al., 2018) software kindly provided by Cameron Wells. All studies used the following parameter settings: out of focus correction = yes, DIC correction = no, split whole image = no, edge correction = yes, size threshold = 650, window size = 300, contaminant intensity = zero, minimum circularity = zero, and segmentation closing structuring element size = 2. Study-specific parameters that depended on overall illumination and focusing were: intensity threshold = 0.5–0.9, edge correction = 0.25–0.35, image reconstruction structuring element size = 2–3, and use reconstructed image for edge correction = true or false. All other parameters were set to the software default. Segments were manually excluded as contaminants if they captured obvious debris, bubbles, 2D growth, or background illumination artifacts; or, if the segment did not accurately reflect an out-of-focus spheroid. Other study-specific refinements included exclusion of partially segmented spheroids, removal of out-of-focus image fields, and splitting of interconnected spheroids when present. From retained image segments, we exported cross-sectional area and circularity for analysis. Area measurements were batch-corrected for experimentalist by normalizing to the global Day 4 mean area calculated after subtracting the segmentation size threshold (650 pixels^2), adding an offset of 10 pixels^2, and log transforming (Przanowska et al., 2024). When necessary, circularities were batch-corrected for experimentalist by normalizing to the global mean circularity after arcsine transformation.

2.5.14 PCSK5 nuclear localization sequence prediction

Nuclear localization sequence predictions for PCSK5A (protein ID NP_006191) were made in March 2025 using cNLS Mapper (Kosugi et al., 2009) with a cutoff score of 2.0 or greater. The entire sequence was searched for bipartite nuclear localization sequences with a long linker.

2.5.15 Intraductal inoculation

For inoculation, PCSK5$^{-/-}$ MCF10DCIS.com cells with PCSK5 addback were transduced with pLenti PGK Blast LUC (w528-1) and selected with 10 µg/ml blasticidin until control plates had cleared. Female, virgin SCID/beige mice (Charles River, 250) were obtained at 7 weeks of age and housed together on a 10-hour dark cycle (8 pm–6 am) and 14-hour light cycle (6 am–8 pm) at 21.5°C and

31.5% relative humidity. Mice were given a standard rodent diet. Mice were anesthetized with isoflurane, depilated, and the nipple tip of the fourth mammary glands were cut off with a fine scissor. Each luciferase-expressing PCSK5 addback variant was suspended at a concentration of 20,000 cells/ml in growth medium, loaded into a 30-gauge blunt needle (Hamilton, 80508), and injected into the fourth and ninth mammary gland (2 µl per gland). Mouse surgical order and left-right gland assignments for the PCSK5 genotypes (N = 10 injections per genotype) were randomized. Mice were switched to rodent food containing 625 mg/kg doxycycline (Harlan, TD.05125, IF060, HF030) starting one week after surgery, which was maintained until the end of the study. All animal work was done in compliance with ethical regulations under University of Virginia IACUC approval #3945, which permitted a maximal tumor size of 2.0 cm that was not exceeded by this study.

2.5.16 Bioluminescent imaging and analysis

Mice were imaged for bioluminescence at 2, 7, 14, 21, 28, 35, 42, 49, and 54 days post-surgery after isoflurane anesthesia and intraperitoneal administration of 150 µg D-luciferin (Promega, E1605) per gram body weight. At 5–10 minutes post-injection of D-luciferin, bioluminescence was collected every 2 minutes for 15–20 minutes on a Lago X (Spectral Instruments Imaging) with Aura Imaging Software (version 4.0.7) at the University of Virginia Molecular Imaging Core. The peak emission (photons/s) across all 2-minute images per gland was taken as the bioluminescence readout for that time point after inoculation. Bioluminescence was compared longitudinally by normalizing each gland to its peak emission averaged across Days 2, 7, and 14. This normalization accounts for gland-to-gland differences in inoculum volume and viability. Multiway ANOVAs considered cage number and left-right gland injections as fixed effects alongside PCSK5 genotype.

2.5.17 Mammary gland harvest and histology

Mice were euthanized at 54 days post-surgery and perfused with 4% paraformaldehyde before gland harvesting (Ip & Asch, 2000) and additional fixation in 4% paraformaldehyde for 24 hours. Samples were paraffin embedded, cut as 4–5 µm sections, and hematoxylin–eosin stained by the University of Virginia Research Histology Core.

2.5.17.1 Histological analysis

One or two representative sections from each mammary gland were selected for analysis after digital acquisition on an Aperio ScanScope. Sections were sub-divided into multiple ductal cross-sections with a distinct outer stroma. Ductal cross-sections were excluded from the analysis if (major axis) x (minor axis) ≤ 12,000 μm^2, if the section was tangential to a duct, or if the minimum Feret diameter of the

lesion was greater than 5 mm at dissection. Ductal cross-sections were scored positive or negative for the pathologic features summarized in **Table 2.02**. Scores were summarized gland-wise as the fraction of ductal cross-sections positive for each feature.

Table 2.02. Criteria for pathological features scored in MCF10DCIS.com intraductal xenografts.

Category	Pathologic feature	Description
DCIS growth patterns	Papillary	MCF10DCIS.com cells arrange around a fibrovascular core
	Micropapillary	MCF10DCIS.com cells arrange around a capillary vascular core without a fibrous component to the core
	Solid	MCF10DCIS.com cells fill the luminal space without any duct formation in the cellular component
	Cribriform	MCF10DCIS.com cells arrange as smaller ducts within the main duct, creating circular or irregular slit-like spaces
Comedo necrosis	Large comedo necrosis	Necrotic regions with at least one dimension greater than 300 μm
	Small comedo necrosis	Necrotic regions consisting of more than a few cells but with no dimension greater than 300 μm
	Punctate necrosis	Necrosis of a single or small number of cells
Stromal characteristics	Hypercellular stroma	Increased abundance of periductal stromal cells, immune cells, or both
	Irregular peripheral interface	Inter-anastomosing small ducts at the inner surface of the main duct, preventing a smooth DCIS-stroma interface, excluding single cell infiltration
	Intraductal stromal proliferation	Stromal cell proliferation that meanders through the ductal space
Other	Gaps	Open regions within the duct that lack proliferation of DCIS cells
	Secretion	Acellular fluid within the lumens, gaps, or regions of comedo necrosis

2.5.18 Statistics

All hypothesis tests are specified in the corresponding figure caption. Nonlinear least squares curve fitting was performed with the nlinfit function in MATLAB (Mathworks, R2023b), with confidence intervals estimated by the nlparci function.

2.6 Authors' Disclosures

No disclosures were reported.

2.7 Authors' Contributions

T. Marohl: Conceptualization, data curation, formal analysis, funding acquisition, investigation, methodology, validation, visualization, writing – original draft, writing – review & editing. **K.A. Atkins:** Formal analysis, methodology, supervision. **L. Wang:** Data curation, funding acquisition, investigation, project administration, validation, writing – original draft, writing – review & editing. **K.A. Janes:** Conceptualization, formal analysis, funding acquisition, investigation, methodology, project administration, supervision, visualization, writing – original draft, writing – review & editing.

2.8 Acknowledgments

We thank Piotr Przanowski for technical help with the mammary gland harvests, Cameron Wells for providing advance access to OrganoSeg2, and Sameer Bajikar and Daniel Gioeli for critically reviewing this manuscript. This work was supported by grants from the NIH (R01-CA214718 to KAJ, KAA and R50-CA265089 to LW), CBIO experimental funding support from the University of Virginia Comprehensive Cancer Center (PJ04191 to KAJ), a graduate research fellowship from the NSF (2018256910 to TM), a Dean's Fellowship from the University of Virginia School of Engineering and Applied Science (to TM), and a Distinguished Fellowship from the Commonwealth of Virginia (to TM). Data were partly generated in the University of Virginia Flow Cytometry Core Facility (RRID: SCR_017829), the Research Histology Core Facility (RRID: SCR_025470), the Biorepository and Tissue Research Facility (RRID: SCR_022971), and the Molecular Imaging Core Facility (RRID: SCR_025472), which are partially supported by the UVA Comprehensive Cancer Center support grant (P30-CA044579).

Chapter 3: Research Significance, Future Directions, and Conclusion

3.1 The Unusual Circumstances of the MCF10DCIS Cell Line

During the derivation of the MCF10 family of cell lines, dozens if not hundreds of mice were injected with myriad derivatives, spanning multiple generations, of the parental MCF10A line. Of all of these cell lines, only MCF10DCIS forms lesions that are predominantly DCIS. Numerous other MCF10 cell lines yield DCIS lesions upon xenograft, but DCIS is just one of many lesion morphologies (e.g. mild, moderate, and atypical hyperplasia; glandular or squamous invasive carcinoma) that arise from those cell lines (Dawson et al., 1996; Miller et al., 1993). This rarity speaks to the specificity of biological circumstances that allow a cell line to survive *in vitro*, a process characterized by the ability to proliferate indefinitely on a rigid substrate (Dai et al., 2017), and also to consistently produce a particular growth pattern *in vivo*, characterized by proliferation but also restraint from invading into the periductal stroma.

Interestingly, the more advanced MCF10CA1 cell lines, which rapidly form advanced tumors upon xenograft, could only be derived from a lesion that grew following multiple generations of *in vivo* passaging of small tumor pieces from one mouse directly to another (H Heppner et al., 2000; Santner et al., 2001; Strickland et al., 2000). In all prior attempts using the $HRAS^{G12V}$-transformed MCF10AneoT cell line and its derivatives to grow lesions and re-establish cells from those lesions *in vitro*, subsequent injection of the cell lines into nude mice resulted first in the growth of normal ducts, followed by the slow and variable progression of those ducts through the stages of proliferative breast disease (Dawson et al., 1996; Miller et al., 1993). It seems that something about the sequential *in vivo* passages permitted the growth of descendant lesions whose cells could grow *in vitro* and also directly produce invasive carcinomas *in vivo*.

Unfortunately, the exact family tree of MCF10DCIS is unclear in the literature (Miller, 2000; Miller et al., 2000). Therefore, we cannot reflect on the exact nature of the mice or the lesions that preceded MCF10DCIS: for example, the sex or strain of mice (male and female, and nude and nude/beige mice were used during derivation of the MCF10 lines), the length of time the lesions grew *in vivo* before harvest, and the morphology of those lesions. However, our study of the $PCSK5^{M452I}$ mutation provides reassurance that this unique aspect of MCF10DCIS, at least, is not a concern in the heterozygous case.

3.2 On the M452I Mutation of PCSK5 in MCF10DCIS Cells

The considerations for interpretation of the M452I mutation that arises in the MCF10A series of cell lines are multifold. The motivation for this project came from a 2016 report on the genomic and

transcriptomic features of 7 MCF10 cell lines (Maguire et al., 2016). Specifically, it was reported that "four predicted cancer driver mutations [were] acquired during transformation of non-malignant MCF10A cells to malignant DCIS.com cells (HRAS, EPHA7, MAP3K12, and PCSK5)" (Maguire et al., 2016). We knew of PCSK5 from its role in the processing of TGFβ-family member GDF11, which plays a tumor suppressive role in triple-negative breast cancer (Bajikar et al., 2017). GDF11 preserves epithelial characteristics and prevents invasion, but its activity is lost in triple-negative breast cancer due to downregulation of its convertase, PCSK5 (Bajikar et al., 2017). Since the MCF10DCIS cell line exhibits restraint from invasion, a characteristic that is rare among cancer cell lines, we reasoned that the PCSK5 mutation might be activating, thereby turning up GDF11 signaling and its pro-epithelial effects. When we looked at the variant allele frequency plot (VAF) for PCSK5 in the MCF10 series (**Figure 3.01, top**), the situation became even more interesting: while the mutation was present in all cell lines from MCF10neoT on, the VAF was highest — 50% — in the MCF10DCIS.COM line. This raised the possibility that the M452I mutation was especially beneficial to MCF10DCIS among MCF10 cell lines. We searched The Cancer Genome Atlas and COSMIC for records of the M452I mutation in clinical cases and found no hits; M452I had not been recorded in any type of cancer. Further, the NIH's dbVar and ClinVar databases did not have record of any germline mutations at this site. Generally, mutation of PCSK5 in cancer is rare. If M452I conveyed properties upon the MCF10 cell lines that specifically contributed to the DCIS characteristics of MCF10DCIS xenografts, then this model of human DCIS had the potential to be very misleading. Because of the importance of MCF10DCIS to the field of DCIS, particularly hormone-negative DCIS, we felt it prudent to evaluate the effects of this mutation on the salient characteristics of the MCF10DCIS model.

Only recently did I realize there was another layer to the PCSK5 mutation in the MCF10 series. The *PCSK5* locus in humans resides in 9q21.13. During the initial cell culture of MCF10 cells before the separation of MCF10A and MCF10F but after spontaneous immortalization, the cells acquired a balanced reciprocal translocation, t(3;9)(3p13:9p22) (Soule et al., 1990). All MCF10 lines also have a homozygous CDN2A deletion that crosses from the p to q arms (Kadota et al., 2010). Neither of these chromosomal alterations affected the PCSK5 locus. However, while chromosome 9 is diploid in MCF10A, it has 3 copies in some of the derivative cell lines (**Figure 3.01, bottom**). A 2010 study shows amplification of chromosome 9 in the MCF10AT1 clonal subline MCF10AT1k.cl2 (referred to as MCF10AT in the text), MCF10CA1a.cl1 (clonal; referred to as MCF10CA1a in the text), and MCF10CA1h (presumably the polyclonal version, but this is not specified) (Kadota et al., 2010). Per the 2016 Maguire, *et al.* analysis, the copy number of chromosome 9 bounces around in the MCF10 cell lines MCF10AT1 (unspecified whether this is actually the polyclonal AT1 or a shorthand for the clonal MCF10AT1k.cl2), MCF10CA1a.cl1 (clonal; referred to as MCF10CA1a in the text), MCF10CA1d.cl1 (clonal; referred to as MCF10CA1d in the text), and MCF10CA1h (presumably the polyclonal version,

but this is not specified) (Maguire et al., 2016). Given the lack of precision in methods sections describing the MCF10 cell line series derivation and the possibility of drift over time, it is highly possible that the lines designated as clonal were actually not clonal at the time of these studies.

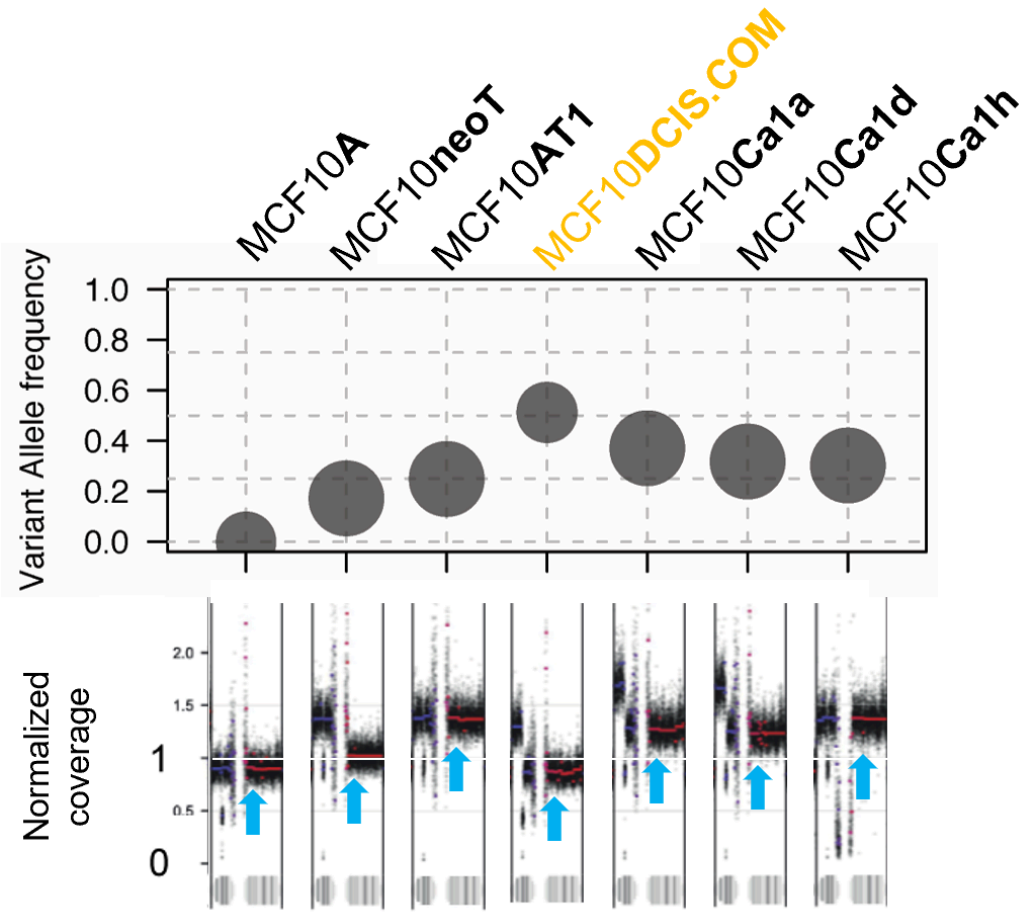

Figure 3.01. PCSK5 variant allele frequency and copy number in MCF10 cell lines. [Adapted from (Maguire et al., 2016)]

Top, Variant allele frequency (VAF) of PCSK5 p.M452I in the MCF10 cell line series. **Bottom**, Copy number alteration for chromosome 9 in the MCF10 cell lines. White horizontal line marks normalized coverage = 1 and blue arrows mark the approximate location of the PCSK5 locus, 9q21.13. *Figures are adapted from an open access article (Creative Commons CC BY license).*

MCF10AT1k.cl2 is a derivative of MCF10AneoT and is the progenitor of all MCF10CA1 lines. I suspect that MCF10DCIS also belongs to this branch, due to its description as being “cloned from a cell culture initiated from a xenograft lesion obtained after two successive trocar passages of a lesion formed by premalignant MCF10AT cells” (Miller et al., 2000), but I cannot be certain. For this discussion we will assume that, like MCF10CA1, MCF10DCIS is a derivative of MCF10AT1k.cl2 (which definitely has amplification of chromosome 9 per Kadota et al., 2010, but may or may not be the exact cell line labeled as MCF10AT1 in **Figure 3.01,** adapted from Maguire et al., 2016). The M452I mutation first arose during derivation of MCF10AneoT, presumably in a subset of cells due to its ~20% VAF; at this

time, the q arm of chromosome 9 was not amplified. From MCF10neoT to MCF10AT1, 9q becomes triploid and M452I is at ~25% VAF (possibly this represents 1 of 3 alleles mutated). From MCF10AT1 to MCF10DCIS, 9q reverts to diploid and the M452I VAF increases to ~50%, indicating that MCF10DCIS cells are heterozygous for the mutation, presumably by losing a copy of 9q harboring wildtype PCSK5. From MCF10AT1 to the MCF10CA1 lines (we have no conclusive evidence that MCF10DCIS is a predecessor of the MCF10CA1 lines), 9q is retained at triploid and a VAF of ~30-35% suggests that one copy harbors M452I. The split chromosome amplification pattern that is shared between MCF10DCIS and MCF10CA1a and MCF10CA1d raises the question whether MCF10DCIS is indeed a progenitor of the MCF10CA1 lines. Alternatively, there could have been a shared intermediate predecessor that was a descendant of MCF10AT1 but not saved and profiled; this is certainly plausible given that the MCF10DCIS and MCF10CA1 lines were derived via successive trocar passages without re-establishment of intermediate generations *in vitro*.

If the copy number and allele variant transitions occurred as described, this suggests that the M452I mutation of PCSK5 became heterozygous in MCF10DCIS by a different mechanism than we initially thought. Instead of a low-prevalence heterozygous subpopulation being selected for (amid a majority of cells that were diploid homozygous wildtype) in the MCF10DCIS derivation process, a heterozygous diploid subpopulation was selected for (amid a majority of cells that were triploid with one copy of M452I). I use “selected for” here simply to mean the subpopulation from which MCF10DCIS arose, not to indicate that any characteristics of that subpopulation actually conferred a selective advantage. I believe our study of PCSK5^{M452I} was still warranted. It is indeed possible that a heterozygous diploid subpopulation could be advantaged by its higher VAF compared to a triploid population with one mutant copy. However, this would suggest that co-expression of the wildtype and mutant alleles results in some interaction effect between the wildtype and mutant that renders it beneficial to have a 1:1 wildtype to mutant ratio rather than 2:1. Our coexpression experiment in 293T cells suggested that the wildtype and M452I variants do not interact, as the concentration of secreted GDF11 was intermediate in the context of heterozygous PCSK5 compared to wildtype or M452I alone. Further, based on our understanding of PC protein synthesis and activation, the first autocatalytic cleavage event in the ER is intramolecular, meaning two PCSK5 variants would not affect one another in *trans* (Leduc et al., 1992). This is true for furin, but I was unable to find any literature directly testing this property in PCSK5. If the pro-domain is missing, the protease settles in a partially folded state and remains in the ER; addition of a recombinant propeptide can rescue trafficking via *trans*-activation (Anderson et al., 2002; Baker et al., 1992; J. W. M. Creemers et al., 1995; De Bie et al., 1996; Eder et al., 1993b; Strausberg et al., 1993). We have no evidence, however, that an endogenous cleaved pro-domain would be present in the ER, as the second cleavage event during which the pro-domain dissociates from the mature protein does not occur until the protein has reached the trans Golgi or the

cell surface (Mayer et al., 2008). Further, our IF experiment did not indicate that M452I accumulates in the ER. Instead, we found a moderate increase in M452I abundance in the trans Golgi. Transport of the proprotein to the trans Golgi has been shown to occur only if the initial cleavage step took place and the pro-domain is still associated with the protease (Anderson et al., 2002; Nour et al., 2003). The final PCSK5 activation step occurs in the trans Golgi or at the cell surface where PCSK5 is tethered by a complex of TIMPs and HSPGs (Nour et al., 2005). While it is known that ACTH or cAMP stimulate PCSK5 activation at the cell surface, the exact mechanism by which PCSK5 is activated has not been elucidated. It is possible that the secondary cleavage occurs in *trans*. There are cell surface-associated ligands for which activation requires the presence of two convertase molecules (Butler et al., 1998; Kai et al., 2002; Nour et al., 2005; Overall et al., 1999; Zucker et al., 1998). By western blot of cell lysates, the ratio of pro-to-mature PCSK5 is slightly higher for the M452I variant than for wildtype. If surface-bound PCSK5 is collected in the cell protein extract, bound but inactive PCSK5^{M452I} could account for this increase. We have not tested the abundance of pro or mature PCSK5 in conditioned medium. Perhaps this could shed light on the question at hand.

3.2.1 Structural Context of M452I in PCSK5

Although the crystal structure of PCSK5 has not been solved, the protein has fairly high identity with furin, the structure of which has been known since the early 2000s. Overall PCSK5 and furin have 60% residue identity, with 65% in the catalytic domain and 48% in the P domain (Henrich et al., 2005). The PC ectodomain (excluding the pro-domain and C-terminal CRD) structure consists of two separate but adjacent domains, the spherical catalytic domain and the barrel-like P domain, which are covalently linked. The catalytic domain consists of a “highly twisted β-sheet” containing seven parallel and one antiparallel β-strands (**Figure 3.02, yellow**) and five adjacent and two peripheral α-helices (**Figure 3.02, pink**) (Henrich et al., 2003, 2005). The β-sheets and α-helices are arranged to form a “deep active-site cleft” that frames the catalytic triad (in furin: Ser368 - His 194 - Asp153, in PCSK5: Ser386 - His212 - Asp171).The catalytic residues are components of α5, α2, and β1, respectively. The α-helix containing M452I is arranged with the helix containing Ser386 and a third helix in a semi-parallel configuration (**Figure 3.02**). The methionine side chain protrudes into the middle of this prism and therefore could contribute to the stability of the tertiary structure that emerges from these three alpha helices. Mutation of methionine to isoleucine has potential to alter those forces, which could result in a conformational change at the active site that hinders substrate access or interaction.

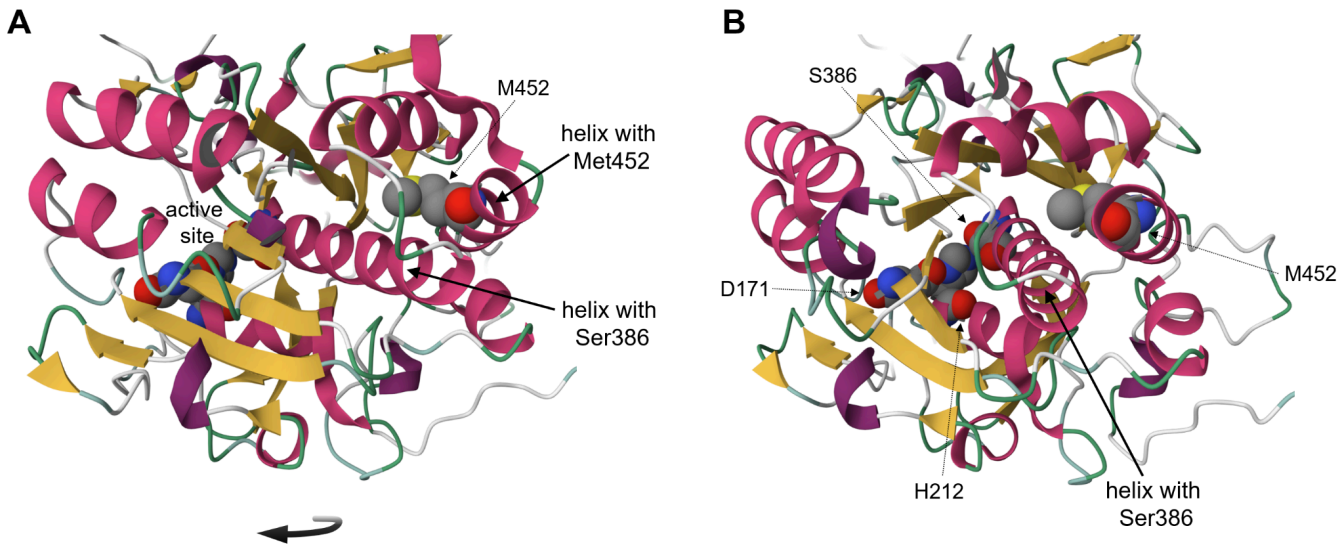

Figure 3.02. 3D rendering of PCSK5 active site and M452. Structure AF-Q92824-F1-v4 from AlphaFold (Jumper et al., 2021; Varadi et al., 2024)).

A, View showing the helix containing M452 and the two adjacent helices, including the helix with S386 on the left side at the active site. **B**, View slightly turned from (A) looking down the helices containing M452 and S386. At the far end of the helix containing S386 is the active site, where S386 meets D171 and H212. *Structure images generated in AlphaFold.*

3.3 MCF10DCIS PCSK5 Addbacks In Vivo

The xenograft lesions resulting from MCF10DCIS PCSK5 addback cells display a remarkable degree of phenotypic diversity. Recalling that the MCF10DCIS cell line is clonal, and that the addback lines were generated from a single PCSK5$^{-/-}$ clone of MCF10DCIS, it is impressive that we see DCIS with cribriform, papillary, micropapillary, and solid growth patterns, as well as comedo necrosis, represented within each individual PCSK5 addback genotype and in many cases, within the same mammary gland. The original paper characterizing the MCF10DCIS cell line found it to consistently form comedo-type DCIS lesions and did not hint at such phenotypic diversity (Miller et al., 2000). The difference is likely due at least in part to the xenograft site; they were initiated subcutaneously in the original work whereas in our study they were initiated intraductally. In the first experiments of MCF10DCIS xenograft via the intraductal model, the authors noted that the DCIS exhibited a cribriform pattern and postulated that the difference was likely due to the site of injection (Behbod et al., 2009). Although we did observe cribriform growth in a high fraction of glands (Supplemental Figure S6A), it was certainly not the only growth pattern present and in most lesions it was not the predominant growth pattern. A larger study may be necessary to discern any genotype-specific differences in DCIS growth pattern; perhaps earlier timepoints would also be useful.

Numerous injected mammary glands formed very large tumors (**Figure 3.03 A**), some in addition to smaller lesions. These tumors were excluded from the histological analysis due to their

extreme size, suggesting they had escaped the mammary duct. At dissection, the diameters of the large tumors ranged from 5-15 mm, whereas the diameters of the smaller lesions that were profiled histologically were on the order of 1-3.5 mm. Out of 10 glands for each genotype, three wildtype, one M452I, and two T288P glands contained large tumors. In the original paper describing the derivation of MCF10DCIS, early-passage and late-passage cells were shown to have different propensities for invasion upon xenograft (Miller et al., 2000). MCF10DCIS "within 22 passages resulted in rapidly growing lesions that are predominantly comedo DCIS… Although early (3-week) lesions are predominantly DCIS, invasive areas develop and may account for half of the older (9-week) lesions." Conversely, "late-passage cells (passage 37) have a more extensive invasive component… [They] formed mixed lesions with major invasive components in three independent experiments" (Miller et al., 2000). Our MCF10DCIS parental stock is passage 4 and the PCSK5 addback cells used for the animal experiment were passage 18, well within the early passage range referenced in the original work. However, the cells did undergo extended time in culture during the multiple transductions and sorting steps involved with PCSK5 knock-out, PCSK5 addback, and addition of luciferase. We harvested mammary glands at nearly 8 weeks post-inoculation; given that half of the lesions had invasive areas at week 9 in the original MCF10DCIS paper, the number of large lesions that we observed seems consistent with past studies.

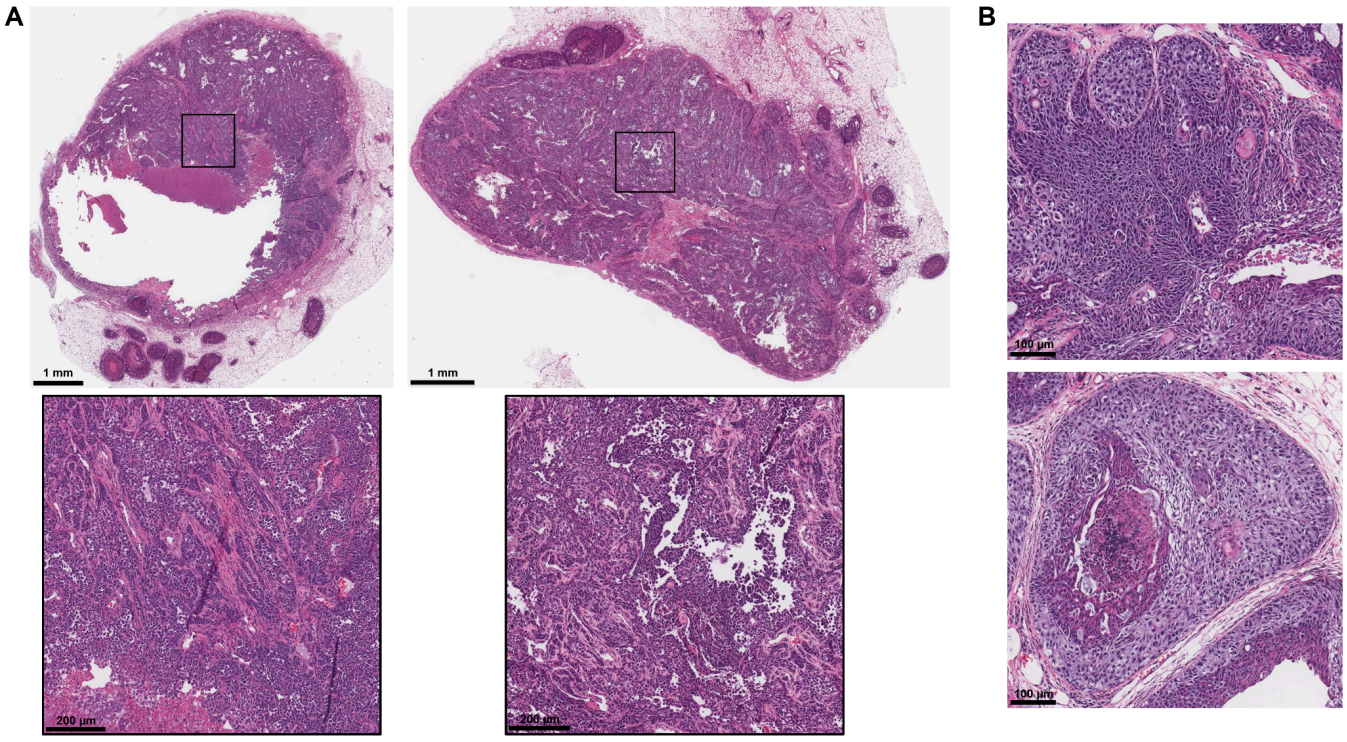

Figure 3.03. MCF10DCIS PCSK5-addback H&E.

A, Two examples of large tumors (top) with zoomed regions (bottom) in PCSK5^{WT} mammary glands. **B**, Two examples of squamoid cells in PCSK5^{M452I} mammary glands.

Squamoid cells were present in a small number of lesions; curiously, we only observed them in the PCSK5^{M452I} condition (**Figure 3.03 B**). Lesions in three PCSK5^{M452I} glands (from three separate mice) contained squamoid cells. Squamoid growth has been described before in the MCF10 series. When inoculated subcutaneously, MCF10AT and its successive transplant generations progress to invasive carcinoma in one-quarter of xenografts; of those that progress, most were adenocarcinomas but one-sixth of the carcinomas were undifferentiated with squamoid features (Iravani et al., 1998). The undifferentiated carcinomas contained only occasional small ducts (in striking opposition to the omnipresent ducts in adenocarcinoma samples), were not proliferative, and stained positive for p53 (Iravani et al., 1998). Xenografts of the malignant MCF10CA1 cell lines also produced some undifferentiated carcinomas that contained focal regions of squamoid cells (Santner et al., 2001). The authors did not postulate an explanation for the emergence of squamoid cells in MCF10-series xenografts; however, squamous differentiation has been observed in the context of anoikis when epithelial ductal cells are deprived of matrix attachment, leading to luminal clearing (Mailleux et al., 2007). In mammary development, breast terminal end buds give rise to a luminal space during ductal expansion, which requires clearance of inner cells via apoptosis. 3D MCF10A spheroids also generate a hollow lumen via apoptosis. In both cases, BIM, a member of the proapoptotic Bcl-2 family, activates cytochrome c release and caspase activation to induce apoptosis. However, BIM-null mice undergo some degree of caspase-independent death which manifests as squamous differentiation prior to ductal hollowing. Similarly, MCF10A cells deprived of ECM attachment *in vitro* underwent squamous differentiation. It is therefore possible that the squamoid cells observed in PCSK5^{M452I} lesions in our study are indicative of anoikis.

As PCSK5 processes a number of substrates associated with ECM remodeling, this result nods to the importance of following up on our PCSK5-GDF11 cleavage assay results by testing the cleavage of other substrates by PCSK5^{M452I}. While it is impossible to rule out a gain-of-function (e.g. the ability to cleave substrates that wildtype PCSK5 cannot), it would be reassuring to find that cleavage assays using other substrates mirror the patterns of GDF11 cleavage by the PCSK5 genotypes. There is precedent for evaluating PCSK5 activity via cotransfection cleavage assay using substrates GDF11, BMP4, or LEFTY1 (Szumska et al., 2008). For measuring PC activity in a general sense, conditioned medium containing secreted PCSK5 is typically incubated with a fluorogenic peptide substrate (pERTKR-AMC; Bachem; Torrance, CA) (Andersson et al., 2006; Essalmani et al., 2006; Heng et al., 2010; Sun et al., 2011; Szumska et al., 2008). While it is common in the literature to directly evaluate PC cleavage of substrates in a test tube, it has been wisely pointed out that "*In vitro* cleavage studies are of limited use for this purpose, as they tend to generate false positives due to non-physiological stoechiometries and the absence of cellular context" (J. W. M. Creemers & Khatib, 2008). Screening of

additional histological sections from PCSK5^{WT} and PCSK5^{T288P} lesions would also be useful to determine if squamoid cells are indeed found uniquely in PCSK5^{M452I} lesions.

3.4 PCSK5 in Embryonic Implantation

The biological context in which PCSK5 has been studied most extensively is in the uterus during embryonic implantation. In many ways, the processes involved in DCIS - both its restraint to remain within the duct and its progression to IDC - resemble those involved in embryonic implantation. I think it would be fruitful for these two fields to collaborate, both in regards to PCSK5 research and also for understanding DCIS and embryonic implantation more generally. I find the parallels between these two contexts fascinating, and therefore dedicate a significant length to a review of the role of PCSK5 in embryonic implantation. It is important to note that PCSK5 in embryonic implantation literature is referred to most commonly as PC6 (or, in older papers, SPC6) due to historical convention; I editorialize here to PCSK5, but it is worth pointing out that this difference in nomenclature may serve as a barrier to organic collaboration between the fields of cancer biology and embryonic implantation.

3.4.1 Biology of Decidualization and the Role of PCSK5

First, the briefest of anatomy and physiology lessons: The endometrium lines the inner cavity of the uterus (**Figure 3.04, "Uterus"**). Interfacing with the lumen are the luminal epithelial cells, which are elongated and display a high degree of polarity (**Figure 3.04, "Endometrial tissue"; Figure 3.05, Panel A, "Surface Epithelium"**). Glandular epithelial cells interface with the glands (**Figure 3.05, Panel A, "Glands"**). Below these lie the endometrial stromal cells, which become decidual cells during decidualization (**Figure 3.05, Panel A, "Stroma"**). For pregnancy to occur, a fertilized egg must travel down the fallopian tube to the uterus; undergo cell division and differentiation to form a blastocyst; and make contact with, adhere to, and invade the uterine epithelium and its underlying stroma. Decidualization is the process by which the endometrial stroma prepares for and accommodates the implantation of the blastocyst into the endometrium (**Figure 3.04, "Endometrial stromal cells (ESCs)"; Figure 3.05, Panel B**).

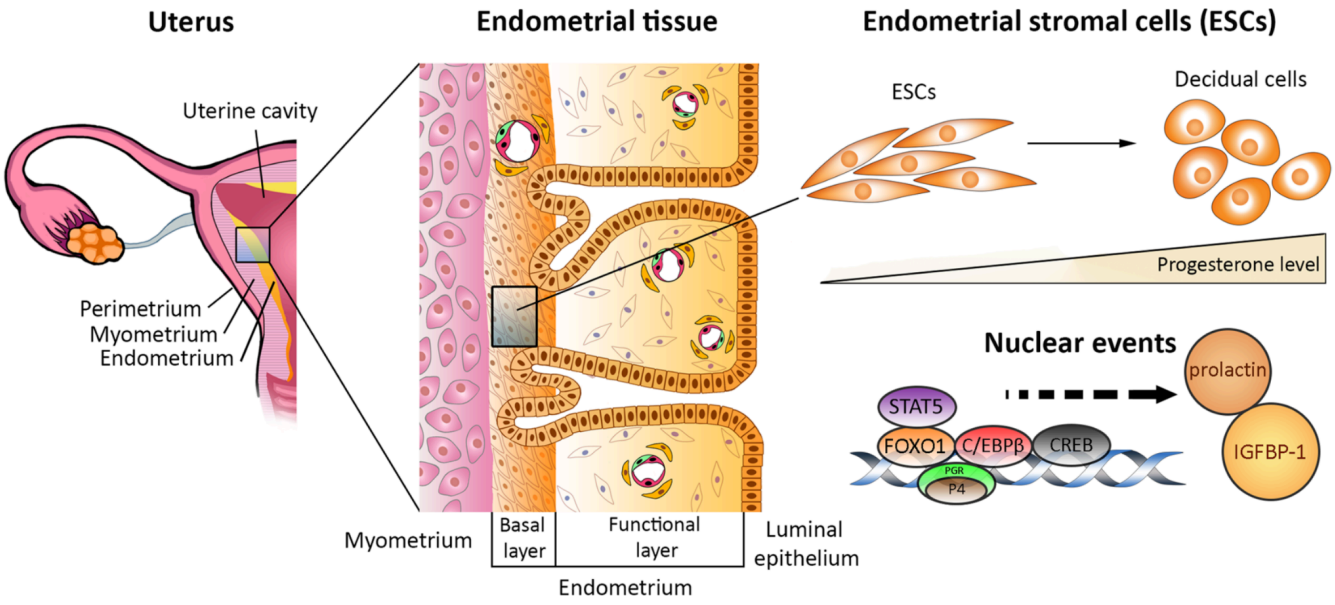

Figure 3.04. Diagram of the uterus, endometrial tissue, and endometrial stromal cells. [Figure 2 from (Deryabin et al., 2020)]

Uterus, Anatomy of the uterus including the central uterine cavity and three tissue layers: endometrium—the inner lining, myometrium—the muscle layer, and perimetrium—the thin outer layer of epithelial cells. **Endometrial tissue**, Anatomy of the endometrium and myometrium showing the basal and functional layers of the endometrium. **Endometrial stromal cells**, Transformation of endometrial stromal cells (ESCs) to decidual cells in response to progesterone and associated nuclear events. *Used with permission from Springer Nature (license number 6013681100118, April 21, 2025).*

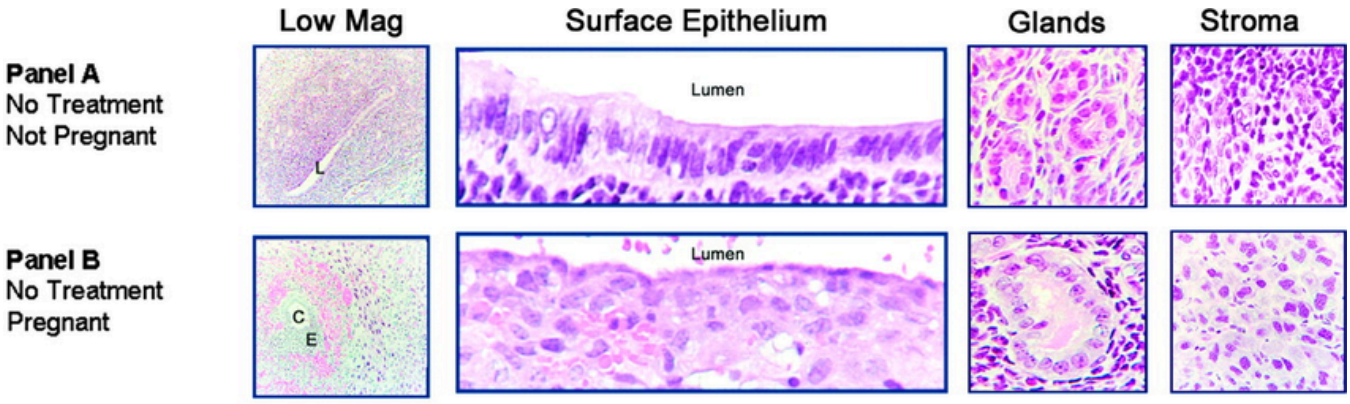

Figure 3.05. Hematoxylin and eosin-stained uterine sections from non-pregnant and pregnant mice. [Figure 1 from (M. Tang, Taylor, et al., 2005)]

Panel A, Appearance of non-pregnant uterine tissue including a slender lumen (marked L in the Low Mag image) and a compact stroma. **Panel B**, Appearance of pregnant uterine tissue including an embryo within the amniotic cavity (marked E and C, respectively, in the Low Mag image) and decidual cells in the surface epithelium characterized by their typical epithelioid appearance and enlarged nuclei. *Used with permission from Oxford University Press (license number 6013690496269, April 21, 2025).*

In mice, blastocyst formation occurs at day 3.5 of gestation (day 1 being the day of the vaginal plug), implantation at days 4.5-6, and formation of the yolk sac at days 6-8 (Cross et al., 1994). Starting

around the time of blastocyst formation, in response to progesterone released by the ovaries (Okada et al., 2005, 2018; Wetendorf & DeMayo, 2012), the uterus enters a “window of receptivity” during which it is responsive to tactile stimuli and can detect contact by the embryo (Carson et al., 2000; Wong et al., 2002). Soon after embryo contact, the uterus begins a critical process known as decidualization, where the fibroblast-like uterine stromal cells differentiate into specialized secretory epithelioid decidual cells (Jia et al., 2024; Wong et al., 2002). The uterine epithelium, normally characterized by distinct organization and strong polarization, undergoes loss of apical and basolateral membrane domains and remodeling of the actin cytoskeleton in a process resembling epithelial-to-mesenchymal transition (Carson et al., 2000; Denker, 1993; Heng, Cervero, et al., 2011). As the embryo begins invading the uterine decidua (i.e. implantation), its trophoblast cells secrete ECM-degrading proteinases, including MMP9, to mediate erosion of the uterine epithelium, stroma, and ultimately maternal blood vessels (Alexander et al., 1996; Schultz & Edwards, 1997; Wong et al., 2002). At the same time, the decidua regulates the extent of embryo invasion. For example, decidual cells immediately surrounding the embryo express mRNA of TIMP-3, a tissue inhibitor known to block MMP9, therefore establishing a guard rail on invasion (Alexander et al., 1996; Das et al., 1997; Rancourt & Rancourt, 1997; Schultz & Edwards, 1997; Wong et al., 2002). This entire complex process takes place over only a few days, with the invasive embryo kept in check by the finely tuned permissiveness of the uterine decidua.

Research spanning multiple decades has repeatedly demonstrated an important role for PCSK5 in uterine remodeling to accommodate blastocyst implantation. Studies in mice have mapped out the specific spatiotemporal expression patterns of PCSK5 during decidualization and implantation. PCSK5 mRNA is detected in the mouse uterus as early as day 3.5, and from days 4.5-6.5 it is strongly expressed in the decidua at the implantation site (Nie et al., 2003; Rancourt & Rancourt, 1997; Wong et al., 2002). From days 7.5-8.5, PCSK5 expression in the uterus shifts toward the site of placental formation, and by day 9.5, expression is gone (Nie et al., 2003; Wong et al., 2002). In multiple studies, PCSK5 mRNA was not detected in the embryo itself at these timepoints (Nie et al., 2003; Rancourt & Rancourt, 1997), although low expression was detected in trophoblasts surrounding the embryo (Rancourt & Rancourt, 1997). Similar patterns of PCSK5 upregulation during decidualization and implantation were observed in rabbits (Nicholls et al., 2011). Studies in mice noted that while both PCSK5 transcripts were detected, the PCSK5a form was more abundant (Nie et al., 2003). An abundance of evidence suggests that PCSK5, and in particular PCSK5a, is closely tied to embryonic implantation in the uterus of small mammals.

The involvement of PCSK5 in mouse and rabbit implantation is upheld in humans. In primary human endometrial stromal cells, PCSK5 is expressed upon treatment with estrogen, progesterone, and cAMP to induce decidualization (Heng et al., 2010; Okada et al., 2005). Because there is some overlap in proprotein convertase substrates, it is notable that furin, PACE4, and PC7 expression in the

human endometrium is not altered by decidualization (Freyer et al., 2007; Heng et al., 2010). In mice, decidualization is triggered by physical contact made between the embryo and the uterus; in contrast, decidualization in higher primates is under maternal control and occurs each month as a part of the menstrual cycle (Gellersen & Brosens, 2014). After menstruation, the primate uterus undergoes a proliferative stage (**Figure 3.06 A**), ovulation, and a secretory phase (**Figure 3.06 B-D**) where the endometrium becomes receptive to implantation (Okada et al., 2018). In humans, PCSK5 is expressed in the glandular epithelium during all menstrual cycle phases but increases significantly during the secretory phase as the uterus prepares for implantation (**Figure 3.06 C-D**) (Heng, Hannan, et al., 2011; Nie et al., 2005). The activity of PCSK5 collected via uterine lavage during the secretory phase is also higher than PCSK5 activity during the proliferative phase (Heng, Hannan, et al., 2011). Strong PCSK5 expression localizes to the stroma in the late secretory phase during decidualization (Nie et al., 2005). In pregnancy, PCSK5 expression remains strong in the decidual cells and present in the glands at least during the first trimester (**Figure 3.06 E-F**) (Nie et al., 2005).

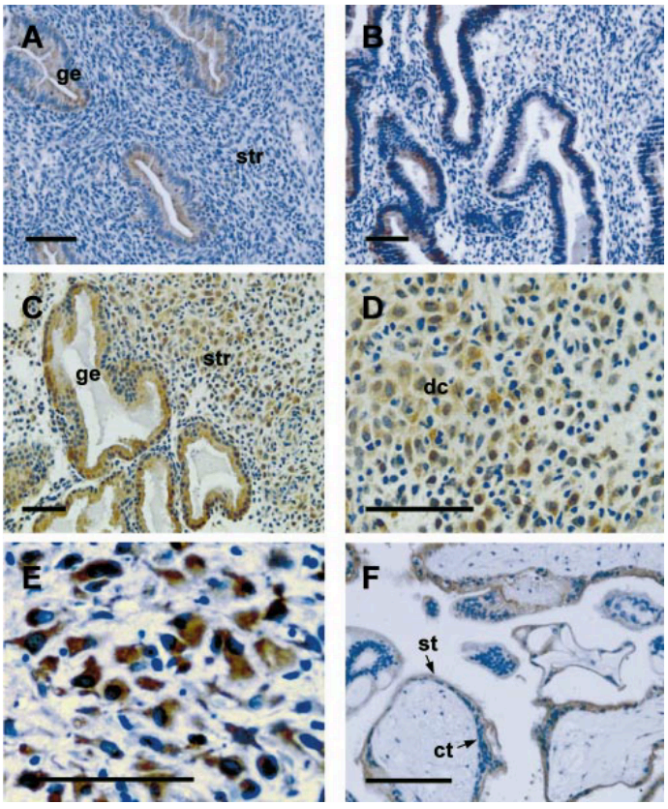

Figure 3.06. PCSK5 immunoreactivity in human endometrial tissue during the menstrual cycle and early pregnancy. [Figure 4 from (Nie et al., 2005)]

A-D, PCSK5 expression in the proliferative (**A**), early secretory (**B**), and late secretory (**C-D**) phases of the menstrual cycle. (**D**) is a higher magnification view of the stromal region in (**C**). Immunoreactivity is highest in decidual dells of the late secretory phase (**D**). **E-F**, PCSK5 expression during pregnancy is high in the maternal decidua (**E**) and low in the trophoblast (**F**). Scale bars = 400 µm. Labels: ge=glandular epithelium,

str=stroma, dc=decidual cells, st=syncytial trophoblast, ct=trophoblast cell column. *Used with permission from Oxford University Press (license number 6013691360657, April 21, 2025).*

PCSK5 expression is not just correlated with decidualization and implantation, it is essential for these processes, as demonstrated in a number of settings. In mice, blockage of uterine PCSK5 production via morpholino antisense oligonucleotides completely inhibits embryonic implantation (Nie et al., 2005). Human endometrial stromal cells cultured *in vitro* can be stimulated to undergo decidualization by treatment with 17β-estradiol and medroxyprogesterone acetate, resulting in prolactin production and intense PCSK5 immunoreactivity in the cytoplasm (Okada et al., 2005). Prolactin, a typical marker for decidualization, was significantly decreased when PCSK5 in decidualized cells was blocked by transfection with morpholino antisense oligonucleotides (Okada et al., 2005). In another study, human endometrial stromal cell cultures prepared from multiple different women exhibited dose-dependent inhibition of decidualization in response to treatment with Poly R, an inhibitor of PCSK5, furin, PC7, and PACE4 (Heng et al., 2010). Poly R was subsequently modified to allow vaginal delivery, yielding C-30k-PEG Poly R (Ho et al., 2012). Drugs administered vaginally localize preferentially to the uterus in humans (Cicinelli & de Ziegler, 1999; De Ziegler et al., 1997), but in mice, vaginal administration has shown more limited uterine uptake (Ho et al., 2012, 2014; Radomsky et al., 1992). Despite C-30k-PEG Poly R reaching the mouse uterus at low levels, the PCSK5 inhibitor completely inhibited embryonic implantation in 24% of mice and partially inhibited it in another 47% (Ho et al., 2014). Using siRNA, PCSK5 mRNA levels and secreted PCSK5 activity were reduced by approximately 50% in human endometrial epithelial carcinoma (HEC1A) cells. Under control conditions, coculture of HEC1A cells with mouse blastocysts serves as a model of human implantation; with PCSK5 knockdown, blastocyst attachment was reduced by approximately 60% (Heng, Cervero, et al., 2011).

Given these findings, it is not surprising that PCSK5 expression is closely associated with fertility. An illustrative study of PCSK5 protein abundance and distribution included endometrial biopsy samples from three cohorts of women (Heng, Cervero, et al., 2011). In women who were fertile or had participated in at least one successful cycle as an oocyte donation recipient, PCSK5 expression in the glandular and luminal epithelium was significantly higher than in women who had exhibited implantation failure (**Figure 3.07 A-D**). Similarly, PCSK5 expression in endometrial epithelial cells was significantly higher in women who were fertile than in women who had endometriosis-associated infertility or unexplained infertility (**Figure 3.07 I-L**). Interestingly, secretory-phase PCSK5 expression in fertile women who presented for insertion of an IUD was significantly higher before IUD placement and after IUD removal than while the IUD was in place (**Figure 3.07 E-H**). In line with these findings, it has been suggested that PCSK5 inhibition is worth exploring as a potential contraceptive (Ho et al., 2012, 2014) with a possible dual role as a sexually transmitted disease preventative since inhibition of PCSK5 has

been shown to block critical steps in both HPV (Kines et al., 2009) and HIV infection (Decroly et al., 1996; Ho et al., 2014; Miranda et al., 1996; Vollenweider et al., 1996). In the context of in vitro fertilization, PCSK5 holds potential as an endometrial fluid-based biomarker for endometrial receptivity (Alves et al., 2023; Heng, Dynon, et al., 2015).

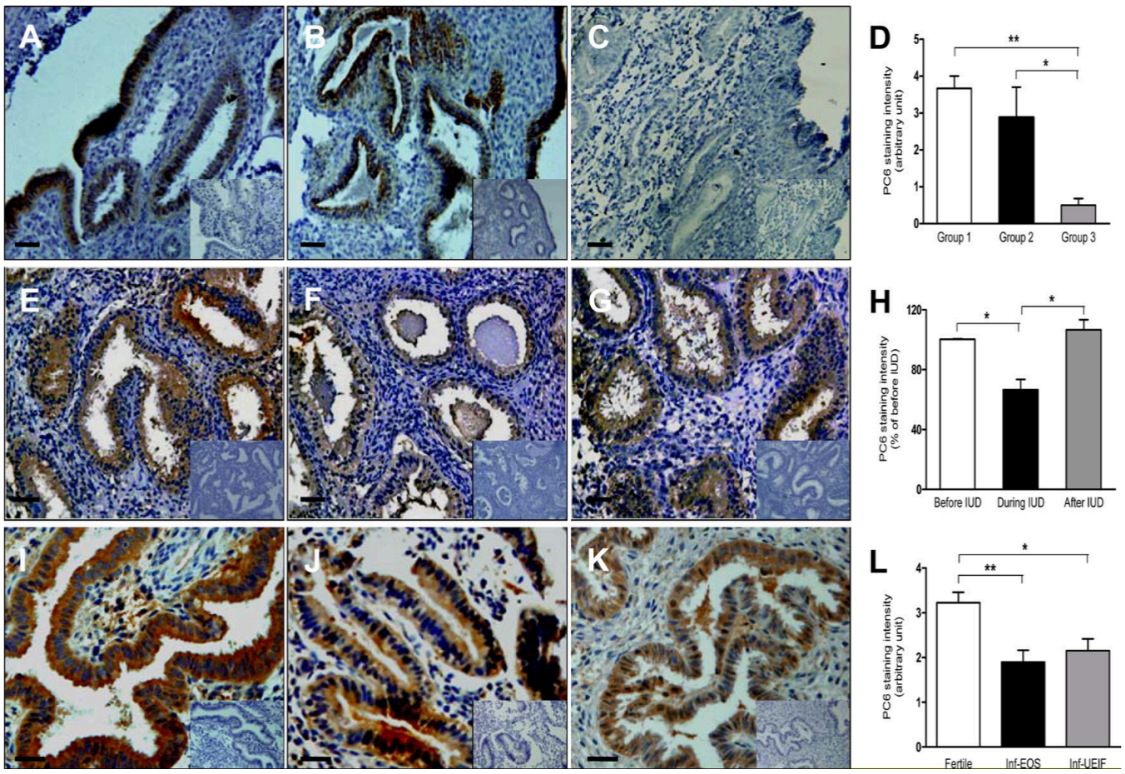

Figure 3.07. PCSK5 immunoreactivity in endometrial tissue of fertile and infertile women. [Figure 1 from (Heng, Cervero, et al., 2011)]

A-D, PCSK5 expression in the endometrial glandular epithelium of a Chilean cohort of fertile women (**A**) and oocyte recipients with implantation success (**B**) or failure (**C**); quantified in (**D**). **E-H**, PCSK5 expression in a Spanish cohort of fertile women before (**E**) during (**F**), or after (**G**) IUD insertion; quantified in (**H**). **I-L**, PCSK5 expression in an Australian cohort of fertile (**I**) or infertile women with endometriosis (**J**) or unexplained infertility (**K**); quantified in (**L**). Inserts are negative controls. Scale bars = 100 μm. *P<0.05, **P<0.005. *Used with permission from The Endocrine Society (license number 6013700202010, April 21, 2025).*

While it is clear that PCSK5 is essential for implantation, its specific role as a promoter of embryonic invasion versus a guardrail limiting the extent of that invasion is less obvious. PCSK5 has been found to cleave a number of substrates in the uterine context, which give us clues into its mechanisms of action. PCSK5 cleaves the TGFβ-family member bone morphogenetic protein (BMP)-2, activating BMP2 signaling through WNT4, β-catenin, and FOXO1 to promote differentiation of endometrial stromal cells into decidual cells (Heng et al., 2010; Q. Li et al., 2013). FOXO1 promotes expression of key decidualization markers such as prolactin and IGFBP-1, but in line with the balanced nature of the decidua, FOXO1 also exhibits negative feedback on expression of WNT4 and other genes

that promote FOXO1 signaling (Gellersen & Brosens, 2014). BMP-2 has been shown to be essential for uterine decidualization and implantation, and the addition of recombinant active BMP2 to human endometrial stromal cells partially rescues decidualization when PCSK5 is inhibited (Heng et al., 2010). The partial rescue speaks highly to the importance of BMP2 in decidualization but also indicates that the role of PCSK5 in decidualization goes beyond activation of BMP2. Another PCSK5 substrate is dystroglycan, which mediates blastocyst adhesion to the human endometrium but requires post-translational removal of its large N-terminus before its adhesive properties are activated. PCSK5 cleaves near the N-terminus of dystroglycan, allowing embryo attachment (Heng, Paule, et al., 2015). An unbiased proteomics approach comparing decidualized human endometrial stromal cells with or without addition of recombinant human PCSK5 identified caldesmon as a substrate (Kilpatrick et al., 2009). In human endometrial tissue, caldesmon and PCSK5 abundance both increase during the secretory phase and are localized to the decidual cells (Kilpatrick et al., 2009). Caldesmon is involved in the organization of actin microfilaments and regulation of cytoskeleton and is a marker for smooth muscle differentiation; it had not previously been implicated in decidualization (Kilpatrick et al., 2009), but the differentiation and increased motility (Grewal et al., 2008; Weimar et al., 2013) of decidual cells makes it plausible that caldesmon could be involved.

Also involved in the regulation of embryo implantation are TIMP-3 and MMP9. MMP9 is expressed by trophoblast cells as the embryo invades the decidua and the MMP9 inhibitor TIMP-3 is expressed by the adjacent decidual cells, suggesting that TIMP-3 functions to moderate the invasiveness of the embryo through regulation of MMP9 activity (Alexander et al., 1996; Rancourt & Rancourt, 1997). In the decidua, an increase in PCSK5 expression slightly precedes an increase in TIMP-3 expression, and PCSK5 and TIMP-3 expression have a high degree of spatial overlap between days 5.5-8.5 of gestation (Nie et al., 2003; Wong et al., 2002). TIMP-3 levels in the decidua are known to be regulated by TGFβ family members, which in turn are known to be activated by PCs (Wong et al., 2002), suggesting a possible indirect mechanism by which PCSK5 could regulate TIMP-3. In the cancer context, PCSK5 has been shown to be capable of binding to all four TIMP family members (Nour et al., 2005). TIMP-2 binds to PCSK5 and tethers the complex to the cell surface by binding to HSPGs; presumably this tethering promotes PCSK5 processing of membrane-bound cell surface precursor proteins, such as integrin alpha-chains, TGFβ-like proteins, and metalloproteinases like ADAM-17 (Nour et al., 2005). Therefore it is possible that PCSK5, through indirect or direct interaction with TIMP-3, could limit embryo invasion.

On the other hand, MMP9, as well as MMP3, have been found to cleave and inactivate IGFBP-1 in the decidua. IGFBP-1 production is triggered by progesterone; the protein is highly enriched in amniotic fluid and it stimulates trophoblast invasion (Gellersen & Brosens, 2014). Therefore TIMP-3-mediated inhibition of MMP9 would promote invasion. Perhaps TIMP-3 regulation of

trophoblast invasion is akin to the relationship between TIMP-2 and MMP2 studied in the context of cancer, where low levels of TIMP-2 promote MMP2 activation, while high levels of TIMP-2 result in MMP2 inhibition and therefore block MMP2-mediated tumor cell invasion and metastasis (Nour et al., 2005). This dual regulation is accomplished by the formation of a ternary complex at the cell surface. First, TIMP-2 binds and inhibits MT1-MMP. MMP2 then binds the TIMP-2—MT1-MMP complex, but MMP2 activation requires a second MT1-MMP, this one active, to cleave the MMP2 pro-domain (Butler et al., 1998; Kai et al., 2002; Nour et al., 2005; Overall et al., 1999; Zucker et al., 1998). Therefore, TIMP-2 is required for MMP2 activation, but a high abundance of TIMP-2 results in more MT1-MMP inactivation, thereby limiting the abundance of active MT1-MMP that can activate MMP2 (Nour et al., 2005).

3.4.2 Questions at the Interface of Embryonic Implantation and DCIS

It is evident that the processes regulating invasion are incredibly complex and involve the function of many competing mechanisms of promotion and inhibition to achieve a properly-regulated embryo implantation, which is essential to successful pregnancy. Indeed, implantation is characterized by a delicate balance between the embryo, working to invade the uterus, and the uterus, working to keep that invasion in check (Schultz & Edwards, 1997; Wong et al., 2002). Similarly, maintenance of DCIS without progression to IDC surely involves forces that moderate the dysmorphic and hyperplastic properties of DCIS cells to restrain their transition to invasive cancer. I therefore amend my suggestion, shared in the opening of this section, for collaboration between the embryonic implantation and DCIS/cancer biology fields: the collaboration should definitely include systems biologists.

A few questions come to mind that could be worth considering. First, is the loss of PCSK5 expression in triple-negative breast cancer related to the lack of progesterone receptor? In breast cancer, the basal-like subgroup is distinguished from its normal-like and luminal A counterparts in part by its low PCSK5 expression (compared to high PCSK5 in normal-like and luminal A) (Bajikar et al., 2017; Perou et al., 2000; Smid et al., 2008). The median abundance of PCSK5 transcripts is only 0.5 copies per cell in the triple-negative and basal-like subgroups of TCGA (Bajikar et al., 2017; M. Cheng et al., 1997). By definition, triple-negative breast cancers lack expression of progesterone receptor, and the basal-like subgroup has high concordance with the triple-negative categorization. Notably, MCF10A, the parental line to MCF10DCIS, lacks functional progesterone receptors (Shekhar et al., 1998). In the uterus, progesterone triggers upregulation of PCSK5 and decidualization. There is a lag period between the postovulatory rise in circulating progesterone and the first morphological changes of decidualization, suggesting that other regulatory factors are at play (Gellersen & Brosens, 2014), but studies of endometrial stromal cells have found PCSK5 transcript and protein expression to be upregulated in response to progesterone treatment (Heng et al., 2010; Okada et al., 2005).

Second, how does the ECM composition influence PCSK5 expression, and how does PCSK5 expression affect ECM composition? In my work, I found that the PCSK5 locus was exceedingly difficult to target by CRISPR under 2D culture conditions, but knock-out was highly successful when MCF10DCIS cells were cultured in the presence of Matrigel basement membrane (Marohl et al., 2025). We have not evaluated which matrix components are essential for the presumed chromatin decondensation at the PCSK5 locus. The major ECM components in Matrigel are laminin, collagen IV, and nidogen (Corning). Separately, in my xenograft study of MCF10DCIS, several stromal characteristics differed significantly between $PCSK5^{WT}$ and $PCSK5^{M452I}$, but we have not characterized the ECM proteins present to know if they differ across PCSK5 genotypes (Marohl et al., 2025). The uterine ECM contains high levels of collagens, particularly collagen I. The uterine stroma undergoes major remodeling during decidualization to accommodate invasion of the embryo, including an increase in collagens I and IV; this is a major area of ongoing research, both in the context of normal decidualization and in cases of infertility, pregnancy complications, and disease (Nallasamy et al., 2025; Rossi et al., 2025).

Finally, what can the study of plasticity in each field tell us about the other? It is common in the literature to comment that the human endometrium exhibits remarkable plasticity. Indeed, each month of the menstrual cycle the endometrium evolves through a range of dissimilar phases; during embryonic implantation and pregnancy, another entire set of programs occur; and after menstrual shedding, miscarriage, or birth, the endometrium completely regenerates (Gellersen & Brosens, 2014). Epithelial stem/progenitor cells and mesenchymal stem cells reside in the endometrium; both are highly proliferative, self-renew *in vitro*, differentiate into mature progeny, and can reconstitute tissue *in vivo* (Gellersen & Brosens, 2014). Similarly, the breast undergoes remodeling of gland architecture during pregnancy and after cessation of breast feeding, processes that could happen numerous times in a woman's lifetype (L. Tait et al., 1996). MCF10 cell lines are characterized as bipotent due to their ability to produce both luminal and myoepithelial cells during *in vivo* duct formation and subsequent DCIS and/or IDC (Hu et al., 2008; Santner et al., 2001). The parallels between the endometrium and the breast are numerous in this regard: both undergo repeated remodeling and harbor stem cell populations that orchestrate these complex remodeling events, and both are exposed to circumstances where a balance between pro- and anti-invasive forces is necessary; for the endometrium, the process of decidualization to accommodate the invading embryo, and for the breast, the disease state of DCIS and its persistence in that state versus its progression to IDC. In the endometrium, the homeostatic program succeeds the majority of the time. The DCIS research community would be wise to tune in to this process.

3.5 Concluding Remarks

The MCF10A series of cell lines is littered with advantages and disadvantages. The fact is, this model has served as a very useful model of breast epithelial cells, transition from healthy to early-stage disease, ductal carcinoma *in situ*, progression to advanced disease, and breast cancer. While new, arguably more relevant models of some of these contexts are becoming available, I doubt that the MCF10 series will go away. Therefore, like any model, it is important to periodically reassess what we know and the assumptions we have made; this process only leads to improvements, both in the model and in our understanding of the underlying biology.

Our work on the unusual PCSK5^{M452I} mutation that arose in the MCF10 series and is heterozygous in MCF10DCIS suggests that it is not a concern for the interpretation of hundreds of studies that leverage the MCF10DCIS cell line as an *in vitro* representative of breast cancer cell lines, a 3D spheroid model, and as an *in vivo* xenograft model of the development and progression of DCIS. In addition, the inclusion of the null PCSK5^{T288P} mutation in our experiments bolstered evidence for the importance of PCSK5 in DCIS.

The study of PCSK5 is difficult. In many tissues, its expression is so low that reliable detection and quantification at the RNA and protein levels is out of reach. However, it is known to play an important role in some widely impactful processes: regulation of the formation of breast alveoli and preservation of an epithelial state, and regulation of endometrial tissue remodeling to facilitate embryonic implantation into the uterus for successful pregnancy. Furthermore, it is known to cleave a number of high-profile substrates (and seems capable of cleaving many more). Generally, biologists assume that important proteins like hormones, ligands, and extracellular matrix modifiers are constitutively active, but this is most definitely not the case. The proprotein convertases are there to activate them and serve as a critical post-translational regulator of their effects. So far, we primarily notice PCs when they are absent. I think we would be well-served to appreciate their contribution when they are present, as well.

Bibliography

Abd El-Rehim, D. M., Pinder, S. E., Paish, C. E., Bell, J., Blamey, R. W., Robertson, J. F. R., Nicholson, R. I., & Ellis, I. O. (2004). Expression of luminal and basal cytokeratins in human breast carcinoma. *The Journal of Pathology*, *203*(2), 661–671. https://doi.org/10.1002/path.1559

Alexander, C. M., Hansell, E. J., Behrendtsen, O., Flannery, M. L., Kishnani, N. S., Hawkes, S. P., & Werb, Z. (1996). Expression and function of matrix metalloproteinases and their inhibitors at the maternal-embryonic boundary during mouse embryo implantation. *Development*, *122*(6), 1723–1736. https://doi.org/10.1242/dev.122.6.1723

Alves, A. R., Dias, M. F., & Silvestre, M. (2023). Endometrial fluid biomarkers and their potential as predictors of successful embryo implantation. *BioMedicine*, *13*(3), 1–8. https://doi.org/10.37796/2211-8039.1413

Anderson, E. D., Molloy, S. S., Jean, F., Fei, H., Shimamura, S., & Thomas, G. (2002). The ordered and compartment-specfific autoproteolytic removal of the furin intramolecular chaperone is required for enzyme activation. *The Journal of Biological Chemistry*, *277*(15), 12879–12890. https://doi.org/10.1074/jbc.M108740200

Anderson, E. D., Peters, R. J., Wilk, B., & Agard, D. A. (1999). alpha-lytic protease precursor: Characterization of a structured folding intermediate. *Biochemistry*, *38*(15), 4728–4735. https://doi.org/10.1021/bi982165e

Anderson, E. D., VanSlyke, J. K., Thulin, C. D., Jean, F., & Thomas, G. (1997). Activation of the furin endoprotease is a multiple‐step process: Requirements for acidification and internal propeptide cleavage. *The EMBO Journal*, *16*(7), 1508–1518. https://doi.org/10.1093/emboj/16.7.1508

Andersson, O., Reissmann, E., & Ibáñez, C. F. (2006). Growth differentiation factor 11 signals through the transforming growth factor-beta receptor ALK5 to regionalize the anterior-posterior axis. *EMBO Reports*, *7*(8), 831–837. https://doi.org/10.1038/sj.embor.7400752

Antebi, Y. E., Linton, J. M., Klumpe, H., Bintu, B., Gong, M., Su, C., McCardell, R., & Elowitz, M. B. (2017). Combinatorial Signal Perception in the BMP Pathway. *Cell*, *170*(6), 1184-1196.e24. https://doi.org/10.1016/j.cell.2017.08.015

Antenos, M., Lei, L., Xu, M., Malipatil, A., Kiesewetter, S., & Woodruff, T. K. (2011). Role of PCSK5 expression in mouse ovarian follicle development: Identification of the inhibin α- and β-subunits as candidate substrates. *PloS One*, *6*(3), e17348. https://doi.org/10.1371/journal.pone.0017348

Bae, J.-A., Park, H.-J., Seo, Y.-M., Roh, J., Hsueh, A. J. W., & Chun, S.-Y. (2008). Hormonal regulation of proprotein convertase subtilisin/kexin type 5 expression during ovarian follicle development in the rat. *Molecular and Cellular Endocrinology*, *289*(1–2), 29–37. https://doi.org/10.1016/j.mce.2008.04.006

Bajikar, S. S., Wang, C.-C., Borten, M. A., Pereira, E. J., Atkins, K. A., & Janes, K. A. (2017). Tumor-Suppressor Inactivation of GDF11 Occurs by Precursor Sequestration in Triple-Negative Breast Cancer. *Developmental Cell*, *43*(4), 418-435.e13. https://doi.org/10.1016/j.devcel.2017.10.027

Baker, D., Shiau, K., & Agard, D. A. (1993). The role of pro regions in protein folding. *Current Opinion in Cell Biology*, *5*(6), 966–970. https://doi.org/10.1016/0955-0674(93)90078-5

Baker, D., Sohl, J. L., & Agard, D. A. (1992). A protein-folding reaction under kinetic control. *Nature*, *356*(6366), 263–265. https://doi.org/10.1038/356263a0

Banaszynski, L. A., Chen, L.-C., Maynard-Smith, L. A., Ooi, A. G. L., & Wandless, T. J. (2006). A rapid, reversible, and tunable method to regulate protein function in living cells using synthetic small molecules. *Cell*, *126*(5), 995–1004. https://doi.org/10.1016/j.cell.2006.07.025

Barnabas, N., & Cohen, D. (2013). Phenotypic and Molecular Characterization of MCF10DCIS and SUM Breast Cancer Cell Lines. *International Journal of Breast Cancer*, *2013*, e872743. https://doi.org/10.1155/2013/872743

Basolo, F., Elliott, J., Tait, L., Chen, X. Q., Maloney, T., Russo, I. H., Pauley, R., Momiki, S., Caamano, J., Klein-Szanto, A. J. P., Koszalka, M., & Russo, J. (1991). Transformation of Human Breast Epithelial Cells by c-Ha-ras Oncogene. *Molecular Carcinogenesis*, *4*(1), 25–35. https://doi.org/10.1002/mc.2940040106

Behbod, F., Gomes, A. M., & Machado, H. L. (2018). Modeling Human Ductal Carcinoma In Situ in the Mouse. *Journal of Mammary Gland Biology and Neoplasia*, *23*(4), 269–278. https://doi.org/10.1007/s10911-018-9408-0

Behbod, F., Kittrell, F. S., LaMarca, H., Edwards, D., Kerbawy, S., Heestand, J. C., Young, E., Mukhopadhyay, P., Yeh, H.-W., Allred, D. C., Hu, M., Polyak, K., Rosen, J. M., & Medina, D. (2009). An intraductal human-in-mouse transplantation model mimics the subtypes of ductal carcinoma in situ. *Breast Cancer Research : BCR*, *11*(5), R66. https://doi.org/10.1186/bcr2358

Bellamy, C. O. C., McDonald, C., Salter, D. M., Chetty, U., & Anderson, T. J. (1993). Noninvasive ductal carcinoma of the breast: The relevance of histologic categorization. *Human Pathology*, *24*(1), 16–23. https://doi.org/10.1016/0046-8177(93)90057-N

Betsill, W. L., Rosen, P. P., Lieberman, P. H., & Robbins, G. F. (1978). Intraductal carcinoma. Long-term follow-up after treatment by biopsy alone. *JAMA*, *239*(18), 1863–1867. https://doi.org/10.1001/jama.239.18.1863

Borten, M. A., Bajikar, S. S., Sasaki, N., Clevers, H., & Janes, K. A. (2018). Automated brightfield morphometry of 3D organoid populations by OrganoSeg. *Scientific Reports*, *8*(1), Article 1. https://doi.org/10.1038/s41598-017-18815-8

Brenton, J. D., Carey, L. A., Ahmed, A. A., & Caldas, C. (2005). Molecular Classification and Molecular Forecasting of Breast Cancer: Ready for Clinical Application? *Journal of Clinical Oncology*, *23*(29), 7350–7360. https://doi.org/10.1200/JCO.2005.03.3845

Brock, E. J., Ji, K., Shah, S., Mattingly, R. R., & Sloane, B. F. (2019). In Vitro Models for Studying Invasive Transitions of Ductal Carcinoma In Situ. *Journal of Mammary Gland Biology and Neoplasia*, *24*(1), 1–15. https://doi.org/10.1007/s10911-018-9405-3

Bryan, B. B., Schnitt, S. J., & Collins, L. C. (2006). Ductal carcinoma in situ with basal-like phenotype: A possible precursor to invasive basal-like breast cancer. *Modern Pathology*, *19*(5), 617–621. https://doi.org/10.1038/modpathol.3800570

Butler, G. S., Butler, M. J., Atkinson, S. J., Will, H., Tamura, T., Schade van Westrum, S., Crabbe, T., Clements, J., d'Ortho, M. P., & Murphy, G. (1998). The TIMP2 membrane type 1 metalloproteinase "receptor" regulates the concentration and efficient activation of progelatinase A. A kinetic study. *The Journal of Biological Chemistry*, *273*(2), 871–880.

https://doi.org/10.1074/jbc.273.2.871

Carson, D. D., Bagchi, I., Dey, S. K., Enders, A. C., Fazleabas, A. T., Lessey, B. A., & Yoshinaga, K. (2000). Embryo Implantation. *Developmental Biology*, *223*(2), 217–237. https://doi.org/10.1006/dbio.2000.9767

Cheang, M. C. U., Voduc, D., Bajdik, C., Leung, S., McKinney, S., Chia, S. K., Perou, C. M., & Nielsen, T. O. (2008). Basal-like breast cancer defined by five biomarkers has superior prognostic value than triple-negative phenotype. *Clinical Cancer Research: An Official Journal of the American Association for Cancer Research*, *14*(5), 1368–1376. https://doi.org/10.1158/1078-0432.CCR-07-1658

Cheng, J., Novati, G., Pan, J., Bycroft, C., Žemgulytė, A., Applebaum, T., Pritzel, A., Wong, L. H., Zielinski, M., Sargeant, T., Schneider, R. G., Senior, A. W., Jumper, J., Hassabis, D., Kohli, P., & Avsec, Ž. (2023). Accurate proteome-wide missense variant effect prediction with AlphaMissense. *Science (New York, N.Y.)*, *381*(6664), eadg7492. https://doi.org/10.1126/science.adg7492

Cheng, M., Watson, P. H., Paterson, J. A., Seidah, N., Chrétien, M., & Shiu, R. P. (1997). Pro-protein convertase gene expression in human breast cancer. *International Journal of Cancer*, *71*(6), 966–971. https://doi.org/10.1002/(sici)1097-0215(19970611)71:6<966::aid-ijc10>3.0.co;2-4

Chrétien, M., & Li, C. H. (1967). ISOLATION, PURIFICATION, AND CHARACTERIZATION OF γ-LIPOTROPIC HORMONE FROM SHEEP PITUITARY GLANDS. *Canadian Journal of Biochemistry*, *45*(7), 1163–1174. https://doi.org/10.1139/o67-133

Chun, S., & Fay, J. C. (2009). Identification of deleterious mutations within three human genomes. *Genome Research*, *19*(9), 1553–1561. https://doi.org/10.1101/gr.092619.109

Cicinelli, E., & de Ziegler, D. (1999). Transvaginal progesterone: Evidence for a new functional “portal system” flowing from the vagina to the uterus. *Human Reproduction Update*, *5*(4), 365–372. https://doi.org/10.1093/humupd/5.4.365

Clark, S. E., Warwick, J., Carpenter, R., Bowen, R. L., Duffy, S. W., & Jones, J. L. (2011). Molecular subtyping of DCIS: Heterogeneity of breast cancer reflected in pre-invasive disease. *British Journal of Cancer*, *104*(1), 120–127. https://doi.org/10.1038/sj.bjc.6606021

Collins, L. C., Tamimi, R. M., Baer, H. J., Connolly, J. L., Colditz, G. A., & Schnitt, S. J. (2005). Outcome of patients with ductal carcinoma in situ untreated after diagnostic biopsy: Results from the Nurses’ Health Study. *Cancer*, *103*(9), 1778–1784. https://doi.org/10.1002/cncr.20979

Constam, D. B. (2014). Regulation of TGFβ and related signals by precursor processing. *Seminars in Cell & Developmental Biology*, *32*, 85–97. https://doi.org/10.1016/j.semcdb.2014.01.008

Cooper, S. A. P. (1840). *On the anatomy of the breast*. Longman, Orme, Green, Brown and Longmans. https://jdc.jefferson.edu/cooper/

Creemers, J. W. M., & Khatib, A.-M. (2008). Knock-out mouse models of proprotein convertases: Unique functions or redundancy? *Frontiers in Bioscience: A Journal and Virtual Library*, *13*, 4960–4971. https://doi.org/10.2741/3055

Creemers, J. W. M., Vey, M., Schäfer, W., Ayoubi, T. A. Y., Roebroek, A. J. M., Klenk, H.-D., Garten, W., & Van De Ven, W. J. M. (1995). Endoproteolytic Cleavage of Its Propeptide Is a Prerequisite for Efficient Transport of Furin Out of the Endoplasmic Reticulum. *Journal of Biological Chemistry*,

270(6), 2695–2702. https://doi.org/10.1074/jbc.270.6.2695

Creemers, J. W., Siezen, R. J., Roebroek, A. J., Ayoubi, T. A., Huylebroeck, D., & Van De Ven, W. J. (1993). Modulation of furin-mediated proprotein processing activity by site-directed mutagenesis. *Journal of Biological Chemistry*, *268*(29), 21826–21834. https://doi.org/10.1016/S0021-9258(20)80616-4

Cross, J., Werb, Z., & Fisher, S. (1994). Implantation and the placenta: Key pieces of the development puzzle. *Science*, *266*(5190), 1508–1518. https://doi.org/10.1126/science.7985020

Cui, Y., Hackenmiller, R., Berg, L., Jean, F., Nakayama, T., Thomas, G., & Christian, J. L. (2001). The activity and signaling range of mature BMP-4 is regulated by sequential cleavage at two sites within the prodomain of the precursor. *Genes & Development*, *15*(21), 2797–2802. https://doi.org/10.1101/gad.940001

Dai, X., Cheng, H., Bai, Z., & Li, J. (2017). Breast Cancer Cell Line Classification and Its Relevance with Breast Tumor Subtyping. *Journal of Cancer*, *8*(16), 3131–3141. https://doi.org/10.7150/jca.18457

Daino, K., Imaoka, T., Morioka, T., Tani, S., Iizuka, D., Nishimura, M., & Shimada, Y. (2013). Loss of the BRCA1-Interacting Helicase BRIP1 Results in Abnormal Mammary Acinar Morphogenesis. *PLoS ONE*, *8*(9). https://doi.org/10.1371/journal.pone.0074013

Das, S. K., Yano, S., Wang, J., Edwards, D. R., Nagase, H., & Dey, S. K. (1997). Expression of matrix metalloproteinases and tissue inhibitors of metalloproteinases in the mouse uterus during the peri-implantation period. *Developmental Genetics*, *21*(1), 44–54. https://doi.org/10.1002/(SICI)1520-6408(1997)21:1<44::AID-DVG5>3.0.CO;2-8

Dawson, P. J., Wolman, S. R., Tait, L., Heppner, G. H., & Miller, F. R. (1996). MCF10AT: A model for the evolution of cancer from proliferative breast disease. *The American Journal of Pathology*, *148*(1), 313–319.

De Bie, I., Marcinkiewicz, M., Malide, D., Lazure, C., Nakayama, K., Bendayan, M., & Seidah, N. G. (1996). The isoforms of proprotein convertase PC5 are sorted to different subcellular compartments. *The Journal of Cell Biology*, *135*(5), 1261–1275. https://doi.org/10.1083/jcb.135.5.1261

De Ziegler, D., Bulletti, C., De Monstier, B., & Jääskeläinen, A.-S. (1997). The First Uterine Pass Effect. *Annals of the New York Academy of Sciences*, *828*(1), 291–299. https://doi.org/10.1111/j.1749-6632.1997.tb48550.x

Debnath, J., Mills, K. R., Collins, N. L., Reginato, M. J., Muthuswamy, S. K., & Brugge, J. S. (2002). The role of apoptosis in creating and maintaining luminal space within normal and oncogene-expressing mammary acini. *Cell*, *111*(1), 29–40. https://doi.org/10.1016/s0092-8674(02)01001-2

Debnath, J., Muthuswamy, S. K., & Brugge, J. S. (2003). Morphogenesis and oncogenesis of MCF-10A mammary epithelial acini grown in three-dimensional basement membrane cultures. *Methods*, *30*(3), 256–268. https://doi.org/10.1016/S1046-2023(03)00032-X

Decroly, E., Wouters, S., Di Bello, C., Lazure, C., Ruysschaert, J. M., & Seidah, N. G. (1996). Identification of the paired basic convertases implicated in HIV gp160 processing based on in vitro assays and expression in CD4(+) cell lines. *The Journal of Biological Chemistry*, *271*(48),

30442–30450. https://doi.org/10.1074/jbc.271.48.30442

Deng, Q., Ramsköld, D., Reinius, B., & Sandberg, R. (2014). Single-cell RNA-seq reveals dynamic, random monoallelic gene expression in mammalian cells. *Science (New York, N.Y.)*, *343*(6167), 193–196. https://doi.org/10.1126/science.1245316

Denker, H.-W. (1993). Implantation: A cell biological paradox. *Journal of Experimental Zoology*, *266*(6), 541–558. https://doi.org/10.1002/jez.1402660606

Deryabin, P., Griukova, A., Nikolsky, N., & Borodkina, A. (2020). The link between endometrial stromal cell senescence and decidualization in female fertility: The art of balance. *Cellular and Molecular Life Sciences*, *77*(7), 1357–1370. https://doi.org/10.1007/s00018-019-03374-0

Deschamps, J., & van Nes, J. (2005). Developmental regulation of the Hox genes during axial morphogenesis in the mouse. *Development (Cambridge, England)*, *132*(13), 2931–2942. https://doi.org/10.1242/dev.01897

Dobrolecki, L. E., Airhart, S. D., Alferez, D. G., Aparicio, S., Behbod, F., Bentires-Alj, M., Brisken, C., Bult, C. J., Cai, S., Clarke, R. B., Dowst, H., Ellis, M. J., Gonzalez-Suarez, E., Iggo, R. D., Kabos, P., Li, S., Lindeman, G. J., Marangoni, E., McCoy, A., … Lewis, M. T. (2016). Patient-derived Xenograft (PDX) Models In Basic and Translational Breast Cancer Research. *Cancer Metastasis Reviews*, *35*(4), 547–573. https://doi.org/10.1007/s10555-016-9653-x

Doebar, S. C., van den Broek, E. C., Koppert, L. B., Jager, A., Baaijens, M. H. A., Obdeijn, I.-M. A. M., & van Deurzen, C. H. M. (2016). Extent of ductal carcinoma in situ according to breast cancer subtypes: A population-based cohort study. *Breast Cancer Research and Treatment*, *158*(1), 179–187. https://doi.org/10.1007/s10549-016-3862-4

Dubrulle, J., & Pourquié, O. (2004). Coupling segmentation to axis formation. *Development (Cambridge, England)*, *131*(23), 5783–5793. https://doi.org/10.1242/dev.01519

Eck, S. M., Côté, A. L., Winkelman, W. D., & Brinckerhoff, C. E. (2009). CXCR4 and matrix metalloproteinase-1 are elevated in breast carcinoma-associated fibroblasts and in normal mammary fibroblasts exposed to factors secreted by breast cancer cells. *Molecular Cancer Research: MCR*, *7*(7), 1033–1044. https://doi.org/10.1158/1541-7786.MCR-09-0015

Eder, J., Rheinnecker, M., & Fersht, A. R. (1993a). Folding of subtilisin BPN': Characterization of a folding intermediate. *Biochemistry*, *32*(1), 18–26. https://doi.org/10.1021/bi00052a004

Eder, J., Rheinnecker, M., & Fersht, A. R. (1993b). Folding of subtilisin BPN': Role of the pro-sequence. *Journal of Molecular Biology*, *233*(2), 293–304. https://doi.org/10.1006/jmbi.1993.1507

Erbas, B., Provenzano, E., Armes, J., & Gertig, D. (2006). The natural history of ductal carcinoma in situ of the breast: A review. *Breast Cancer Research and Treatment*, *97*(2), 135–144. https://doi.org/10.1007/s10549-005-9101-z

Esquela, A. F., & Lee, S. e-J. (2003). Regulation of metanephric kidney development by growth/differentiation factor 11. *Developmental Biology*, *257*(2), 356–370. https://doi.org/10.1016/S0012-1606(03)00100-3

Essalmani, R., Hamelin, J., Marcinkiewicz, J., Chamberland, A., Mbikay, M., Chrétien, M., Seidah, N. G., & Prat, A. (2006). Deletion of the Gene Encoding Proprotein Convertase 5/6 Causes Early Embryonic Lethality in the Mouse. *Molecular and Cellular Biology*, *26*(1), 354–361. https://doi.org/10.1128/MCB.26.1.354-361.2006

Essalmani, R., Zaid, A., Marcinkiewicz, J., Chamberland, A., Pasquato, A., Seidah, N. G., & Prat, A. (2008). In vivo functions of the proprotein convertase PC5/6 during mouse development: Gdf11 is a likely substrate. *Proceedings of the National Academy of Sciences of the United States of America*, *105*(15), 5750–5755. https://doi.org/10.1073/pnas.0709428105

Fattet, L., Jung, H.-Y., Matsumoto, M. W., Aubol, B. E., Kumar, A., Adams, J. A., Chen, A. C., Sah, R. L., Engler, A. J., Pasquale, E. B., & Yang, J. (2020). Matrix Rigidity Controls Epithelial-Mesenchymal Plasticity and Tumor Metastasis via a Mechanoresponsive EPHA2/LYN Complex. *Developmental Cell*, *54*(3), 302-316.e7. https://doi.org/10.1016/j.devcel.2020.05.031

Freedman, R. B. (1984). Native disulphide bond formation in protein biosynthesis: Evidence for the role of protein disulphide isomerase. *Trends in Biochemical Sciences*, *9*(10), 438–441. https://doi.org/10.1016/0968-0004(84)90152-X

Freyer, C., Kilpatrick, L. M., Salamonsen, L. A., & Nie, G. (2007). Pro-protein convertases (PCs) other than PC6 are not tightly regulated for implantation in the human endometrium. *Reproduction (Cambridge, England)*, *133*(6), 1189–1197. https://doi.org/10.1530/REP-06-0285

Frittoli, E., Palamidessi, A., Iannelli, F., Zanardi, F., Villa, S., Barzaghi, L., Abdo, H., Cancila, V., Beznoussenko, G. V., Della Chiara, G., Pagani, M., Malinverno, C., Bhattacharya, D., Pisati, F., Yu, W., Galimberti, V., Bonizzi, G., Martini, E., Mironov, A. A., … Scita, G. (2023). Tissue fluidification promotes a cGAS–STING cytosolic DNA response in invasive breast cancer. *Nature Materials*, *22*(5), 644–655. https://doi.org/10.1038/s41563-022-01431-x

Frohlich, J., & Vinciguerra, M. (2020). Candidate rejuvenating factor GDF11 and tissue fibrosis: Friend or foe? *GeroScience*, *42*(6), 1475–1498. https://doi.org/10.1007/s11357-020-00279-w

Fuller, R. S., Brake, A. J., & Thorner, J. (1989a). Intracellular targeting and structural conservation of a prohormone-processing endoprotease. *Science (New York, N.Y.)*, *246*(4929), 482–486. https://doi.org/10.1126/science.2683070

Fuller, R. S., Brake, A., & Thorner, J. (1989b). Yeast prohormone processing enzyme (KEX2 gene product) is a Ca2+-dependent serine protease. *Proceedings of the National Academy of Sciences*, *86*(5), 1434–1438. https://doi.org/10.1073/pnas.86.5.1434

Gamer, L. W., Wolfman, N. M., Celeste, A. J., Hattersley, G., Hewick, R., & Rosen, V. (1999). A Novel BMP Expressed in Developing Mouse Limb, Spinal Cord, and Tail Bud Is a Potent Mesoderm Inducer inXenopusEmbryos. *Developmental Biology*, *208*(1), 222–232. https://doi.org/10.1006/dbio.1998.9191

Ge, G., Hopkins, D. R., Ho, W.-B., & Greenspan, D. S. (2005). GDF11 Forms a Bone Morphogenetic Protein 1-Activated Latent Complex That Can Modulate Nerve Growth Factor-Induced Differentiation of PC12 Cells. *Molecular and Cellular Biology*, *25*(14), 5846–5858. https://doi.org/10.1128/MCB.25.14.5846-5858.2005

Gellersen, B., & Brosens, J. J. (2014). Cyclic Decidualization of the Human Endometrium in Reproductive Health and Failure. *Endocrine Reviews*, *35*(6), 851–905. https://doi.org/10.1210/er.2014-1045

Gerardo-Ramírez, M., Lazzarini-Lechuga, R., Hernández-Rizo, S., Jiménez-Salazar, J. E., Simoni-Nieves, A., García-Ruiz, C., Fernández-Checa, J. C., Marquardt, J. U., Coulouarn, C., Gutiérrez-Ruiz, M. C., Pérez-Aguilar, B., & Gomez-Quiroz, L. E. (2019). GDF11 exhibits tumor suppressive properties in hepatocellular carcinoma cells by restricting clonal expansion and

invasion. *Biochimica et Biophysica Acta (BBA) - Molecular Basis of Disease*, *1865*(6), 1540–1554. https://doi.org/10.1016/j.bbadis.2019.03.003

Girotti, M., & Banting, G. (1996). TGN38-green fluorescent protein hybrid proteins expressed in stably transfected eukaryotic cells provide a tool for the real-time, in vivo study of membrane traffic pathways and suggest a possible role for ratTGN38. *Journal of Cell Science*, *109 (Pt 12)*, 2915–2926. https://doi.org/10.1242/jcs.109.12.2915

Gluschankof, P., & Fuller, R. S. (1994). A C-terminal domain conserved in precursor processing proteases is required for intramolecular N-terminal maturation of pro-Kex2 protease. *The EMBO Journal*, *13*(10), 2280–2288. https://doi.org/10.1002/j.1460-2075.1994.tb06510.x

Green, J. E., Shibata, M.-A., Yoshidome, K., Liu, M., Jorcyk, C., Anver, M. R., Wigginton, J., Wiltrout, R., Shibata, E., Kaczmarczyk, S., Wang, W., Liu, Z., Calvo, A., & Couldrey, C. (2000). The C3(1)/SV40 T-antigen transgenic mouse model of mammary cancer: Ductal epithelial cell targeting with multistage progression to carcinoma. *Oncogene*, *19*(8), 1020–1027. https://doi.org/10.1038/sj.onc.1203280

Grewal, S., Carver, J. G., Ridley, A. J., & Mardon, H. J. (2008). Implantation of the human embryo requires Rac1-dependent endometrial stromal cell migration. *Proceedings of the National Academy of Sciences of the United States of America*, *105*(42), 16189–16194. https://doi.org/10.1073/pnas.0806219105

H Heppner, G., R Miller, F., & Malathy Shekhar, P. (2000). Nontransgenic models of breast cancer. *Breast Cancer Research*, *2*(5), 331. https://doi.org/10.1186/bcr77

Hassiotou, F., & Geddes, D. (2013). Anatomy of the human mammary gland: Current status of knowledge. *Clinical Anatomy*, *26*(1), 29–48. https://doi.org/10.1002/ca.22165

Hayashida, K., Aquino, R. S., & Park, P. W. (2022). Coreceptor functions of cell surface heparan sulfate proteoglycans. *American Journal of Physiology. Cell Physiology*, *322*(5), C896–C912. https://doi.org/10.1152/ajpcell.00050.2022

Heng, S., Cervero, A., Simon, C., Stephens, A. N., Li, Y., Zhang, J., Paule, S., Rainczuk, A., Singh, H., Quinonero, A., Tapia, A., Velasquez, L., Salamonsen, L., Rombauts, L. J. F., & Nie, G. (2011). Proprotein Convertase 5/6 Is Critical for Embryo Implantation in Women: Regulating Receptivity by Cleaving EBP50, Modulating Ezrin Binding, and Membrane-Cytoskeletal Interactions. *Endocrinology*, *152*(12), 5041–5052. https://doi.org/10.1210/en.2011-1273

Heng, S., Dynon, K., Li, Y., Edgell, T., Walton, K., Rombauts, L. J., Vollenhoven, B., & Nie, G. (2015). Development of a high-throughput assay for human proprotein convertase 5/6 for detecting uterine receptivity. *Analytical Biochemistry*, *475*, 14–21. https://doi.org/10.1016/j.ab.2014.12.012

Heng, S., Hannan, N. J., Rombauts, L. J. F., Salamonsen, L. A., & Nie, G. (2011). PC6 levels in uterine lavage are closely associated with uterine receptivity and significantly lower in a subgroup of women with unexplained infertility. *Human Reproduction*, *26*(4), 840–846. https://doi.org/10.1093/humrep/der002

Heng, S., Paule, S. G., Li, Y., Rombauts, L. J., Vollenhoven, B., Salamonsen, L. A., & Nie, G. (2015). Posttranslational removal of α-dystroglycan N terminus by PC5/6 cleavage is important for uterine preparation for embryo implantation in women. *The FASEB Journal*, *29*(9), 4011–4022. https://doi.org/10.1096/fj.14-269456

Heng, S., Paule, S., Hardman, B., Li, Y., Singh, H., Rainczuk, A., Stephens, A. N., & Nie, G. (2010). Posttranslational activation of bone morphogenetic protein 2 is mediated by proprotein convertase 6 during decidualization for pregnancy establishment. *Endocrinology*, *151*(8), 3909–3917. https://doi.org/10.1210/en.2010-0326

Henrich, S., Cameron, A., Bourenkov, G. P., Kiefersauer, R., Huber, R., Lindberg, I., Bode, W., & Than, M. E. (2003). The crystal structure of the proprotein processing proteinase furin explains its stringent specificity. *Nature Structural & Molecular Biology*, *10*(7), 520–526. https://doi.org/10.1038/nsb941

Henrich, S., Lindberg, I., Bode, W., & Than, M. E. (2005). Proprotein Convertase Models based on the Crystal Structures of Furin and Kexin: Explanation of their Specificity. *Journal of Molecular Biology*, *345*(2), 211–227. https://doi.org/10.1016/j.jmb.2004.10.050

Ho, H., Li, Y., & Nie, G. (2014). Inhibition of embryo implantation in mice through vaginal administration of a proprotein convertase 6 inhibitor. *Reproductive Biology*, *14*(2), 155–159. https://doi.org/10.1016/j.repbio.2013.12.008

Ho, H., Nero, T. L., Singh, H., Parker, M. W., & Nie, G. (2012). PEGylation of a proprotein convertase peptide inhibitor for vaginal route of drug delivery: In vitro bioactivity, stability and in vivo pharmacokinetics. *Peptides*, *38*(2), 266–274. https://doi.org/10.1016/j.peptides.2012.09.014

Hoadley, K. A., Yau, C., Hinoue, T., Wolf, D. M., Lazar, A. J., Drill, E., Shen, R., Taylor, A. M., Cherniack, A. D., Thorsson, V., Akbani, R., Bowlby, R., Wong, C. K., Wiznerowicz, M., Sanchez-Vega, F., Robertson, A. G., Schneider, B. G., Lawrence, M. S., Noushmehr, H., … Laird, P. W. (2018). Cell-of-Origin Patterns Dominate the Molecular Classification of 10,000 Tumors from 33 Types of Cancer. *Cell*, *173*(2), 291-304.e6. https://doi.org/10.1016/j.cell.2018.03.022

Hong, Y., Limback, D., Elsarraj, H. S., Harper, H., Haines, H., Hansford, H., Ricci, M., Kaufman, C., Wedlock, E., Xu, M., Zhang, J., May, L., Cusick, T., Inciardi, M., Redick, M., Gatewood, J., Winblad, O., Aripoli, A., Huppe, A., … Consortium, the G. C. P. (2022). Mouse-INtraDuctal (MIND): An in vivo model for studying the underlying mechanisms of DCIS malignancy. *The Journal of Pathology*, *256*(2), 186–201. https://doi.org/10.1002/path.5820

Horlbeck, M. A., Witkowsky, L. B., Guglielmi, B., Replogle, J. M., Gilbert, L. A., Villalta, J. E., Torigoe, S. E., Tjian, R., & Weissman, J. S. (2016). Nucleosomes impede Cas9 access to DNA in vivo and in vitro. *eLife*, *5*, e12677. https://doi.org/10.7554/eLife.12677

Hu, M., Yao, J., Carroll, D. K., Weremowicz, S., Chen, H., Carrasco, D., Richardson, A., Violette, S., Nikolskaya, T., Nikolsky, Y., Bauerlein, E. L., Hahn, W. C., Gelman, R. S., Allred, C., Bissell, M. J., Schnitt, S., & Polyak, K. (2008). Regulation of In Situ to Invasive Breast Carcinoma Transition. *Cancer Cell*, *13*(5), 394–406. https://doi.org/10.1016/j.ccr.2008.03.007

Hutten, S. J., de Bruijn, R., Lutz, C., Badoux, M., Eijkman, T., Chao, X., Ciwinska, M., Sheinman, M., Messal, H., Herencia-Ropero, A., Kristel, P., Mulder, L., van der Waal, R., Sanders, J., Almekinders, M. M., Llop-Guevara, A., Davies, H. R., van Haren, M. J., Martin, N. I., … Jonkers, J. (2023). A living biobank of patient-derived ductal carcinoma in situ mouse-intraductal xenografts identifies risk factors for invasive progression. *Cancer Cell*, *41*(5), 986-1002.e9. https://doi.org/10.1016/j.ccell.2023.04.002

Hutten, S. J., & Jonkers, J. (2023). MIND the translational gap: Preclinical models of ductal carcinoma in situ. *Clinical and Translational Medicine*, *13*(8). https://doi.org/10.1002/ctm2.1376

Ip, M., & Asch, B. (2000). *Methods in mammary gland biology and breast cancer research*. Kluwer Academic/Plenum Publishers.

Iravani, S., Mora, L., Miller, F. R., & Dawson, P. J. (1998). Altered expression of c-erbB-2, DF3, b72.3, p53 and Ki-67 with progression and differentiation to two distinct histologic types of invasive carcinoma in the MCF10AT human xenograft model of proliferative breast disease. *International Journal of Oncology*. https://doi.org/10.3892/ijo.12.2.369

Janda, E., Lehmann, K., Killisch, I., Jechlinger, M., Herzig, M., Downward, J., Beug, H., & Grünert, S. (2002). Ras and TGF[beta] cooperatively regulate epithelial cell plasticity and metastasis: Dissection of Ras signaling pathways. *The Journal of Cell Biology*, *156*(2), 299–313. https://doi.org/10.1083/jcb.200109037

Janes, K. A. (2015). An analysis of critical factors for quantitative immunoblotting. *Science Signaling*, *8*(371), rs2. https://doi.org/10.1126/scisignal.2005966

Janes, K. A., Wang, C.-C., Holmberg, K. J., Cabral, K., & Brugge, J. S. (2010). Identifying single-cell molecular programs by stochastic profiling. *Nature Methods*, *7*(4), Article 4. https://doi.org/10.1038/nmeth.1442

Jedeszko, C., Victor, B. C., Podgorski, I., & Sloane, B. F. (2009). Fibroblast hepatocyte growth factor promotes invasion of human mammary ductal carcinoma in situ. *Cancer Research*, *69*(23), 9148–9155. https://doi.org/10.1158/0008-5472.CAN-09-1043

Jia, Z., Wei, Y., Zhang, Y., Song, K., & Yuan, J. (2024). Metabolic reprogramming and heterogeneity during the decidualization process of endometrial stromal cells. *Cell Communication and Signaling*, *22*(1), 385. https://doi.org/10.1186/s12964-024-01763-y

Jin, W., Fuki, I. V., Seidah, N. G., Benjannet, S., Glick, J. M., & Rader, D. J. (2005). Proprotein convertases [corrected] are responsible for proteolysis and inactivation of endothelial lipase. *The Journal of Biological Chemistry*, *280*(44), 36551–36559. https://doi.org/10.1074/jbc.M502264200

Jin, W., Millar, J. S., Broedl, U., Glick, J. M., & Rader, D. J. (2003). Inhibition of endothelial lipase causes increased HDL cholesterol levels in vivo. *The Journal of Clinical Investigation*, *111*(3), 357–362. https://doi.org/10.1172/JCI16146

Jumper, J., Evans, R., Pritzel, A., Green, T., Figurnov, M., Ronneberger, O., Tunyasuvunakool, K., Bates, R., Žídek, A., Potapenko, A., Bridgland, A., Meyer, C., Kohl, S. A. A., Ballard, A. J., Cowie, A., Romera-Paredes, B., Nikolov, S., Jain, R., Adler, J., … Hassabis, D. (2021). Highly accurate protein structure prediction with AlphaFold. *Nature*, *596*(7873), 583–589. https://doi.org/10.1038/s41586-021-03819-2

Kadota, M., Yang, H. H., Gomez, B., Sato, M., Clifford, R. J., Meerzaman, D., Dunn, B. K., Wakefield, L. M., & Lee, M. P. (2010). Delineating Genetic Alterations for Tumor Progression in the MCF10A Series of Breast Cancer Cell Lines. *PLOS ONE*, *5*(2), e9201. https://doi.org/10.1371/journal.pone.0009201

Kai, H. S.-T., Butler, G. S., Morrison, C. J., King, A. E., Pelman, G. R., & Overall, C. M. (2002). Utilization of a novel recombinant myoglobin fusion protein expression system to characterize the tissue inhibitor of metalloproteinase (TIMP)-4 and TIMP-2 C-terminal domain and tails by mutagenesis. The importance of acidic residues in binding the MMP-2 hemopexin C-domain. *The Journal of Biological Chemistry*, *277*(50), 48696–48707.

https://doi.org/10.1074/jbc.M209177200

Kalaany, N. Y., & Sabatini, D. M. (2009). Tumours with PI3K activation are resistant to dietary restriction. *Nature*, *458*(7239), 725–731. https://doi.org/10.1038/nature07782

Kao, J., Salari, K., Bocanegra, M., Choi, Y.-L., Girard, L., Gandhi, J., Kwei, K. A., Hernandez-Boussard, T., Wang, P., Gazdar, A. F., Minna, J. D., & Pollack, J. R. (2009). Molecular Profiling of Breast Cancer Cell Lines Defines Relevant Tumor Models and Provides a Resource for Cancer Gene Discovery. *PLoS ONE*, *4*(7), e6146. https://doi.org/10.1371/journal.pone.0006146

Kelly, R. B. (1985). Pathways of Protein Secretion in Eukaryotes. *Science*, *230*(4721), 25–32. https://doi.org/10.1126/science.2994224

Kilpatrick, L. M., Stephens, A. N., Hardman, B. M., Salamonsen, L. A., Li, Y., Stanton, P. G., & Nie, G. (2009). Proteomic identification of caldesmon as a physiological substrate of proprotein convertase 6 in human uterine decidual cells essential for pregnancy establishment. *Journal of Proteome Research*, *8*(11), 4983–4992. https://doi.org/10.1021/pr900381a

Kines, R. C., Thompson, C. D., Lowy, D. R., Schiller, J. T., & Day, P. M. (2009). The initial steps leading to papillomavirus infection occur on the basement membrane prior to cell surface binding. *Proceedings of the National Academy of Sciences of the United States of America*, *106*(48), 20458–20463. https://doi.org/10.1073/pnas.0908502106

Kittrell, F., Valdez, K., Elsarraj, H., Hong, Y., Medina, D., & Behbod, F. (2016). Mouse Mammary Intraductal (MIND) Method for Transplantation of Patient Derived Primary DCIS Cells and Cell Lines. *Bio-Protocol*, *6*(5), e1744.

Koboldt, D. C., Fulton, R. S., McLellan, M. D., Schmidt, H., Kalicki-Veizer, J., McMichael, J. F., Fulton, L. L., Dooling, D. J., Ding, L., Mardis, E. R., Wilson, R. K., Ally, A., Balasundaram, M., Butterfield, Y. S. N., Carlsen, R., Carter, C., Chu, A., Chuah, E., Chun, H.-J. E., … Palchik, J. D. (2012). Comprehensive molecular portraits of human breast tumours. *Nature*, *490*(7418), 61–70. https://doi.org/10.1038/nature11412

Kosugi, S., Hasebe, M., Matsumura, N., Takashima, H., Miyamoto-Sato, E., Tomita, M., & Yanagawa, H. (2009). Six classes of nuclear localization signals specific to different binding grooves of importin alpha. *The Journal of Biological Chemistry*, *284*(1), 478–485. https://doi.org/10.1074/jbc.M807017200

Kraler, S., Balbi, C., Vdovenko, D., Lapikova-Bryhinska, T., Camici, G. G., Liberale, L., Bonetti, N., Canestro, C. D., Burger, F., Roth, A., Carbone, F., Vassalli, G., Mach, F., Bhasin, S., Wenzl, F. A., Muller, O., Räber, L., Matter, C. M., Montecucco, F., … Akhmedov, A. (2023). Circulating GDF11 exacerbates myocardial injury in mice and associates with increased infarct size in humans. *Cardiovascular Research*, *119*(17), 2729–2742. https://doi.org/10.1093/cvr/cvad153

Lander, A. D., Gokoffski, K. K., Wan, F. Y. M., Nie, Q., & Calof, A. L. (2009). Cell lineages and the logic of proliferative control. *PLoS Biology*, *7*(1), e15. https://doi.org/10.1371/journal.pbio.1000015

Lazure, C., Seidah, N. G., Pélaprat, D., & Chrétien, M. (1983). Proteases and posttranslational processing of prohormones: A review. *Canadian Journal of Biochemistry and Cell Biology*, *61*(7), 501–515. https://doi.org/10.1139/o83-066

Leduc, R., Molloy, S. S., Thorne, B. A., & Thomas, G. (1992). Activation of human furin precursor processing endoprotease occurs by an intramolecular autoproteolytic cleavage. *Journal of*

Biological Chemistry, *267*(20), 14304–14308. https://doi.org/10.1016/S0021-9258(19)49712-3

Lee, S., Stewart, S., Nagtegaal, I., Luo, J., Wu, Y., Colditz, G., Medina, D., & Allred, D. C. (2012). Differentially Expressed Genes Regulating the Progression of Ductal Carcinoma In Situ to Invasive Breast Cancer. *Cancer Research*, *72*(17), 4574–4586. https://doi.org/10.1158/0008-5472.CAN-12-0636

Li, C., Zhi, D., Wang, K., & Liu, X. (2022). MetaRNN: Differentiating rare pathogenic and rare benign missense SNVs and InDels using deep learning. *Genome Medicine*, *14*(1), 115. https://doi.org/10.1186/s13073-022-01120-z

Li, Q., Kannan, A., Das, A., Demayo, F. J., Hornsby, P. J., Young, S. L., Taylor, R. N., Bagchi, M. K., & Bagchi, I. C. (2013). WNT4 acts downstream of BMP2 and functions via β-catenin signaling pathway to regulate human endometrial stromal cell differentiation. *Endocrinology*, *154*(1), 446–457. https://doi.org/10.1210/en.2012-1585

Li, Q., & Mattingly, R. R. (2008). Restoration of E-cadherin cell-cell junctions requires both expression of E-cadherin and suppression of ERK MAP kinase activation in Ras-transformed breast epithelial cells. *Neoplasia (New York, N.Y.)*, *10*(12), 1444–1458. https://doi.org/10.1593/neo.08968

Lin, E. Y., Jones, J. G., Li, P., Zhu, L., Whitney, K. D., Muller, W. J., & Pollard, J. W. (2003). Progression to malignancy in the polyoma middle T oncoprotein mouse breast cancer model provides a reliable model for human diseases. *The American Journal of Pathology*, *163*(5), 2113–2126. https://doi.org/10.1016/S0002-9440(10)63568-7

Liu, X., Li, C., Mou, C., Dong, Y., & Tu, Y. (2020). dbNSFP v4: A comprehensive database of transcript-specific functional predictions and annotations for human nonsynonymous and splice-site SNVs. *Genome Medicine*, *12*(1), 103. https://doi.org/10.1186/s13073-020-00803-9

Livasy, C. A., Perou, C. M., Karaca, G., Cowan, D. W., Maia, D., Jackson, S., Tse, C.-K., Nyante, S., & Millikan, R. C. (2007). Identification of a basal-like subtype of breast ductal carcinoma in situ. *Human Pathology*, *38*(2), 197–204. https://doi.org/10.1016/j.humpath.2006.08.017

Lonsdale, J., Thomas, J., Salvatore, M., Phillips, R., Lo, E., Shad, S., Hasz, R., Walters, G., Garcia, F., Young, N., Foster, B., Moser, M., Karasik, E., Gillard, B., Ramsey, K., Sullivan, S., Bridge, J., Magazine, H., Syron, J., … Moore, H. F. (2013). The Genotype-Tissue Expression (GTEx) project. *Nature Genetics*, *45*(6), 580–585. https://doi.org/10.1038/ng.2653

Lopacinski, A. B., Sweatt, A. J., Smolko, C. M., Gray-Gaillard, E., Borgman, C. A., Shah, M., & Janes, K. A. (2021). Modeling the complete kinetics of coxsackievirus B3 reveals human determinants of host-cell feedback. *Cell Systems*, *12*(4), 304-323.e13. https://doi.org/10.1016/j.cels.2021.02.004

Lopez-Garcia, M. A., Geyer, F. C., Lacroix-Triki, M., Marchió, C., & Reis-Filho, J. S. (2010). Breast cancer precursors revisited: Molecular features and progression pathways. *Histopathology*, *57*(2), 171–192. https://doi.org/10.1111/j.1365-2559.2010.03568.x

Lusson, J., Vieau, D., Hamelin, J., Day, R., Chrétien, M., & Seidah, N. G. (1993). cDNA structure of the mouse and rat subtilisin/kexin-like PC5: A candidate proprotein convertase expressed in endocrine and nonendocrine cells. *Proceedings of the National Academy of Sciences of the United States of America*, *90*(14), 6691–6695. https://doi.org/10.1073/pnas.90.14.6691

Maguire, S. L., Peck, B., Wai, P. T., Campbell, J., Barker, H., Gulati, A., Daley, F., Vyse, S., Huang, P., Lord, C. J., Farnie, G., Brennan, K., & Natrajan, R. (2016). Three-dimensional modelling identifies novel genetic dependencies associated with breast cancer progression in the isogenic MCF10 model. *The Journal of Pathology*, *240*(3), 315–328. https://doi.org/10.1002/path.4778

Mailleux, A. A., Overholtzer, M., Schmelzle, T., Bouillet, P., Strasser, A., & Brugge, J. S. (2007). BIM Regulates Apoptosis during Mammary Ductal Morphogenesis, and Its Absence Reveals Alternative Cell Death Mechanisms. *Developmental Cell*, *12*(2), 221–234. https://doi.org/10.1016/j.devcel.2006.12.003

Marohl, T., Atkins, K. A., Wang, L., & Janes, K. A. (2025). *PCSK5M452I is a recessive hypomorph exclusive to MCF10DCIS.com cells* (p. 2025.03.03.641323). bioRxiv. https://doi.org/10.1101/2025.03.03.641323

Matsuuchi, L., Buckley, K. M., Lowe, A. W., & Kelly, R. B. (1988). Targeting of secretory vesicles to cytoplasmic domains in AtT-20 and PC-12 cells. *The Journal of Cell Biology*, *106*(2), 239–251. https://doi.org/10.1083/jcb.106.2.239

Mayer, G., Hamelin, J., Asselin, M.-C., Pasquato, A., Marcinkiewicz, E., Tang, M., Tabibzadeh, S., & Seidah, N. G. (2008). The Regulated Cell Surface Zymogen Activation of the Proprotein Convertase PC5A Directs the Processing of Its Secretory Substrates *. *Journal of Biological Chemistry*, *283*(4), 2373–2384. https://doi.org/10.1074/jbc.M708763200

McKeen Polizzotti, L., Oztan, B., Bjornsson, C. S., Shubert, K. R., Yener, B., & Plopper, G. E. (2012). Novel Image Analysis Approach Quantifies Morphological Characteristics of 3D Breast Culture Acini with Varying Metastatic Potentials. *Journal of Biomedicine and Biotechnology*, *2012*, 1–16. https://doi.org/10.1155/2012/102036

McPherron, A. C., Lawler, A. M., & Lee, S.-J. (1997). Regulation of skeletal muscle mass in mice by a new TGF-p superfamily member. *Nature*, *387*(6628), 83–90. https://doi.org/10.1038/387083a0

McPherron, A. C., Lawler, A. M., & Lee, S.-J. (1999). Regulation of anterior/posterior patterning of the axial skeleton by growth/differentiation factor 11. *Nature Genetics*, *22*(3), Article 3. https://doi.org/10.1038/10320

Mei, W., Faraj Tabrizi, S., Godina, C., Lovisa, A. F., Isaksson, K., Jernström, H., & Tavazoie, S. F. (2025). A commonly inherited human PCSK9 germline variant drives breast cancer metastasis via LRP1 receptor. *Cell*, *188*(2), 371-389.e28. https://doi.org/10.1016/j.cell.2024.11.009

Miller, F. R. (2000). Xenograft Models of Premalignant Breast Disease. *Journal of Mammary Gland Biology and Neoplasia*, *5*(4), 379–391. https://doi.org/10.1023/A:1009577811584

Miller, F. R., Santner, S. J., Tait, L., & Dawson, P. J. (2000). MCF10DCIS.com Xenograft Model of Human Comedo Ductal Carcinoma In Situ. *JNCI: Journal of the National Cancer Institute*, *92*(14), 1185a–11186. https://doi.org/10.1093/jnci/92.14.1185a

Miller, F. R., Soule, H. D., Tait, L., Pauley, R. J., Wolman, S. R., Dawson, P. J., & Heppner, G. H. (1993). Xenograft Model of Progressive Human Proliferative Breast Disease. *JNCI Journal of the National Cancer Institute*, *85*(21), 1725–1732. https://doi.org/10.1093/jnci/85.21.1725

Miranda, L., Wolf, J., Pichuantes, S., Duke, R., & Pranzusoff, A. (1996). Isolation of the human PC6 gene encoding the putative host protease for HIV-1 gp160 processing in CD4+ T lymphocytes. *Proceedings of the National Academy of Sciences of the United States of America*, *93*(15),

7695–7700. Scopus. https://doi.org/10.1073/pnas.93.15.7695

Muthuswamy, S. K., Li, D., Lelievre, S., Bissell, M. J., & Brugge, J. S. (2001). ErbB2, but not ErbB1, reinitiates proliferation and induces luminal repopulation in epithelial acini. *Nature Cell Biology*, *3*(9), 785–792. https://doi.org/10.1038/ncb0901-785

Nakagawa, T., Hosaka, M., Torii, S., Watanabe, T., Murakami, K., & Nakayama, K. (1993). Identification and Functional Expression of a New Member of the Mammalian Kex2-Like Processing Endoprotease Family: Its Striking Structural Similarity to PACE41. *The Journal of Biochemistry*, *113*(2), 132–135. https://doi.org/10.1093/oxfordjournals.jbchem.a124015

Nakagawa, T., Murakami, K., & Nakayama, K. (1993). Identification of an isoform with an extremely large Cys-rich region of PC6, a Kex2-like processing endoprotease. *FEBS Letters*, *327*(2), 165–171. https://doi.org/10.1016/0014-5793(93)80163-O

Nakamura, N., Rabouille, C., Watson, R., Nilsson, T., Hui, N., Slusarewicz, P., Kreis, T. E., & Warren, G. (1995). Characterization of a cis-Golgi matrix protein, GM130. *The Journal of Cell Biology*, *131*(6 Pt 2), 1715–1726. https://doi.org/10.1083/jcb.131.6.1715

Nakashima, M., Toyono, T., Akamine, A., & Joyner, A. (1999). Expression of growth/differentiation factor 11, a new member of the BMP/ TGFb superfamily during mouse embryogenesis. *Mechanisms of Development*.

Nallasamy, S., Gebril, M., Mulder, S., & Das, R. (2025). *Extracellular Matrix Reorganization During Endometrial Decidualization* (p. 2025.03.22.644728). bioRxiv. https://doi.org/10.1101/2025.03.22.644728

Neve, R. M., Chin, K., Fridlyand, J., Yeh, J., Baehner, F. L., Fevr, T., Clark, L., Bayani, N., Coppe, J.-P., Tong, F., Speed, T., Spellman, P. T., DeVries, S., Lapuk, A., Wang, N. J., Kuo, W.-L., Stilwell, J. L., Pinkel, D., Albertson, D. G., … Gray, J. W. (2006). A collection of breast cancer cell lines for the study of functionally distinct cancer subtypes. *Cancer Cell*, *10*(6), 515–527. https://doi.org/10.1016/j.ccr.2006.10.008

Nicholls, P. K., Sun, Z., Heng, S., Li, Y., Wang, J., & Nie, G. (2011). Embryo implantation is closely associated with dynamic expression of proprotein convertase 5/6 in the rabbit uterus. *Reproductive Biology and Endocrinology: RB&E*, *9*, 43. https://doi.org/10.1186/1477-7827-9-43

Nie, G., Li, Y., Minoura, H., Findlay, J. K., & Salamonsen, L. A. (2003). Specific and Transient Up-Regulation of Proprotein Convertase 6 at the Site of Embryo Implantation and Identification of a Unique Transcript in Mouse Uterus During Early Pregnancy1. *Biology of Reproduction*, *68*(2), 439–447. https://doi.org/10.1095/biolreprod.102.006676

Nie, G., Li, Y., Wang, M., Liu, Y. X., Findlay, J. K., & Salamonsen, L. A. (2005). Inhibiting Uterine PC6 Blocks Embryo Implantation: An Obligatory Role for a Proprotein Convertase in Fertility1. *Biology of Reproduction*, *72*(4), 1029–1036. https://doi.org/10.1095/biolreprod.104.036889

Nielsen, T. O. (2004). Immunohistochemical and Clinical Characterization of the Basal-Like Subtype of Invasive Breast Carcinoma. *Clinical Cancer Research*, *10*(16), 5367–5374. https://doi.org/10.1158/1078-0432.CCR-04-0220

Nielsen, T. O., & Perou, C. M. (2015). CCR 20th Anniversary Commentary: The Development of Breast Cancer Molecular Subtyping. *Clinical Cancer Research*, *21*(8), 1779–1781. https://doi.org/10.1158/1078-0432.CCR-14-2552

Nour, N., Basak, A., Chrétien, M., & Seidah, N. G. (2003). Structure-function analysis of the prosegment of the proprotein convertase PC5A. *The Journal of Biological Chemistry*, *278*(5), 2886–2895. https://doi.org/10.1074/jbc.M208009200

Nour, N., Mayer, G., Mort, J. S., Salvas, A., Mbikay, M., Morrison, C. J., Overall, C. M., & Seidah, N. G. (2005). The cysteine-rich domain of the secreted proprotein convertases PC5A and PACE4 functions as a cell surface anchor and interacts with tissue inhibitors of metalloproteinases. *Molecular Biology of the Cell*, *16*(11), 5215–5226. https://doi.org/10.1091/mbc.e05-06-0504

Odeniyide, P., Yohe, M. E., Pollard, K., Vaseva, A. V., Calizo, A., Zhang, L., Rodriguez, F. J., Gross, J. M., Allen, A. N., Wan, X., Somwar, R., Schreck, K. C., Kessler, L., Wang, J., & Pratilas, C. A. (2022). Targeting farnesylation as a novel therapeutic approach in HRAS-mutant rhabdomyosarcoma. *Oncogene*, *41*(21), 2973–2983. https://doi.org/10.1038/s41388-022-02305-x

Oft, M., Peli, J., Rudaz, C., Schwarz, H., Beug, H., & Reichmann, E. (1996). TGF-beta1 and Ha-Ras collaborate in modulating the phenotypic plasticity and invasiveness of epithelial tumor cells. *Genes & Development*, *10*(19), 2462–2477. https://doi.org/10.1101/gad.10.19.2462

Oh, S. P., Yeo, C.-Y., Lee, Y., Schrewe, H., Whitman, M., & Li, E. (2002). Activin type IIA and IIB receptors mediate Gdf11 signaling in axial vertebral patterning. *Genes & Development*, *16*(21), 2749–2754. https://doi.org/10.1101/gad.1021802

Okada, H., Nie, G., & Salamonsen, L. A. (2005). Requirement for proprotein convertase 5/6 during decidualization of human endometrial stromal cells in vitro. *The Journal of Clinical Endocrinology and Metabolism*, *90*(2), 1028–1034. https://doi.org/10.1210/jc.2004-0904

Okada, H., Tsuzuki, T., & Murata, H. (2018). Decidualization of the human endometrium. *Reproductive Medicine and Biology*, *17*(3), 220–227. https://doi.org/10.1002/rmb2.12088

Overall, C. M., King, A. E., Sam, D. K., Ong, A. D., Lau, T. T., Wallon, U. M., DeClerck, Y. A., & Atherstone, J. (1999). Identification of the tissue inhibitor of metalloproteinases-2 (TIMP-2) binding site on the hemopexin carboxyl domain of human gelatinase A by site-directed mutagenesis. The hierarchical role in binding TIMP-2 of the unique cationic clusters of hemopexin modules III and IV. *The Journal of Biological Chemistry*, *274*(7), 4421–4429. https://doi.org/10.1074/jbc.274.7.4421

Page, D. L., Dupont, W. D., Rogers, L. W., Jensen, R. A., & Schuyler, P. A. (1995). Continued local recurrence of carcinoma 15–25 years after a diagnosis of low grade ductal carcinoma in situ of the breast treated only by biopsy. *Cancer*, *76*(7), 1197–1200. Scopus. https://doi.org/10.1002/1097-0142(19951001)76:7<1197::AID-CNCR2820760715>3.0.CO;2-0

Page, D. L., Dupont, W. D., Rogers, L. W., & Landenberger, M. (1982). Intraductal carcinoma of the breast: Follow‐up after biopsy only. *Cancer*, *49*(4), 751–758. Scopus. https://doi.org/10.1002/1097-0142(19820215)49:4<751::AID-CNCR2820490426>3.0.CO;2-Y

Palade, G. (1975). Intracellular Aspects of the Process of Protein Synthesis. *Science*, *189*(4200), 347–358. https://doi.org/10.1126/science.1096303

Pereira, E. J., Burns, J. S., Lee, C. Y., Marohl, T., Calderon, D., Wang, L., Atkins, K. A., Wang, C.-C., & Janes, K. A. (2020). Sporadic activation of an oxidative stress–dependent NRF2-p53 signaling network in breast epithelial spheroids and premalignancies. *Science Signaling*, *13*(627), eaba4200. https://doi.org/10.1126/scisignal.aba4200

Perez, C. A., Ott, J., Mays, D. J., & Pietenpol, J. A. (2007). p63 consensus DNA-binding site: Identification, analysis and application into a p63MH algorithm. *Oncogene*, *26*(52), 7363–7370. https://doi.org/10.1038/sj.onc.1210561

Perou, C. M., Sørlie, T., Eisen, M. B., van de Rijn, M., Jeffrey, S. S., Rees, C. A., Pollack, J. R., Ross, D. T., Johnsen, H., Akslen, L. A., Fluge, Ø., Pergamenschikov, A., Williams, C., Zhu, S. X., Lønning, P. E., Børresen-Dale, A.-L., Brown, P. O., & Botstein, D. (2000). Molecular portraits of human breast tumours. *Nature*, *406*(6797), 747–752. https://doi.org/10.1038/35021093

Peuhu, E., Jacquemet, G., Scheele, C. L. G. J., Isomursu, A., Laisne, M.-C., Koskinen, L. M., Paatero, I., Thol, K., Georgiadou, M., Guzmán, C., Koskinen, S., Laiho, A., Elo, L. L., Boström, P., Hartiala, P., Rheenen, J. van, & Ivaska, J. (2022). MYO10-filopodia support basement membranes at pre-invasive tumor boundaries. *Developmental Cell*, *57*(20), 2350-2364.e7. https://doi.org/10.1016/j.devcel.2022.09.016

Pfefferle, A. D., Herschkowitz, J. I., Usary, J., Harrell, J. C., Spike, B. T., Adams, J. R., Torres-Arzayus, M. I., Brown, M., Egan, S. E., Wahl, G. M., Rosen, J. M., & Perou, C. M. (2013). Transcriptomic classification of genetically engineered mouse models of breast cancer identifies human subtype counterparts. *Genome Biology*, *14*(11), R125. https://doi.org/10.1186/gb-2013-14-11-r125

Polyak, K., & Hu, M. (2005). Do Myoepithelial Cells Hold the Key for Breast Tumor Progression? *Journal of Mammary Gland Biology and Neoplasia*, *10*(3), 231–247. https://doi.org/10.1007/s10911-005-9584-6

Possemato, R., Marks, K. M., Shaul, Y. D., Pacold, M. E., Kim, D., Birsoy, K., Sethumadhavan, S., Woo, H.-K., Jang, H. G., Jha, A. K., Chen, W. W., Barrett, F. G., Stransky, N., Tsun, Z.-Y., Cowley, G. S., Barretina, J., Kalaany, N. Y., Hsu, P. P., Ottina, K., … Sabatini, D. M. (2011). Functional genomics reveal that the serine synthesis pathway is essential in breast cancer. *Nature*, *476*(7360), 346–350. https://doi.org/10.1038/nature10350

Przanowska, R. K., Labban, N., Przanowski, P., Hawes, R. B., Atkins, K. A., Showalter, S. L., & Janes, K. A. (2024). Patient-derived response estimates from zero-passage organoids of luminal breast cancer. *Breast Cancer Research: BCR*, *26*(1), 192. https://doi.org/10.1186/s13058-024-01931-5

Puleo, J., & Polyak, K. (2021). The MCF10 Model of Breast Tumor Progression. *Cancer Research*, *81*(16), 4183–4185. https://doi.org/10.1158/0008-5472.CAN-21-1939

Qin, X., Kuang, H., Chen, L., Wei, S., Yu, D., & Liang, F. (2017). Coexpression of growth differentiation factor 11 and reactive oxygen species in metastatic oral cancer and its role in inducing the epithelial to mesenchymal transition. *Oral Surgery, Oral Medicine, Oral Pathology and Oral Radiology*, *123*(6), 697–706. https://doi.org/10.1016/j.oooo.2017.03.010

Radomsky, M. L., Whaley, K. J., Cone, R. A., & Mark Saltzman, W. (1992). Controlled Vaginal Delivery of Antibodies in the Mouse1. *Biology of Reproduction*, *47*(1), 133–140. https://doi.org/10.1095/biolreprod47.1.133

Rancourt, S. L., & Rancourt, D. E. (1997). Murine subtilisin-like proteinase SPC6 is expressed during embryonic implantation, somitogenesis, and skeletal formation. *Developmental Genetics*, *21*(1), 75–81. https://doi.org/10.1002/(SICI)1520-6408(1997)21:1<75::AID-DVG9>3.0.CO;2-5

Rizki, A., Weaver, V. M., Lee, S.-Y., Rozenberg, G. I., Chin, K., Myers, C. A., Bascom, J. L., Mott, J. D., Semeiks, J. R., Grate, L. R., Mian, I. S., Borowsky, A. D., Jensen, R. A., Idowu, M. O., Chen, F.,

Chen, D. J., Petersen, O. W., Gray, J. W., & Bissell, M. J. (2008). A Human Breast Cell Model of Preinvasive to Invasive Transition. *Cancer Research*, *68*(5), 1378–1387. https://doi.org/10.1158/0008-5472.CAN-07-2225

Rogers, M. F., Gaunt, T. R., & Campbell, C. (2021). CScape-somatic: Distinguishing driver and passenger point mutations in the cancer genome. *Bioinformatics (Oxford, England)*, *37*(22), 4298. https://doi.org/10.1093/bioinformatics/btab654

Rogers, M. F., Shihab, H. A., Gaunt, T. R., & Campbell, C. (2017). CScape: A tool for predicting oncogenic single-point mutations in the cancer genome. *Scientific Reports*, *7*(1), 11597. https://doi.org/10.1038/s41598-017-11746-4

Rossi, F., Luppi, S., Fejza, A., Giolo, E., Ricci, G., & Andreuzzi, E. (2025). Extracellular matrix and pregnancy: Functions and opportunities caught in the net. *Reproductive Biology and Endocrinology*, *23*(1), 24. https://doi.org/10.1186/s12958-025-01348-5

Russell, T. D., Jindal, S., Agunbiade, S., Gao, D., Troxell, M., Borges, V. F., & Schedin, P. (2015). Myoepithelial Cell Differentiation Markers in Ductal Carcinoma in Situ Progression. *The American Journal of Pathology*, *185*(11), 3076–3089. https://doi.org/10.1016/j.ajpath.2015.07.004

Russo, J., Tait, L., & Russo, I. H. (1991). Morphological expression of cell transformation induced by c-Ha-ras oncogene in human breast epithelial cells. *Journal of Cell Science*, *99*, 453–463.

Samson, J., Derlipanska, M., Zaheed, O., & Dean, K. (2021). Molecular and cellular characterization of two patient-derived ductal carcinoma in situ (DCIS) cell lines, ETCC-006 and ETCC-010. *BMC Cancer*, *21*(1), 790. https://doi.org/10.1186/s12885-021-08511-2

Sanati, S. (2019). Morphologic and Molecular Features of Breast Ductal Carcinoma in Situ. *The American Journal of Pathology*, *189*(5), 946–955. https://doi.org/10.1016/j.ajpath.2018.07.031

Sanders, M. E., Schuyler, P. A., Dupont, W. D., & Page, D. L. (2005). The natural history of low-grade ductal carcinoma in situ of the breast in women treated by biopsy only revealed over 30 years of long-term follow-up. *Cancer*, *103*(12), 2481–2484. https://doi.org/10.1002/cncr.21069

Santner, S. J., Dawson, P. J., Tait, L., Soule, H. D., Eliason, J., Mohamed, A. N., Wolman, S. R., Heppner, G. H., & Miller, F. R. (2001). Malignant MCF10CA1 Cell Lines Derived from Premalignant Human Breast Epithelial MCF10AT Cells. *Breast Cancer Research and Treatment*, *65*(2), 101–110. https://doi.org/10.1023/A:1006461422273

Schnell, S. A., Staines, W. A., & Wessendorf, M. W. (1999). Reduction of lipofuscin-like autofluorescence in fluorescently labeled tissue. *The Journal of Histochemistry and Cytochemistry: Official Journal of the Histochemistry Society*, *47*(6), 719–730. https://doi.org/10.1177/002215549904700601

Schultz, G. A., & Edwards, D. R. (1997). Biology and genetics of implantation. *Developmental Genetics*, *21*(1), 1–5. https://doi.org/10.1002/(SICI)1520-6408(1997)21:1<1::AID-DVG1>3.0.CO;2-B

Schwartz, G. F., Solin, L. J., Olivotto, I. A., Ernster, V. L., & Pressman, P. I. (2000). Consensus Conference on the Treatment of In Situ Ductal Carcinoma of the Breast, April 22-25, 1999. *Cancer*, *88*(4), 946–954.

Scripcaru, G., & Zardawi, I. M. (2012). Mammary ductal carcinoma in situ: A fresh look at architectural patterns. *International Journal of Surgical Oncology*, *2012*, 979521.

https://doi.org/10.1155/2012/979521

Seidah, N. G. (2011). The Proprotein Convertases, 20 Years Later. In M. Mbikay & N. G. Seidah (Eds.), *Proprotein Convertases* (pp. 23–57). Humana Press. https://doi.org/10.1007/978-1-61779-204-5_3

Seidah, N. G., & Chrétien, M. (1992). Proprotein and prohormone convertases of the subtilisin family: Recent developments and future perspectives. *Trends in Endocrinology & Metabolism*, *3*(4), 133–140. https://doi.org/10.1016/1043-2760(92)90102-7

Seidah, N. G., & Chrétien, M. (1999). Proprotein and prohormone convertases: A family of subtilases generating diverse bioactive polypeptides. *Brain Research*, *848*(1), 45–62. https://doi.org/10.1016/S0006-8993(99)01909-5

Seidah, N. G., Gaspar, L., Mion, P., Marcinkiewicz, M., Mbikay, M., & Chrétien, M. (1990). cDNA Sequence of Two Distinct Pituitary Proteins Homologous to Kex2 and Furin Gene Products: Tissue-Specific mRNAs Encoding Candidates for Pro-Hormone Processing Proteinases. *DNA and Cell Biology*, *9*(6), 415–424. https://doi.org/10.1089/dna.1990.9.415

Seidah, N. G., Marcinkiewicz, M., Benjannet, S., Gaspar, L., Beaubien, G., Mattei, M. G., Lazure, C., Mbikay, M., & Chrétien, M. (1991). Cloning and primary sequence of a mouse candidate prohormone convertase PC1 homologous to PC2, Furin, and Kex2: Distinct chromosomal localization and messenger RNA distribution in brain and pituitary compared to PC2. *Molecular Endocrinology (Baltimore, Md.)*, *5*(1), 111–122. https://doi.org/10.1210/mend-5-1-111

Seidah, N. G., Mayer, G., Zaid, A., Rousselet, E., Nassoury, N., Poirier, S., Essalmani, R., & Prat, A. (2008). The activation and physiological functions of the proprotein convertases. *The International Journal of Biochemistry & Cell Biology*, *40*(6), 1111–1125. https://doi.org/10.1016/j.biocel.2008.01.030

Seidah, N. G., & Prat, A. (2012). The biology and therapeutic targeting of the proprotein convertases. *Nature Reviews. Drug Discovery*, *11*(5), 367–383. https://doi.org/10.1038/nrd3699

Seidah, N. G., Sadr, M. S., Chrétien, M., & Mbikay, M. (2013). The multifaceted proprotein convertases: Their unique, redundant, complementary, and opposite functions. *The Journal of Biological Chemistry*, *288*(30), 21473–21481. https://doi.org/10.1074/jbc.R113.481549

Senturk, S., Shirole, N. H., Nowak, D. G., Corbo, V., Pal, D., Vaughan, A., Tuveson, D. A., Trotman, L. C., Kinney, J. B., & Sordella, R. (2017). Rapid and tunable method to temporally control gene editing based on conditional Cas9 stabilization. *Nature Communications*, *8*, 14370. https://doi.org/10.1038/ncomms14370

Shekhar, M. P. V., Chen, M. L., Werdell, J., Heppner, G. H., Miller, F. R., & Christman, J. K. (1998). Transcriptional activation of functional endogenous estrogen receptor gene expression in MCF10AT cells: A model for early breast cancer. *International Journal of Oncology*, *13*(5), 907–922. https://doi.org/10.3892/ijo.13.5.907

Shihab, H. A., Gough, J., Cooper, D. N., Stenson, P. D., Barker, G. L. A., Edwards, K. J., Day, I. N. M., & Gaunt, T. R. (2013). Predicting the Functional, Molecular, and Phenotypic Consequences of Amino Acid Substitutions using Hidden Markov Models. *Human Mutation*, *34*(1), 57–65. https://doi.org/10.1002/humu.22225

Shinde, U., Fu, X., & Inouye, M. (1999). A pathway for conformational diversity in proteins mediated by

intramolecular chaperones. *The Journal of Biological Chemistry*, *274*(22), 15615–15621. https://doi.org/10.1074/jbc.274.22.15615

Siezen, R. J., & Leunissen, J. A. M. (1997). Subtilases: The superfamily of subtilisin-like serine proteases: Subtilases. *Protein Science*, *6*(3), 501–523. https://doi.org/10.1002/pro.5560060301

Sim, N.-L., Kumar, P., Hu, J., Henikoff, S., Schneider, G., & Ng, P. C. (2012). SIFT web server: Predicting effects of amino acid substitutions on proteins. *Nucleic Acids Research*, *40*(Web Server issue), W452–W457. https://doi.org/10.1093/nar/gks539

Simoni-Nieves, A., Gerardo-Ramírez, M., Pedraza-Vázquez, G., Chávez-Rodríguez, L., Bucio, L., Souza, V., Miranda-Labra, R. U., Gomez-Quiroz, L. E., & Gutiérrez-Ruiz, M. C. (2019). GDF11 Implications in Cancer Biology and Metabolism. Facts and Controversies. *Frontiers in Oncology*, *9*. https://doi.org/10.3389/fonc.2019.01039

Smeekens, S. P., & Steiner, D. F. (1990). Identification of a human insulinoma cDNA encoding a novel mammalian protein structurally related to the yeast dibasic processing protease Kex2. *The Journal of Biological Chemistry*, *265*(6), 2997–3000.

Smid, M., Wang, Y., Zhang, Y., Sieuwerts, A. M., Yu, J., Klijn, J. G. M., Foekens, J. A., & Martens, J. W. M. (2008). Subtypes of Breast Cancer Show Preferential Site of Relapse. *Cancer Research*, *68*(9), 3108–3114. https://doi.org/10.1158/0008-5472.CAN-07-5644

Sorlie, T., Perou, C. M., Tibshirani, R., Aas, T., Geisler, S., Johnsen, H., Hastie, T., Eisen, M. B., van de Rijn, M., Jeffrey, S. S., Thorsen, T., Quist, H., Matese, J. C., Brown, P. O., Botstein, D., Lonning, P. E., & Borresen-Dale, A.-L. (2001). Gene expression patterns of breast carcinomas distinguish tumor subclasses with clinical implications. *Proceedings of the National Academy of Sciences*, *98*(19), 10869–10874. https://doi.org/10.1073/pnas.191367098

Soule, H. D., Maloney, T. M., Wolman, S. R., Peterson, W. D., Brenz, R., McGrath, C. M., Russo, J., Pauley, R. J., Jones, R. F., & Brooks, S. C. (1990). Isolation and Characterization of a Spontaneously Immortalized Human Breast Epithelial Cell Line, MCF-10. *Cancer Research*, *50*(18), 6075–6086.

Stawowy, P., Blaschke, F., Kilimnik, A., Goetze, S., Kallisch, H., Chrétien, M., Marcinkiewicz, M., Fleck, E., & Graf, K. (2002). Proprotein convertase PC5 regulation by PDGF-BB involves PI3-kinase/p70(s6)-kinase activation in vascular smooth muscle cells. *Hypertension (Dallas, Tex.: 1979)*, *39*(2 Pt 2), 399–404. https://doi.org/10.1161/hy0202.103000

Steiner, D. F. (2011). On the discovery of precursor processing. *Methods in Molecular Biology (Clifton, N.J.)*, *768*, 3–11. https://doi.org/10.1007/978-1-61779-204-5_1

Steiner, D. F., Cunningham, D., Spigelman, L., & Aten, B. (1967). Insulin Biosynthesis: Evidence for a Precursor. *Science*, *157*(3789), 697–700. https://doi.org/10.1126/science.157.3789.697

Steiner, D. F., Quinn, P. S., Chan, S. J., Marsh, J., & Tager, H. S. (1980). Processing Mechanisms in the Biosynthesis of Proteins. *Annals of the New York Academy of Sciences*, *343*(1), 1–16. https://doi.org/10.1111/j.1749-6632.1980.tb47238.x

Steinhaus, R., Proft, S., Schuelke, M., Cooper, D. N., Schwarz, J. M., & Seelow, D. (2021). MutationTaster2021. *Nucleic Acids Research*, *49*(W1), W446–W451. https://doi.org/10.1093/nar/gkab266

Stirling, D. R., Swain-Bowden, M. J., Lucas, A. M., Carpenter, A. E., Cimini, B. A., & Goodman, A.

(2021). CellProfiler 4: Improvements in speed, utility and usability. *BMC Bioinformatics*, *22*(1), 433. https://doi.org/10.1186/s12859-021-04344-9

Strand, S. H., Rivero-Gutiérrez, B., Houlahan, K. E., Seoane, J. A., King, L. M., Risom, T., Simpson, L. A., Vennam, S., Khan, A., Cisneros, L., Hardman, T., Harmon, B., Couch, F., Gallagher, K., Kilgore, M., Wei, S., DeMichele, A., King, T., McAuliffe, P. F., … West, R. B. (2022). Molecular classification and biomarkers of clinical outcome in breast ductal carcinoma in situ: Analysis of TBCRC 038 and RAHBT cohorts. *Cancer Cell*, *40*(12), 1521-1536.e7. https://doi.org/10.1016/j.ccell.2022.10.021

Strausberg, S., Alexander, P., Wang, L., Schwarz, F., & Bryan, P. (1993). Catalysis of a protein folding reaction: Thermodynamic and kinetic analysis of subtilisin BPN' interactions with its propeptide fragment. *Biochemistry*, *32*(32), 8112–8119. https://doi.org/10.1021/bi00083a009

Strickland, L. B., Dawson, P. J., Santner, S. J., & Miller, F. R. (2000). Progression of Premalignant MCF10AT Generates Heterogeneous Malignant Variants with Characteristic Histologic Types and Immunohistochemical Markers. *Breast Cancer Research and Treatment*, *64*(3), 235–240. https://doi.org/10.1023/A:1026562720218

Stuart, K. E., Houssami, N., Taylor, R., Hayen, A., & Boyages, J. (2015). Long-term outcomes of ductal carcinoma in situ of the breast: A systematic review, meta-analysis and meta-regression analysis. *BMC Cancer*, *15*, 890. https://doi.org/10.1186/s12885-015-1904-7

Su, C. J., Murugan, A., Linton, J. M., Yeluri, A., Bois, J., Klumpe, H., Langley, M. A., Antebi, Y. E., & Elowitz, M. B. (2022). Ligand-receptor promiscuity enables cellular addressing. *Cell Systems*, *13*(5), 408-425.e12. https://doi.org/10.1016/j.cels.2022.03.001

Sun, X., Essalmani, R., Susan-Resiga, D., Prat, A., & Seidah, N. G. (2011). Latent transforming growth factor beta-binding proteins-2 and -3 inhibit the proprotein convertase 5/6A. *The Journal of Biological Chemistry*, *286*(33), 29063–29073. https://doi.org/10.1074/jbc.M111.242479

Szumska, D., Pieles, G., Essalmani, R., Bilski, M., Mesnard, D., Kaur, K., Franklyn, A., El Omari, K., Jefferis, J., Bentham, J., Taylor, J. M., Schneider, J. E., Arnold, S. J., Johnson, P., Tymowska-Lalanne, Z., Stammers, D., Clarke, K., Neubauer, S., Morris, A., … Bhattacharya, S. (2008). VACTERL/caudal regression/Currarino syndrome-like malformations in mice with mutation in the proprotein convertase Pcsk5. *Genes & Development*, *22*(11), 1465–1477. https://doi.org/10.1101/gad.479408

Tait, L., Dawson, P., Wolman, S., Galea, K., & Miller, F. (1996). Multipotent human breast stem cell line MCF10AT. *International Journal of Oncology*. https://doi.org/10.3892/ijo.9.2.263

Tait, L. R., Pauley, R. J., Santner, S. J., Heppner, G. H., Heng, H. H., Rak, J. W., & Miller, F. R. (2007). Dynamic stromal-epithelial interactions during progression of MCF10DCIS.com xenografts. *International Journal of Cancer*, *120*(10), 2127–2134. https://doi.org/10.1002/ijc.22572

Tait, L., Soule, H. D., & Russo, J. (1990). Ultrastructural and immunocytochemical characterization of an immortalized human breast epithelial cell line, MCF-10. *Cancer Research*, *50*(18), 6087–6094.

Tamimi, R. M., Baer, H. J., Marotti, J., Galan, M., Galaburda, L., Fu, Y., Deitz, A. C., Connolly, J. L., Schnitt, S. J., Colditz, G. A., & Collins, L. C. (2008). Comparison of molecular phenotypes of ductal carcinoma in situ and invasive breast cancer. *Breast Cancer Research*, *10*(4), R67. https://doi.org/10.1186/bcr2128

Tang, H., & Thomas, P. D. (2016). PANTHER-PSEP: Predicting disease-causing genetic variants using position-specific evolutionary preservation. *Bioinformatics (Oxford, England)*, *32*(14), 2230–2232. https://doi.org/10.1093/bioinformatics/btw222

Tang, M., Mikhailik, A., Pauli, I., Giudice, L. C., Fazelabas, A. T., Tulac, S., Carson, D. D., Kaufman, D. G., Barbier, C., Creemers, J. W. M., & Tabibzadeh, S. (2005). Decidual differentiation of stromal cells promotes Proprotein Convertase 5/6 expression and lefty processing. *Endocrinology*, *146*(12), 5313–5320. https://doi.org/10.1210/en.2005-0684

Tang, M., Taylor, H. S., & Tabibzadeh, S. (2005). In vivo gene transfer of lefty leads to implantation failure in mice. *Human Reproduction*, *20*(7), 1772–1778. https://doi.org/10.1093/humrep/deh849

Tate, J. G., Bamford, S., Jubb, H. C., Sondka, Z., Beare, D. M., Bindal, N., Boutselakis, H., Cole, C. G., Creatore, C., Dawson, E., Fish, P., Harsha, B., Hathaway, C., Jupe, S. C., Kok, C. Y., Noble, K., Ponting, L., Ramshaw, C. C., Rye, C. E., … Forbes, S. A. (2019). COSMIC: The Catalogue Of Somatic Mutations In Cancer. *Nucleic Acids Research*, *47*(D1), D941–D947. https://doi.org/10.1093/nar/gky1015

Tordai, H., Torres, O., Csepi, M., Padányi, R., Lukács, G. L., & Hegedűs, T. (2024). Analysis of AlphaMissense data in different protein groups and structural context. *Scientific Data*, *11*(1), 495. https://doi.org/10.1038/s41597-024-03327-8

Tortorella, M. D., Arner, E. C., Hills, R., Gormley, J., Fok, K., Pegg, L., Munie, G., & Malfait, A.-M. (2005). ADAMTS-4 (aggrecanase-1): N-terminal activation mechanisms. *Archives of Biochemistry and Biophysics*, *444*(1), 34–44. https://doi.org/10.1016/j.abb.2005.09.018

Turnbull, J., Powell, A., & Guimond, S. (2001). Heparan sulfate: Decoding a dynamic multifunctional cell regulator. *Trends in Cell Biology*, *11*(2), 75–82. https://doi.org/10.1016/s0962-8924(00)01897-3

Ueda, K., Lipkind, G. M., Zhou, A., Zhu, X., Kuznetsov, A., Philipson, L., Gardner, P., Zhang, C., & Steiner, D. F. (2003). Mutational analysis of predicted interactions between the catalytic and P domains of prohormone convertase 3 (PC3/PC1). *Proceedings of the National Academy of Sciences of the United States of America*, *100*(10), 5622–5627. https://doi.org/10.1073/pnas.0631617100

Valdez, K. E., Fan, F., Smith, W., Allred, D. C., Medina, D., & Behbod, F. (2011). Human primary ductal carcinoma in situ (DCIS) subtype-specific pathology is preserved in a mouse intraductal (MIND) xenograft model. *The Journal of Pathology*, *225*(4), 565–573. https://doi.org/10.1002/path.2969

van Amerongen, R., Bentires-Alj, M., van Boxtel, A. L., Clarke, R. B., Fre, S., Suarez, E. G., Iggo, R., Jechlinger, M., Jonkers, J., Mikkola, M. L., Koledova, Z. S., Sørlie, T., & Vivanco, M. dM. (2023). Imagine beyond: Recent breakthroughs and next challenges in mammary gland biology and breast cancer research. *Journal of Mammary Gland Biology and Neoplasia*, *28*(1), 17. https://doi.org/10.1007/s10911-023-09544-y

van de Loo, J. W., Creemers, J. W., Kas, K., Roebroek, A. J., & Van de Ven, W. J. (1996). Assignment of the human proprotein convertase gene PCSK5 to chromosome 9q21.3. *Cytogenetics and Cell Genetics*, *75*(4), 227–229. https://doi.org/10.1159/000134489

Varadi, M., Bertoni, D., Magana, P., Paramval, U., Pidruchna, I., Radhakrishnan, M., Tsenkov, M., Nair, S., Mirdita, M., Yeo, J., Kovalevskiy, O., Tunyasuvunakool, K., Laydon, A., Žídek, A., Tomlinson, H., Hariharan, D., Abrahamson, J., Green, T., Jumper, J., … Velankar, S. (2024). AlphaFold Protein Structure Database in 2024: Providing structure coverage for over 214 million protein

sequences. *Nucleic Acids Research*, *52*(D1), D368–D375. https://doi.org/10.1093/nar/gkad1011

Vaser, R., Adusumalli, S., Leng, S. N., Sikic, M., & Ng, P. C. (2016). SIFT missense predictions for genomes. *Nature Protocols*, *11*(1), 1–9. https://doi.org/10.1038/nprot.2015.123

Vollenweider, F., Benjannet, S., Decroly, E., Savaria, D., Lazure, C., Thomas, G., Chrétien, M., & Seidah, N. G. (1996). Comparative cellular processing of the human immunodeficiency virus (HIV-1) envelope glycoprotein gp160 by the mammalian subtilisin/kexin-like convertases. *Biochemical Journal*, *314*(2), 521–532. https://doi.org/10.1042/bj3140521

Wagner, K.-U. (2022). Know thy cells: Commonly used triple-negative human breast cancer cell lines carry mutations in RAS and effectors. *Breast Cancer Research*, *24*(1), 44. https://doi.org/10.1186/s13058-022-01538-8

Wang, J., Li, B., Luo, M., Huang, J., Zhang, K., Zheng, S., Zhang, S., & Zhou, J. (2024). Progression from ductal carcinoma in situ to invasive breast cancer: Molecular features and clinical significance. *Signal Transduction and Targeted Therapy*, *9*(1), 1–28. https://doi.org/10.1038/s41392-024-01779-3

Wang, L., Brugge, J. S., & Janes, K. A. (2011). Intersection of FOXO- and RUNX1-mediated gene expression programs in single breast epithelial cells during morphogenesis and tumor progression. *Proceedings of the National Academy of Sciences of the United States of America*, *108*(40), E803-812. https://doi.org/10.1073/pnas.1103423108

Wang, L., Paudel, B. B., McKnight, R. A., & Janes, K. A. (2023). Nucleocytoplasmic transport of active HER2 causes fractional escape from the DCIS-like state. *Nature Communications*, *14*(1), 2110. https://doi.org/10.1038/s41467-023-37914-x

Wang, Z., Dou, M., Liu, F., Jiang, P., Ye, S., Ma, L., Cao, H., Du, X., Sun, P., Su, N., Lin, F., Zhang, R., & Li, C. (2018). GDF11 induces differentiation and apoptosis and inhibits migration of C17.2 neural stem cells via modulating MAPK signaling pathway. *PeerJ*, *6*, e5524. https://doi.org/10.7717/peerj.5524

Wei, S. C., Fattet, L., Tsai, J. H., Guo, Y., Pai, V. H., Majeski, H. E., Chen, A. C., Sah, R. L., Taylor, S. S., Engler, A. J., & Yang, J. (2015). Matrix stiffness drives epithelial-mesenchymal transition and tumour metastasis through a TWIST1-G3BP2 mechanotransduction pathway. *Nature Cell Biology*, *17*(5), 678–688. https://doi.org/10.1038/ncb3157

Weimar, C. H. E., Macklon, N. S., Post Uiterweer, E. D., Brosens, J. J., & Gellersen, B. (2013). The motile and invasive capacity of human endometrial stromal cells: Implications for normal and impaired reproductive function. *Human Reproduction Update*, *19*(5), 542–557. https://doi.org/10.1093/humupd/dmt025

Wellings, S. R., & Jensen, H. M. (1973). On the Origin and Progression of Ductal Carcinoma in the Human Breast. *JNCI: Journal of the National Cancer Institute*, *50*(5), 1111–1118. https://doi.org/10.1093/jnci/50.5.1111

Wetendorf, M., & DeMayo, F. J. (2012). The progesterone receptor regulates implantation, decidualization, and glandular development via a complex paracrine signaling network. *Molecular and Cellular Endocrinology*, *357*(1–2), 108–118. https://doi.org/10.1016/j.mce.2011.10.028

Wong, B. S. Y., Liu, S., Schultz, G. A., & Rancourt, D. E. (2002). Subtilisin proprotein convertase-6

expression in the mouse uterus during implantation and artificially induced decidualization. *Molecular Reproduction and Development*, *61*(4), 453–459. https://doi.org/10.1002/mrd.10113

Yokoe, T., Ohmachi, T., Inoue, H., Mimori, K., Tanaka, F., Kusunoki, M., & Mori, M. (2007). Clinical significance of growth differentiation factor 11 in colorectal cancer. *International Journal of Oncology*, *31*(5), 1097–1101. https://doi.org/10.3892/ijo.31.5.1097

Yong, J. W., Choong, M. L., Wang, S., Wang, Y., Lim, S. Q., & Lee, M. A. (2014). Characterization of ductal carcinoma in situ cell lines established from breast tumor of a Singapore Chinese patient. *Cancer Cell International*, *14*(1), 94. https://doi.org/10.1186/s12935-014-0094-8

Yu, K.-D., Wu, L.-M., Liu, G.-Y., Wu, J., Di, G.-H., Shen, Z.-Z., & Shao, Z.-M. (2011). Different distribution of breast cancer subtypes in breast ductal carcinoma in situ (DCIS), DCIS with microinvasion, and DCIS with invasion component. *Annals of Surgical Oncology*, *18*(5), 1342–1348. https://doi.org/10.1245/s10434-010-1407-3

Zhou, A., Martin, S., Lipkind, G., LaMendola, J., & Steiner, D. F. (1998). Regulatory Roles of the P Domain of the Subtilisin-like Prohormone Convertases. *Journal of Biological Chemistry*, *273*(18), 11107–11114. https://doi.org/10.1074/jbc.273.18.11107

Zhou, W., Fong, M. Y., Min, Y., Somlo, G., Liu, L., Palomares, M. R., Yu, Y., Chow, A., O'Connor, S. T. F., Chin, A. R., Yen, Y., Wang, Y., Marcusson, E. G., Chu, P., Wu, J., Wu, X., Li, A. X., Li, Z., Gao, H., … Wang, S. E. (2014). Cancer-Secreted miR-105 Destroys Vascular Endothelial Barriers to Promote Metastasis. *Cancer Cell*, *25*(4), 501–515. https://doi.org/10.1016/j.ccr.2014.03.007

Zucker, S., Drews, M., Conner, C., Foda, H. D., DeClerck, Y. A., Langley, K. E., Bahou, W. F., Docherty, A. J., & Cao, J. (1998). Tissue inhibitor of metalloproteinase-2 (TIMP-2) binds to the catalytic domain of the cell surface receptor, membrane type 1-matrix metalloproteinase 1 (MT1-MMP). *The Journal of Biological Chemistry*, *273*(2), 1216–1222. https://doi.org/10.1074/jbc.273.2.1216

Appendix: Sporadic activation of an oxidative stress–dependent NRF2-p53 signaling network in breast epithelial spheroids and premalignancies[#]

Elizabeth J. Pereira[1], Joseph S. Burns[1*], Christina Y. Lee[1†], **Taylor Marohl[1]**, Delia Calderon[2], Lixin Wang[1], Kristen A. Atkins[3], Chun-Chao Wang[4], Kevin A. Janes[1,5‡]

[1]Department of Biomedical Engineering, University of Virginia, Charlottesville, VA 22908, USA.

[2]Biology and Chemistry Programs, California State University Channel Islands, Camarillo, CA 93012, USA.

[3]Department of Pathology, University of Virginia, Charlottesville, VA 22908, USA.

[4]Institute of Molecular Medicine and Department of Medical Science, National Tsing Hua University, Hsinchu 30013, Taiwan.

[5]Department of Biochemistry and Molecular Genetics, University of Virginia, Charlottesville, VA 22908, USA.

[*]Present address: Department of Biomedical Engineering, University of Wisconsin, Madison, WI 53706, USA.

[†]Present address: Department of Biomedical Engineering, University of Michigan, Ann Arbor, MI 48109, USA.

[‡]Corresponding author. Email: kjanes@virginia.edu

[#]This work has been published in *Science Signaling* and is available online in full at: https://www.science.org/doi/10.1126/scisignal.aba4200/.

Author contributions: Unless otherwise noted, E.J.P. performed the experiments, modeling, and bioinformatic analyses in the manuscript and drafted the manuscript. J.S.B. performed qPCR, led the image analysis of local NRF2 stabilization, and contributed experiments related to the NRF2-p53 computational model. C.Y.L. built the initial draft of the NRF2-p53 computational model and contributed experiments related to model construction. **T.M. assisted with immunocytochemistry and imaging.** D.C. and L.W. provided cloning assistance. K.A.A. identified the clinical samples, performed the p53 immunohistochemical scoring, and reviewed the pathology images in the manuscript. C.-C.W. completed the promoter bioinformatics along with the initial genetic perturbations and phenotyping related to the work. K.A.J. assisted with image acquisition for the clinical samples, edited the final manuscript, supervised all research, and secured funding for the work.

SELECTED RESULTS

Statistical bioinformatics links gene cluster regulation to NRF2 and p53

We began by looking within the gene cluster (Fig. 1A, top) for potential regulatory mechanisms. The only TF in the cluster is JUND, and we showed previously that its chronic knockdown in MCF10A-5E cells (20) causes specific morphometric defects during spheroid growth (24). We revisited these results by acutely knocking down the expression of JUND with inducible short hairpin RNA (shRNA) and measuring transcript abundance of cluster genes by quantitative polymerase chain reaction (qPCR) (see Materials and Methods). Unexpectedly, other than JUND itself, no transcripts were reliably altered by its knockdown (see later in this section), supporting a regulatory role for other factors outside of the cluster.

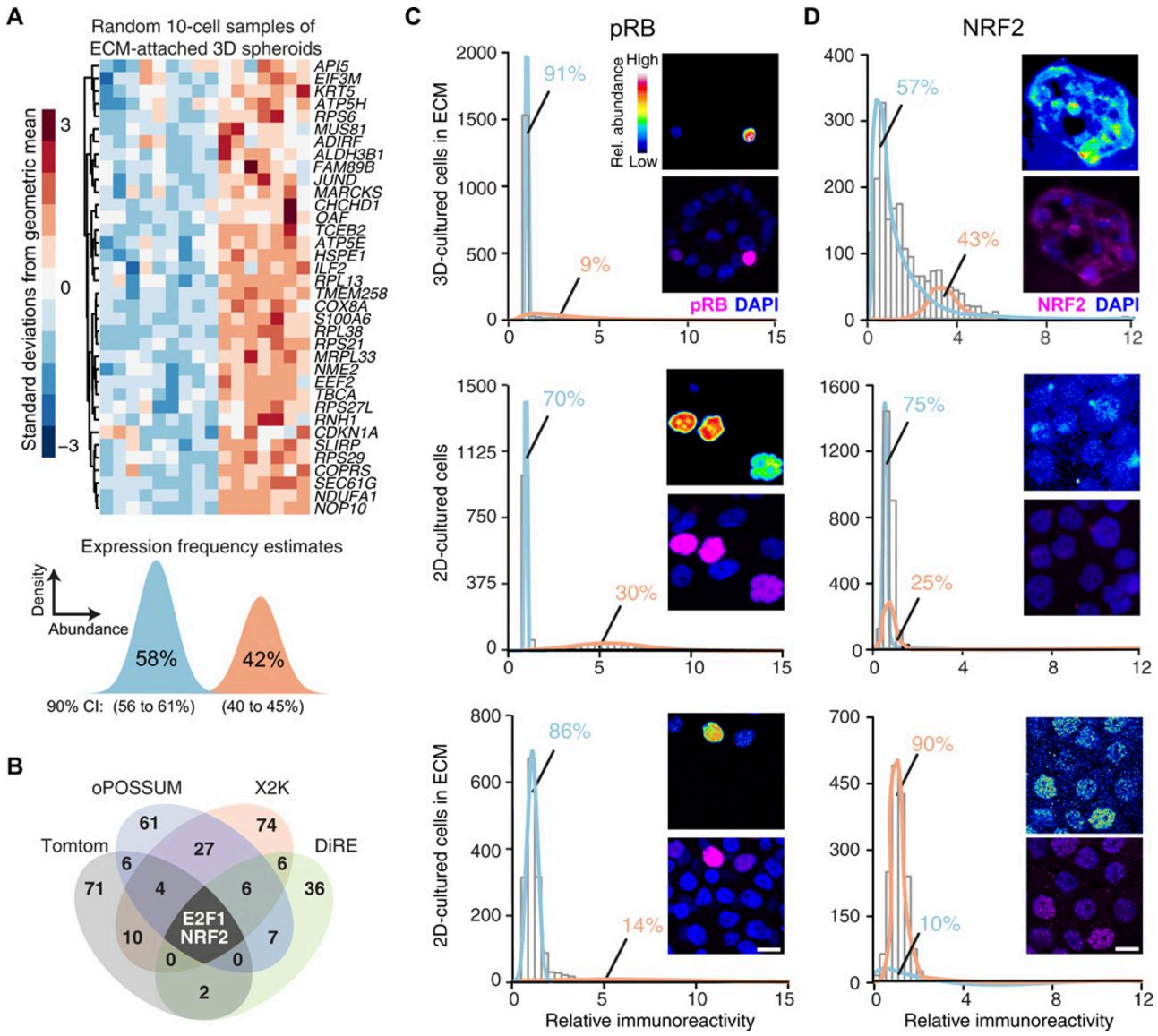

Fig. 1 Transcriptomic fluctuations of ECM-cultured breast epithelial spheroids reveal a gene cluster associated with heterogeneous NRF2 stabilization in a 3D-specific environment.

(A) Maximum likelihood inference parameterization (bottom) of a two-state distribution of transcript abundances for the gene cluster from microarray profiles (top) of ECM-attached basal-like MCF10A-5E breast epithelial cells, randomly collected as 10-cell pools (n = 16) from 3D-cultured spheroids after 10 days, extracted from (20). Inferred expression frequencies are the maximum likelihood estimate with 90% confidence interval (CI). (B) Venn diagram summarizing the candidate TFs predicted from four different bioinformatics algorithms (data file S1). (C and D) Quantitative immunofluorescence of (C) hyperphosphorylated RB (pRB, an upstream proxy of active E2F1) and (D) NRF2 in 3D culture with ECM (top), 2D culture (middle), and 2D culture with ECM (bottom). Expression frequencies for a two-state lognormal mixture model (preferred over a one-state model by F test; $P < 0.05$) were calculated by nonlinear least squares of 60 histogram bins collected from n = 1100 to 1600 of cells quantified from 100 to 200 spheroids from two separate 3D cultures. For each subpanel, representative pseudocolored images are shown in the top right inset and merged (magenta) with DAPI nuclear counterstain (blue) in the bottom right inset. Scale bars, 10 μm.

We constrained the search for candidate regulators by using maximum likelihood inference (38) to estimate a frequency of bimodal transcriptional regulation (39) for the gene cluster. Given the 10-cell-averaged fluctuations from the original study (20), the maximum likelihood approach inferred two lognormal regulatory states defined by transcript abundance (Fig. 1A, bottom). The data supported a low-abundance regulatory state predominating in 58% of ECM-attached cells along with a second, high-abundance subpopulation in the remaining 42%. The frequency estimates placed quantitative bounds on the bimodal characteristics of upstream regulatory mechanisms.

Next, we applied a panel of bioinformatics approaches to search for TFs that might impinge upon the gene cluster (see Materials and Methods). The informatic methods adopt different strategies for assessing binding site overrepresentation (40–43). Therefore, we intersected their respective outputs to arrive at predictions that were robust to algorithmic details. The analysis converged upon two TFs: the G1/S regulator E2F1 and the stress response effector NRF2 (Fig. 1B and data file S1). We assessed the relative activation of the NRF2 and E2F1 pathways in single cells by quantitative immunofluorescence for the total stabilized NRF2 protein or phosphorylated RB1 (pRB indicates disinhibited E2F1; see Materials and Methods). In 3D spheroid cultures, pRB immunostaining was bimodal, but high-pRB cells were much rarer than the inferred regulatory frequency of the gene cluster (Fig. 1C, top). In 2D cultures, pRB staining was more than twice as immunoreactive and nearly twice as prevalent in the population (Fig. 1C, middle). The reduced proportion of high-pRB cells in 3D is consistent with the proliferative suppression of late-stage spheroid cultures (23). A 3D-like distribution of pRB was achieved in 2D cultures upon addition of dilute ECM (Fig. 1C, bottom), stemming from soluble proliferation-suppressing factors in the reconstituted basement membrane preparation (44). By contrast, NRF2 stabilization was only distinctly bimodal in 3D spheroids, and the observed frequency of low- and high-NRF2 states almost exactly coincided with that inferred for the gene cluster (Fig. 1D). Stabilization of hypoxia-inducible factor 1α (HIF-1α) was negligible in 3D spheroids overall (fig. S1, A

and B), excluding irregular hypoxic stress as a contributor to the two-state distribution of NRF2. These results build a strong statistical argument for NRF2 as a covarying regulator of the gene cluster.

The NRF2-associated gene cluster (Fig. 1A, top) was originally identified by quantitative analysis of transcriptomic fluctuations among 4557 genes profiled by oligonucleotide microarray (20). The same samples were later reprofiled by 10-cell RNA sequencing (10cRNA-seq) (45), creating an opportunity to look more deeply at covariates with the NRF2-associated gene cluster. We used the median ranked fluctuations of the cluster across 10 cell samples (Fig. 1A, top) and surveyed the 10cRNA-seq data for genes that covaried (Spearman $\rho > 0.5$), identifying 633 candidates (Fig. 2A). When this expanded cluster was assessed for functional enrichments by Gene Ontology (GO) (data file S2) (46), we noted multiple GO terms linked to cell stress (“Response to stress” and “Oxidative stress”) and the TF p53 (“DNA damage response” and “p53 pathway”). p53 is sporadically stabilized in regenerating epithelia such as the intestine and skin, but p53 activation in quiescent tissues is rare (47). Recognizing the residual proliferation observed in 3D cultures (Fig. 1C), we immunostained for p53 and found nonuniform stabilization associated with the abundance of NRF2 in single cells [Fig. 2B, estimated mutual information (MI) = 0.15 (0.12 to 0.18); see Materials and Methods]. The analysis raised the possibility of a coordinated NRF2-p53 regulatory event triggered heterogeneously when breast epithelial cells proliferate and organize in reconstituted ECM.

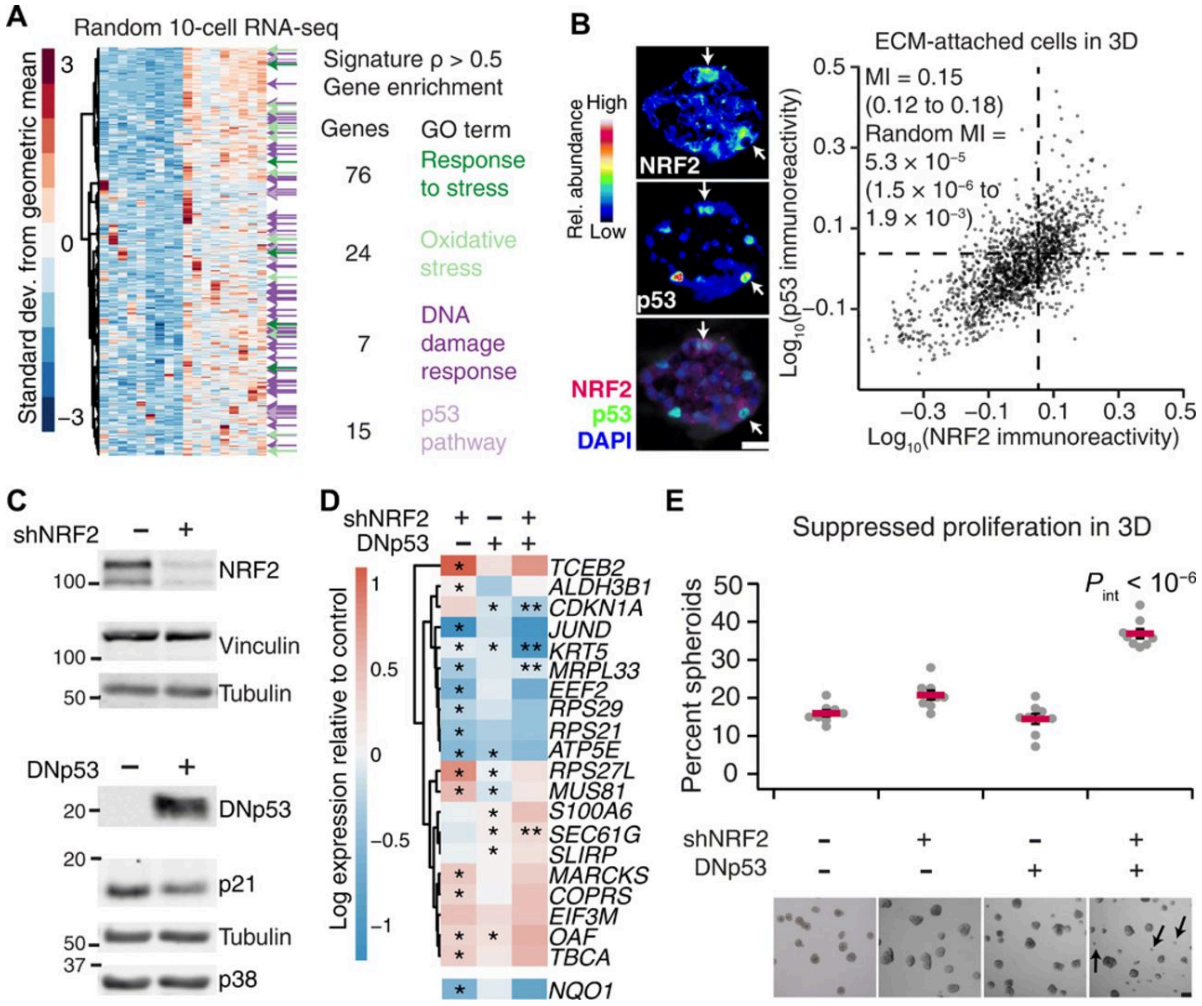

Fig. 2 Transcriptome-wide covariate analysis of the NRF2-associated gene cluster suggests a coordinated adaptive-stress response involving p53.

(A) Transcripts covarying with the median NRF2-associated fluctuation signature (Fig. 1AOpens in image viewer, top) (20) measured by 10cRNA-seq (45) of ECM-attached MCF10A-5E cells grown as 3D spheroids (n = 18 10-cell pools from GSE120261). Selected GO enrichment analysis (green and purple) is shown for the transcripts with a Spearman correlation (ρ) greater than 0.5. The complete list of enrichments is available in data file S2. (B) Quantitative immunofluorescence of NRF2 and p53 abundance in ECM-attached MCF10A-5E cells grown as 3D spheroids. Representative pseudocolored images for NRF2 (top left) and p53 (middle left) are shown merged with DAPI nuclear counterstain (bottom left). White arrows indicate concurrent NRF2 and p53 stabilization. Median-scaled two-color average fluorescence intensities are quantified (right) along with the log-scaled and background-subtracted mutual information (MI) with 90% CI for n = 1691 cells segmented from 50 to 100 spheroids from two separate 3D cultures. (C) Genetic perturbation of NRF2 by inducible shRNA knockdown (top) and p53 by inducible expression of a FLAG-tagged carboxy terminal (residues 1 to 13 and 302 to 390) dominant-negative p53 (DNp53; bottom). NRF2 knockdown reduced NRF2 protein abundance to 22 ± 4% of control knockdown (fig. S3B). MCF10A-5E cells were treated with doxycycline (1 μg/ml) for 72 (top) or 24 (bottom) hours and immunoblotted for NRF2 or FLAG with vinculin, tubulin, and p38 used as loading controls and p21 used to confirm efficacy of DNp53. The negative control for shNRF2 was an inducible shGFP, and the negative control for DNp53 was an inducible FLAG-tagged LacZ. (D) Abundance changes in the gene cluster after single and combined perturbations of NRF2 and p53. NQO1 was used as a control for efficacy of shNRF2, and CDKN1A shows efficacy of DNp53. MCF10A-5E cells with or without NRF2 knockdown or DNp53 were

treated with doxycycline (1 μg/ml) for 48 hours, grown as 3D spheroids for 10 days, and profiled for the indicated genes by qPCR. Data are log2 geometric mean relative to the negative control (shGFP + FLAG-tagged LacZ), with asterisks indicating statistically significant changes (left and middle columns) or interaction effects (right column) by two-way ANOVA of n = 8 independent 3D-cultured samples and an FDR of 5%. The complete set of transcripts in the gene cluster is shown in fig. S2C. (E) Dual inactivation of NRF2 and p53 causes synergistic proliferative suppression in MCF10A-5E 3D spheroids. Black arrows indicate proliferation-suppressed spheroids. Data are mean percentage of proliferation-suppressed spheroids ± SEM of n = 8 independent 3D-cultured samples after 10 days. Statistical interaction between NRF2 and p53 (Pint) was assessed by two-way ANOVA with replication. Scale bars, 20 μm (B) and 100 μm (E).

NRF2 coimmunoprecipitates with p53 in TNBC cells harboring gain-of-function p53 mutations, but this complex is absent in MCF10A cells with wild-type p53 (37). Loss of wild-type p53 function in MCF10A cells yields only minor 3D culture defects, but gain-of-function p53 mutants strongly perturb 3D architecture (48). Suspecting that some of p53's effects could be explained through NRF2, we inducibly knocked down NRF2 with shRNA and inducibly coexpressed a truncated p53 (49) that acts as a dominant negative (DNp53; Fig. 2C). Compared with the gene cluster response to JUND knockdown or constitutive E2F1 activation through RB inhibition with overexpressed human papillomavirus E7 protein, we observed substantially more alterations upon NRF2 knockdown (66%) or inhibition of p53 (31%; Fig. 2D and fig. S2, A to D). Using public chromatin immunoprecipitation sequencing (ChIP-seq) datasets (50, 51), we found significant enrichment of proximal NRF2 binding among transcripts reduced by NRF2 knockdown and a slight enrichment in p53 binding among those increased by NRF2 knockdown (fig. S2C). Compound perturbation of NRF2 and p53 elicited further nonadditive changes to multiple genes in the cluster, including synergistic reduction in CDKN1A, encoding a cyclin-dependent kinase inhibitor, and KRT5, encoding a basal cytokeratin. Although p53 can antagonize certain NRF2 target genes in reporter assays (52), significant antagonism was detected for only one transcript in the cluster (MRPL33; fig. S2C). Phenotypically, disruption of NRF2 reduced mean 3D growth by 10 to 13% (fig. S3, A to D), but dual perturbation with p53 gave rise to an increase in aborted spheroids unable to grow in the culture (Fig. 2E). The penetrance of the phenotype (37%; range, 34 to 44%) was close to the percentage of cells showing stabilized NRF2 at the same time point in 3D culture (43%; Fig. 1E). For this clonal basal-like breast epithelial line (20), we conclude that 3D culture heterogeneously elicits NRF2- and p53-inducing stresses, which must be withstood for extended proliferation.

NRF2 disruption in basal-like premalignancy causes similar p53 adaptations but different 3D phenotypes

We next asked how the cellular, molecular, and phenotypic relationships between NRF2 and p53 change in basal-like premalignancy by using isogenic MCF10DCIS.com cells (53) as a proxy for DCIS (54). MCF10DCIS.com cells express oncogenic HRAS (55) and hyperproliferate as 3D spheroids (confirmed in fig. S4A), but they retain wild-type p53 function, albeit at reduced levels compared with parental MCF10A cells (fig. S4, B and C). By two-color immunostaining, we found that NRF2-p53

costabilization was even more pronounced in MCF10DCIS.com cells [MI = 0.30 (0.27 to 0.33); Fig. 3A]. To identify common adaptive programs downstream of NRF2 deficiency, we inducibly knocked down NRF2 and profiled 3D spheroids by RNA-seq (see Materials and Methods). Among transcripts consistently increased or decreased in both MCF10A-5E and MCF10DCIS.com spheroids, there was a significant enrichment in gene signatures encompassing p53, including transcriptional programs downstream of BRCA1, ATM, and CHEK2 (Fig. 3B and data file S3). Consistent with these results, NRF2 knockdown in MCF10DCIS.com cells was sufficient to significantly stabilize p53 (fig. S5A). Stabilization of wild-type p53 upon NRF2 knockdown was also observed in premalignant CHEK21100delC SUM102PT cells (56) and became even more pronounced when these cells were reconstituted with inducible wild-type CHEK2 (fig. S5, B and C), as expected, given the feedforward stabilization of p53 by ATM and ATM-activated CHEK2 (57). Thus, NRF2 impairment promotes p53 pathway activity in basal-like breast epithelia without the need for specific oncogenic drivers.

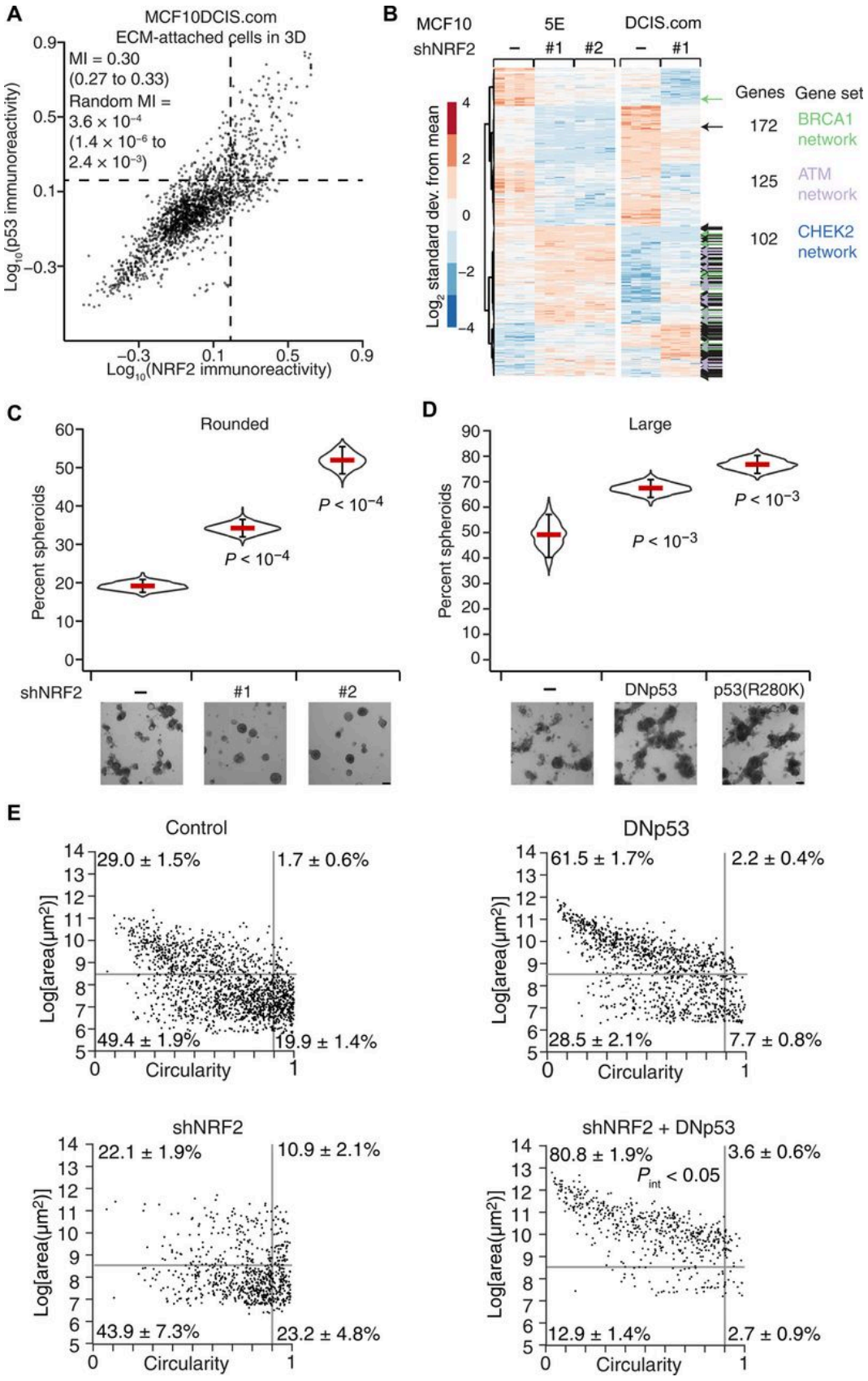

Fig. 3 NRF2-p53 costabilization is enhanced, and shNRF2-induced p53 adaptations are preserved in basal-like premalignancy but have different morphometric consequences.

(A) Quantitative immunofluorescence of NRF2 and p53 abundance in ECM-attached MCF10DCIS.com cells grown as 3D spheroids. Median-scaled two-color average fluorescence intensities are quantified along with the log-scaled and background-subtracted MI with 90% CI for n = 1832 cells segmented from 70 to 110 spheroids from two separate 3D cultures. (B) Common changes in transcript abundance identified by RNA-seq of MCF10A-5E (5E) and MCF10DCIS.com (DCIS.com) cells grown as 3D spheroids with or without NRF2 knockdown. The negative control for shNRF2 was an inducible shGFP (5E) or shLacZ (DCIS.com). Data are log2-transformed Z scores for genes detected at >5 transcripts per million from n = 4 biological replicates. Enriched gene sets for the BRCA1, ATM, and CHEK2 networks are indicated, with black denoting multiple enrichments. The complete list of enrichments is available in data file S3. (C) Quantification of rounded spheroids (circularity >0.9) in 3D-cultured MCF10DCIS.com cells with or without NRF2 knockdown. The negative control for shNRF2 was an inducible shLacZ. (D) Quantification of large spheroids (size > e8.5 ≈ 5000 μm2) in 3D-cultured MCF10DCIS.com cells with or without p53 disruption. The negative control for p53 constructs was an inducible FLAG-tagged LacZ. (E) Quantification of size and circularity in 3D-cultured MCF10DCIS.com cells with or without NRF2 knockdown, p53 disruption, or both. For (C) to (E), cells with or without inducible perturbations were treated with doxycycline (1 μg/ml) for 48 hours, grown as 3D spheroids for 10 days, imaged by brightfield microscopy, and segmented. For (C) and (D), data are mean ± 90% bootstrap-estimated CI from n = 8 biological replicates, with P values by rank sum test estimated by bootstrapping. For (E), data are means ± SEM of n = 8 biological replicates. Statistical interaction between NRF2 and p53 perturbations (Pint) was assessed by two-way ANOVA with replication. Scale bars, 100 μm.

Despite many transcriptomic alterations in common with MCF10A-5E cells (Fig. 3B), MCF10DCIS.com cells yielded very different 3D phenotypes when NRF2 or p53 was perturbed. NRF2 knockdown did not detectably alter 3D growth (fig. S6A) but instead gave rise to more rounded, organized MCF10DCIS.com spheroids of high circularity compared with control (Fig. 3C), which reverted upon addback of an RNA interference (RNAi)–resistant (RR) NRF2 mutant (fig. S6B). NRF2 deficiency also increased rounding in 3D cultures of SUM102PT cells with or without CHEK2 reconstitution (fig. S6C). By contrast, p53 disruption in MCF10DCIS.com cells with either DNp53 or a gain-of-function p53R280K mutant increased the prevalence of hyper-enlarged outgrowths (Fig. 3D). Combined NRF2-p53 perturbation elicited a synergistic increase in nonspherical hyper-enlargement (Fig. 3E), starkly contrasting the proliferative suppression observed with the same combination in nontransformed MCF10A-5E cells (Fig. 2E). The data suggested that the coordinate transcriptional adaptations of NRF2 and p53 are conserved in premalignant cells but insufficient to buffer the cellular phenotypes caused by single-gene perturbations in either pathway.

NRF2 and p53 are coordinately stabilized by sporadic oxidative stress

Coordination of the NRF2-p53 pathways could be achieved if they shared the same inducer. We thus considered various potential upstream and intermediate triggers for NRF2 and p53 stabilization in basal-like breast epithelia. Inhibition of KEAP1 with the electrophile sulforaphane (58) stabilized NRF2 but not p53, and pharmacologic inhibition of MDM2 with nutlin-3 (59) stabilized p53 but not NRF2 (fig. S4, B to E), suggesting they act as parallel pathways downstream of a common inducer. An obvious candidate was DNA damage, given CDKN1A and MUS81 in the gene cluster (Fig. 1A, top) and the

most recognized function of p53 (60). However, chemotherapy-induced double-strand breaks did not appreciably stabilize NRF2 in cells with wild-type p53 (Fig. 4A and fig. S7, A and B), and genetically driving increased proliferation (61) did not detectably affect regulation of the gene cluster in 3D spheroids (fig. S2, B and D). The lack of NRF2-p53 coinduction by conventional agonists prompted a search for less canonical activators.

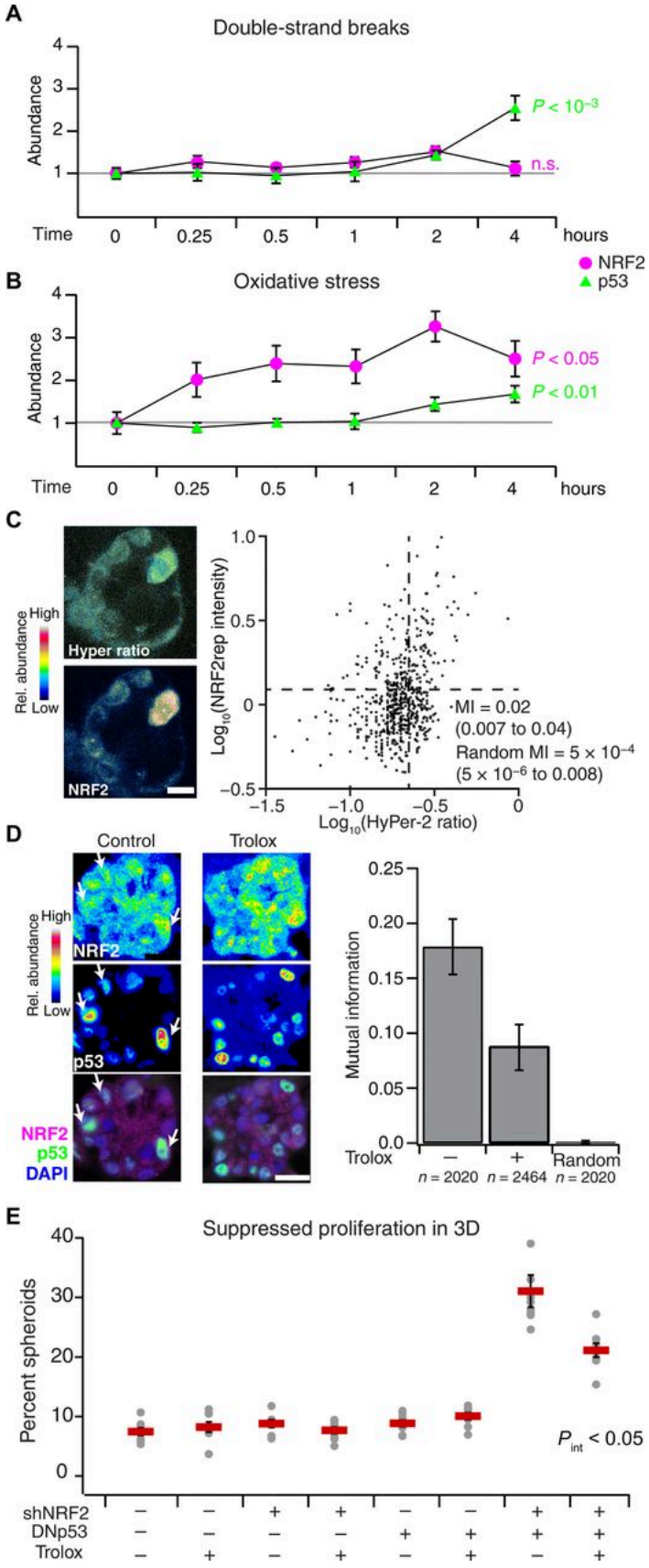

Fig. 4 NRF2-p53 signaling coordination and 3D phenotypes arise from spontaneous and oncogene-induced oxidative stress.

(A and B) NRF2 and p53 stabilization by oxidative stress compared with DNA double-strand breaks. MCF10A-5E cells were treated with 5 μM doxorubicin (double-strand breaks) or 200 μM H2O2 (oxidative stress) for the indicated time points, and NRF2 (magenta) or p53 (green) protein abundance was estimated by quantitative immunoblotting. Data are means ± SEM of n = 3 (A) or 4 (B) independent perturbations. n.s., not significant. (C) Endogenous oxidative stress association with NRF2 stabilization in 3D spheroids. MCF10A-5E cells stably expressing HyPer-2 (67) and mRFP1-NRF2 reporter (NRF2rep) were grown as 3D spheroids for 10 days and imaged by laser scanning confocal microscopy. Representative pseudocolored images for HyPer-2 ratio (top left) and mRFP1-NRF2 reporter (bottom left) are shown. HyPer-2 ratios and mRFP1-NRF2 reporter fluorescence are quantified (right) along with the log-scaled MI with 90% CI for n = 605 cells segmented from 10 to 25 spheroids from four separate 3D cultures. (D) Suppression of endogenous NRF2-p53 coordination during 3D culture with the antioxidant Trolox. Representative pseudocolored images for NRF2 (top left) and p53 (middle left) are shown merged with DAPI nuclear counterstain (bottom left). White arrows indicate concurrent NRF2 and p53 stabilization. The log-scaled and background-subtracted MI (right) is shown with 90% CI estimated from n = 1000 bootstrap replicates. (E) Trolox interference with the synergistic proliferative suppression caused by dual inactivation of NRF2 and p53 in MCF10A-5E cells. Data are mean percentage of proliferation-suppressed spheroids ± SEM of n = 8 independent 3D-cultured samples after 10 days. The overall effect of Trolox on spheroid size is shown in fig. S10. Statistical interaction between Trolox and NRF2-p53 (Pint) was assessed by three-way ANOVA with replication. For (A) and (B), change in protein abundance over time was assessed by one-way ANOVA. For (D) and (E), MCF10A-5E cells cultured for 10 days in 3D with or without 50 μM Trolox supplemented every 2 days. Scale bars, 10 μm (C) and 20 μm (D).

One shared inducer of the KEAP1-NRF2 and ATM-CHEK2-p53 pathways is oxidative stress (62, 63). In human breast tissue, increased levels of reactive oxygen species (ROS) are generated and tolerated by basoluminal progenitors (64), which are the cells of origin for basal-like breast cancer (65). We documented local niches of Nrf2 stabilization in the murine mammary gland during puberty (fig. S8, A to F), potentially linking NRF2 and oxidative stress in expanding progenitor(-like) cells, such as MCF10A. When MCF10A-5E cells were exogenously stimulated with H2O2, NRF2 was rapidly stabilized, and p53 also accumulated after several hours (Fig. 4B and fig. S7, A and B). Recognizing oxidative stress heterogeneities in 3D spheroids (21, 22, 66), we used the genetically encoded sensor HyPer-2 (67) together with an engineered mRFP1-NRF2 reporter (NRF2rep) to colocalize intracellular H2O2 with stabilized NRF2 (see Materials and Methods and fig. S9, A to F). We observed a small but nonzero MI between HyPer-2 fluorescence ratios and NRF2rep [MI = 0.05 (0.02 to 0.10); randomized MI = 0.0004 (0.0001 to 0.0007); Fig. 4C], suggesting a complex connection between the two reporters (see next section). Next, we evaluated whether oxidative stress resided upstream of NRF2-p53 coordination by using the cell-permeable, vitamin E analog Trolox to quench overall ROS in the 3D cultures. Trolox treatment halved the MI between stabilized NRF2-p53 and significantly reduced the synergistic proliferative suppression caused by dual perturbation of NRF2 and p53 (Fig. 4, D and E, and fig. S10). Together, the data suggested that the NRF2 and p53 pathway coregulation involves upstream heterogeneities in oxidative stress.

SELECTED METHODS

Immunofluorescence

MCF10A-5E and MCF10DCIS.com 3D cultures were embedded at day 10 of morphogenesis, and 5-μm sections were cut and mounted on Superfrost Plus slides (Fisher Scientific). For clinical samples, paraffin tissue sections were dewaxed and antigens were retrieved on a PT Link (Dako) with low-pH EnVision FLEX Target Retrieval Solution (Dako) for 20 min at 97°C. Immunofluorescence on cryosections and antigen-retrieved slides was performed as previously described (20) with the following primary antibodies: NRF2 (1:100; Santa Cruz Biotechnology, #sc-13032), phospho-Rb (1:1600; Cell Signaling, #8516), HIF-1α (1:800; Cell Signaling, #79233), and p53 (1:200; Santa Cruz Biotechnology, #sc-126). Slides were incubated the next day for 1 hour in the following secondary antibodies: Alexa Fluor 555–conjugated goat anti-rabbit (1:200; Invitrogen) and Alexa Fluor 647–conjugated goat anti-mouse (1:200; Invitrogen).

Image acquisition analysis and MI calculation

Fluorescence images were collected unblinded on an Olympus BX51 fluorescence microscope with a 40× 1.3 numerical aperture (NA) UPlanFL oil immersion objective and an Orca R2 charge-coupled device (CCD) camera (Hamamatsu) with no binning. Images were segmented in CellProfiler (117) using 4′,6-diamidino-2-phenylindole (DAPI) to identify nuclei. Nuclear objects were dilated to a median diameter of 15 μm to capture about one whole cell. NRF2 staining was quantified in the nucleus, the whole cell, and the cytoplasm (whole cell area − nuclear area). p53 staining was quantified in the whole cell. Immunoreactivity was quantified as the median fluorescence intensity of the whole cell unless otherwise noted.

SELECTED REFERENCES

20. K. A. Janes, C. C. Wang, K. J. Holmberg, K. Cabral, J. S. Brugge, Identifying single-cell molecular programs by stochastic profiling. Nat. Methods 7, 311–317 (2010).

23. J. Debnath, K. R. Mills, N. L. Collins, M. J. Reginato, S. K. Muthuswamy, J. S. Brugge, The role of apoptosis in creating and maintaining luminal space within normal and oncogene-expressing mammary acini. Cell 111, 29–40 (2002).

24. C.-C. Wang, S. S. Bajikar, L. Jamal, K. A. Atkins, K. A. Janes, A time- and matrix-dependent TGFBR3-JUND-KRT5 regulatory circuit in single breast epithelial cells and basal-like premalignancies. Nat. Cell Biol. 16, 345–356 (2014).

37. D. Walerych, K. Lisek, R. Sommaggio, S. Piazza, Y. Ciani, E. Dalla, K. Rajkowska, K. Gaweda-Walerych, E. Ingallina, C. Tonelli, M. J. Morelli, A. Amato, V. Eterno, A. Zambelli, A. Rosato, B. Amati, J. R. Wisniewski, G. Del Sal, Proteasome machinery is instrumental in a common gain-of-function program of the p53 missense mutants in cancer. Nat. Cell Biol. 18, 897–909 (2016).

38. S. S. Bajikar, C. Fuchs, A. Roller, F. J. Theis, K. A. Janes, Parameterizing cell-to-cell regulatory heterogeneities via stochastic transcriptional profiles. Proc. Natl. Acad. Sci. U.S.A. 111, E626–E635 (2014).

39. A. K. Shalek, R. Satija, X. Adiconis, R. S. Gertner, J. T. Gaublomme, R. Raychowdhury, S. Schwartz, N. Yosef, C. Malboeuf, D. Lu, J. J. Trombetta, D. Gennert, A. Gnirke, A. Goren, N. Hacohen, J. Z. Levin, H. Park, A. Regev, Single-cell transcriptomics reveals bimodality in expression and splicing in immune cells. Nature 498, 236–240 (2013).

40. V. Gotea, I. Ovcharenko, DiRE: Identifying distant regulatory elements of co-expressed genes. Nucleic Acids Res. 36, W133–W139 (2008).

41. E. Y. Chen, H. Xu, S. Gordonov, M. P. Lim, M. H. Perkins, A. Ma'ayan, Expression2Kinases: mRNA profiling linked to multiple upstream regulatory layers. Bioinformatics 28, 105–111 (2012).

42. T. L. Bailey, J. Johnson, C. E. Grant, W. S. Noble, The MEME Suite. Nucleic Acids Res. 43, W39–W49 (2015).

43. A. T. Kwon, D. J. Arenillas, R. Worsley Hunt, W. W. Wasserman, oPOSSUM-3: Advanced analysis of regulatory motif over-representation across genes or ChIP-Seq datasets. G3 2, 987–1002 (2012).

44. H. K. Kleinman, G. R. Martin, Matrigel: Basement membrane matrix with biological activity. Semin. Cancer Biol. 15, 378–386 (2005).

45. S. Singh, L. Wang, D. L. Schaff, M. D. Sutcliffe, A. F. Koeppel, J. Kim, S. Onengut-Gumuscu, K. S. Park, H. Zong, K. A. Janes, In situ 10-cell RNA sequencing in tissue and tumor biopsy samples. Sci. Rep. 9, 4836 (2019).

46. The Gene Ontology Consortium, The Gene Ontology Resource: 20 years and still GOing strong. Nucleic Acids Res. 47, D330–D338 (2019).

47. A. Loewer, E. Batchelor, G. Gaglia, G. Lahav, Basal dynamics of p53 reveal transcriptionally attenuated pulses in cycling cells. Cell 142, 89–100 (2010).

48. Y. Zhang, W. Yan, X. Chen, Mutant p53 disrupts MCF-10A cell polarity in three-dimensional culture via epithelial-to-mesenchymal transitions. J. Biol. Chem. 286, 16218–16228 (2011).

49. T. Bowman, H. Symonds, L. Gu, C. Yin, M. Oren, T. Van Dyke, Tissue-specific inactivation of p53 tumor suppression in the mouse. Genes Dev. 10, 826–835 (1996).

50. ENCODE Project Consortium, An integrated encyclopedia of DNA elements in the human genome. Nature 489, 57–74 (2012).

51. Z. Andrysik, M. D. Galbraith, A. L. Guarnieri, S. Zaccara, K. D. Sullivan, A. Pandey, M. MacBeth, A. Inga, J. M. Espinosa, Identification of a core TP53 transcriptional program with highly distributed tumor suppressive activity. Genome Res. 27, 1645–1657 (2017).

52. R. Faraonio, P. Vergara, D. Di Marzo, M. G. Pierantoni, M. Napolitano, T. Russo, F. Cimino, p53 suppresses the Nrf2-dependent transcription of antioxidant response genes. J. Biol. Chem. 281, 39776–39784 (2006).

53. F. R. Miller, S. J. Santner, L. Tait, P. J. Dawson, MCF10DCIS.com xenograft model of human comedo ductal carcinoma in situ. J. Natl. Cancer Inst. 92, 1185–1186 (2000).

54. M. Hu, J. Yao, D. K. Carroll, S. Weremowicz, H. Chen, D. Carrasco, A. Richardson, S. Violette, T. Nikolskaya, Y. Nikolsky, E. L. Bauerlein, W. C. Hahn, R. S. Gelman, C. Allred, M. J. Bissell, S.

Schnitt, K. Polyak, Regulation of in situ to invasive breast carcinoma transition. Cancer Cell 13, 394–406 (2008).

55. P. J. Dawson, S. R. Wolman, L. Tait, G. H. Heppner, F. R. Miller, MCF10AT: A model for the evolution of cancer from proliferative breast disease. Am. J. Pathol. 148, 313–319 (1996).

56. M. Wasielewski, P. Hanifi-Moghaddam, A. Hollestelle, S. D. Merajver, A. van den Ouweland, J. G. Klijn, S. P. Ethier, M. Schutte, Deleterious CHEK2 1100delC and L303X mutants identified among 38 human breast cancer cell lines. Breast Cancer Res. Treat. 113, 285–291 (2009).

57. A. Hirao, A. Cheung, G. Duncan, P. M. Girard, A. J. Elia, A. Wakeham, H. Okada, T. Sarkissian, J. A. Wong, T. Sakai, E. De Stanchina, R. G. Bristow, T. Suda, S. W. Lowe, P. A. Jeggo, S. J. Elledge, T. W. Mak, Chk2 is a tumor suppressor that regulates apoptosis in both an ataxia telangiectasia mutated (ATM)-dependent and an ATM-independent manner. Mol. Cell. Biol. 22, 6521–6532 (2002).

58. F. Hong, M. L. Freeman, D. C. Liebler, Identification of sensor cysteines in human Keap1 modified by the cancer chemopreventive agent sulforaphane. Chem. Res. Toxicol. 18, 1917–1926 (2005).

59. L. T. Vassilev, B. T. Vu, B. Graves, D. Carvajal, F. Podlaski, Z. Filipovic, N. Kong, U. Kammlott, C. Lukacs, C. Klein, N. Fotouhi, E. A. Liu, In vivo activation of the p53 pathway by small-molecule antagonists of MDM2. Science 303, 844–848 (2004).

60. D. P. Lane, Cancer. p53, guardian of the genome. Nature 358, 15–16 (1992).

61. A. R. Barr, S. Cooper, F. S. Heldt, F. Butera, H. Stoy, J. Mansfeld, B. Novak, C. Bakal, DNA damage during S-phase mediates the proliferation-quiescence decision in the subsequent G1 via p21 expression. Nat. Commun. 8, 14728 (2017).

62. T. Suzuki, A. Muramatsu, R. Saito, T. Iso, T. Shibata, K. Kuwata, S. I. Kawaguchi, T. Iwawaki, S. Adachi, H. Suda, M. Morita, K. Uchida, L. Baird, M. Yamamoto, Molecular Mechanism of Cellular Oxidative Stress Sensing by Keap1. Cell Rep 28, 746–758.e4 (2019).

63. Z. Guo, S. Kozlov, M. F. Lavin, M. D. Person, T. T. Paull, ATM activation by oxidative stress. Science 330, 517–521 (2010).

64. N. Kannan, L. V. Nguyen, M. Makarem, Y. Dong, K. Shih, P. Eirew, A. Raouf, J. T. Emerman, C. J. Eaves, Glutathione-dependent and -independent oxidative stress-control mechanisms distinguish normal human mammary epithelial cell subsets. Proc. Natl. Acad. Sci. U.S.A. 111, 7789–7794 (2014).

65. G. Molyneux, F. C. Geyer, F. A. Magnay, A. McCarthy, H. Kendrick, R. Natrajan, A. Mackay, A. Grigoriadis, A. Tutt, A. Ashworth, J. S. Reis-Filho, M. J. Smalley, BRCA1 basal-like breast cancers originate from luminal epithelial progenitors and not from basal stem cells. Cell Stem Cell 7, 403–417 (2010).

66. N. Takahashi, H. Y. Chen, I. S. Harris, D. G. Stover, L. M. Selfors, R. T. Bronson, T. Deraedt, K. Cichowski, A. L. Welm, Y. Mori, G. B. Mills, J. S. Brugge, Cancer cells co-opt the neuronal redox-sensing channel TRPA1 to promote oxidative-stress tolerance. Cancer Cell 33, 985–1003.e7 (2018).

117. C. McQuin, A. Goodman, V. Chernyshev, L. Kamentsky, B. A. Cimini, K. W. Karhohs, M. Doan, L. Ding, S. M. Rafelski, D. Thirstrup, W. Wiegraebe, S. Singh, T. Becker, J. C. Caicedo, A. E. Carpenter, CellProfiler 3.0: Next-generation image processing for biology. PLOS Biol. 16, e2005970 (2018).